

HYDROLOGIC CONTROLS OF LANDSLIDING IN TSITIKA  
BASIN, VANCOUVER ISLAND

by

Scott Charles Davidson

B.Sc. University of British Columbia 1992

A THESIS SUBMITTED IN PARTIAL FUFILLMENT OF  
THE REQUIREMENTS FOR THE DEGREE OF  
MASTER OF SCIENCE

In

THE FACULTY OF GRADUATE STUDIES

(Department of Geography)

We accept this thesis as conforming

to the required standard

THE UNIVERSITY OF BRITISH COLUMBIA

August 1998

© Scott Charles Davidson, 1998

In presenting this thesis in partial fulfilment of the requirements for an advanced degree at the University of British Columbia, I agree that the Library shall make it freely available for reference and study. I further agree that permission for extensive copying of this thesis for scholarly purposes may be granted by the head of my department or by his or her representatives. It is understood that copying or publication of this thesis for financial gain shall not be allowed without my written permission.

Department of GEOGRAPHY

The University of British Columbia  
Vancouver, Canada

Date AUGUST 28, 1998

## ABSTRACT

Landslides are common occurrences in steep mountainous terrain of the Pacific Northwest. Many resource industry activities occur in locations and at times when there is potential for instability to occur. Limiting the exposure of workers during periods of high risk is seen as one way of minimizing worker fatalities. In order to minimize the exposure of workers it is necessary to understand the linkages between rainfall episodes, groundwater fluctuations, and landslide events.

An intensive groundwater and precipitation study was conducted in Russell Creek basin within the Tsitika River basin on Vancouver Island. This basin is the site of a Ministry of Forests study examining fine sediment contributions from logging and natural sediment sources.

The results of this study show that slope instability can result from either high intensity rainfall or rain-on-snow meltwater production. Instability associated with high intensity rainfall occurs in rainstorms with approximately a two-year return period. Instability associated with rain-on-snow meltwater production can be associated with storms with return periods of less than a year. Thresholds for instability need to be refined to allow for the development of an effective shutdown system for forest harvesting operations.

Measurement of groundwater response during storm events showed that there is rapid response of the groundwater system to precipitation inputs. Under high intensity rainfall, the response may be considered almost instantaneous. Modeling of the groundwater responses based on observed groundwater records showed that it is possible

to closely model the response of the groundwater system. The key use of calibrated models for groundwater response is their ability to correctly predict the timing of groundwater peaks rather than estimation of the exact magnitude of the response.

## Acknowledgements

There are many people who I would like to take this space to thank for their input into my thesis. Most prominently I would like to thank the women in my family for their relentless goading of me to “finish that thesis Scott!” That goes triple for Tara Leduc who had to live with me for the entire experience.

This thesis would not have been possible without the assistance of Craig Nistor with whom I endured most of the major rainstorms in the Tsitika over three years of data collection. Along with Craig special thanks must be given to Rob Hudson for his support of the project both physically, financially, and comically. Thanks also to Dan Hogan who in his kindly manner arranged for the initial funding of this study and provided many hours of amusement even when not present. Sorry it took so long. Keno, Scott Weston, Brett Easton, Darren Ham, Drew Brayshaw, Tom Millard, John “funky” Fraser, Shannon Sterling, Rhys Evans, Hjalmar and Osa Langdon all provided field assistance at various stages of the study and their help is appreciated. Thanks to Gord Wright for technical support and equipment advice.

I would like to thank the staff of the Department of Geography for their wisdom and insights. This goes double for Mrs. North for her support and Dr. Mackay for his friendship.

I would also like to thank MacMillan Bloedel Eve River “We Deliver” Division for continuing support throughout the field data collection. Lastly I would like to thank my supervisor Dr. Michael Bovis of the Mendicino Elves for providing me with the opportunity to conduct this study and the patience to wait for me to finish.

## TABLE OF CONTENTS

Abstract .....	ii
Acknowledgements .....	iv
Table of Contents .....	v
List of Figures .....	ix
List of Tables .....	xii
Chapter 1 Introduction .....	1
1.1 Study objectives.....	3
Chapter 2 Study outline .....	6
2.1 Overview .....	6
2.2 Relations between rainfall and landslide events.....	10
2.2.1 Rainfall intensity-duration studies.....	10
2.2.2 Antecedent moisture conditions.....	13
2.3 Definition of the rainfall-groundwater relation .....	16
2.3.1 Influence of static variables on the groundwater system .....	19
2.3.2 Groundwater studies .....	25
2.4 The groundwater-landslide relation.....	29
2.4 Summary of the links between rainfall, groundwater, and landsliding .....	30
Chapter 3 Study Sites.....	33
3.1 Overview.....	33
3.2 Climate.....	33
3.3 Hydrology .....	36
3.4 Bedrock Geology .....	37
3.5 Quaternary Geologic Setting .....	38
3.6 Basin morphometry .....	40
3.7 Vegetation.....	40
3.8 Russell Creek sub-basin.....	41
3.8.1 Overview of Russell Creek sub-basin soils .....	41
3.8.1.1 Grain-size distribution of Russell Creek soils .....	41

3.8.1.3	Clay content of study area soils .....	50
3.8.1.4	Soil porosity determination.....	50
3.8.2	Clear-cut study site.....	51
3.8.3	Old-growth study site.....	53
3.9	Field instrumentation.....	53
Chapter 4	Methods of analysis.....	57
4.1	Rainfall records.....	57
4.1.1	Analysis of synoptic-scale characteristics of storms.....	59
4.1.2	Analysis of averaged storm values.....	59
4.1.3	Analysis of rainfall intensity and duration.....	60
4.2	Groundwater analysis .....	61
4.2.1	Soil parameter determination.....	62
4.2.2	Analysis of groundwater hydrograph.....	64
4.2.3	Estimation of snowmelt and rain-on-snow inputs .....	68
Chapter 5	Rainfall analysis .....	70
5.1	Overview of precipitation during the study period.....	70
5.2	Analysis of storm rainfall .....	75
5.2.1	Storm averaged rainfall analysis .....	75
5.2.2.1	Storm rainfall intensity analysis.....	80
5.2.2.2	Regional rainfall intensity-duration thresholds.....	82
Chapter 6	Groundwater analysis.....	86
6.1	Saturated hydraulic conductivity .....	86
6.2	Soil moisture considerations.....	91
6.3	Groundwater response during storms .....	93
6.3.1	Observed groundwater responses during storms.....	95
6.3.2	Analysis of groundwater responses.....	103
6.3.2.1	Groundwater response to storm input lag determination .....	103
6.3.2.2	Determination of groundwater response rate .....	107
6.3.2.3	Groundwater recession.....	110
6.3.2.4	Snow melt contributions to groundwater.....	111

6.3.2.4	Snow melt contributions to groundwater .....	111
Chapter 7	Groundwater modeling .....	114
7.1	Inputs to the groundwater model .....	115
7.1.1	Rainfall events during the modeled period .....	115
7.1.2	Snowmelt inputs to the groundwater model .....	122
7.1.3	Parameter determination for the groundwater model.....	122
7.2	Results of modeling of the groundwater system.....	126
7.2.1	Calibration of model using individual or grouped rainfall events .....	126
7.2.2	Application of the model to storms known to have initiated instability in the .....	133
Russell Creek basin .....		133
7.3	Synthesis of groundwater modeling results .....	136
Chapter 8	Description of failures during the study period .....	138
8.1	January 28, 1993 failure .....	138
8.2	February 28-March 1, 1994 failures .....	141
8.3	October 25, 1994 failure .....	146
Chapter 9	Discussion .....	150
9.1	Rainfall events .....	150
9.2	Groundwater relations .....	153
9.3	Groundwater modeling at the clear-cut site.....	154
9.4	Relations to landsliding .....	155
9.5	Implications for a warning system to shutdown logging operations during periods of potential slope instability.....	157
9.5.1	Interfor Shutdown System.....	157
9.5.2	Wet and Dry Coastal Shutdown Systems.....	158
9.5.3	Relation of current shutdown thresholds to regional intensity-duration instability thresholds .....	159
9.5.4	Design of a warning system for operational shutdown .....	160
Chapter 10	Conclusions and Recommendations .....	164
10.1	Rainfall and landsliding conclusions.....	164

10.3 Groundwater modeling conclusions.....	165
10.4 Comparison of study findings to the study hypothesis .....	165
10.5 Recommendations .....	167
References.....	170
Appendix A.....	176

## LIST OF FIGURES

Figure 2.1 Forces acting on a soil block with perched watertable .....	7
Figure 2.2 Reported intensity-duration envelopes for triggering instability .....	12
Figure 2.3 Nomograph for soil meltwater production.....	15
Figure 2.4a Flownet for a planar hillslope .....	18
Figure 2.4b Flownet for a hillslope with slope breaks.....	18
Figure 2.5 Representation of the groundwater configuration as a series of slices .....	27
Figure 3.1 Vancouver Island map showing location of Tsitika basin.....	34
Figure 3.2 Tsitika basin map showing geology, elevation and monitoring sites .....	35
Figure 3.3 Typical Karmutsen Formation mountain.....	39
Figure 3.4 Typical island intrusive hill .....	39
Figure 3.5 Russell Creek sub-basin map.....	42
Figure 3.6 Grain-size distribution summary curves for Russell Creek.....	43
Figure 3.7 Soil profile for Pit CC1.....	45
Figure 3.8 Soil profile for Pit CC2.....	45
Figure 3.9 Soil profile for Pit CC3.....	45
Figure 3.10 Soil profile for Pit CC4.....	45
Figure 3.11 Soil profile for Pit OG1 .....	46
Figure 3.12 Soil profile for Pit OG2 .....	46
Figure 3.13 Soil profile for Pit OG3 .....	46
Figure 3.14 Soil profile for Pit OG4 .....	46
Figure 3.15 Road cut into soils near the clear-cut monitoring site .....	48
Figure 3.16 Road cut into soils near the old growth monitoring site.....	49
Figure 3.17 Clear-cut monitoring site map .....	52
Figure 3.18 Old growth monitoring site map.....	54
Figure 3.19 Schematic drawing of a typical groundwater well.....	56
Figure 4.1 Schematic illustrating response lag .....	67
Figure 5.1 Rainfall time series for the Tsitika basin .....	71
Figure 5.2 Air temperature time series for the Tsitika basin.....	72

Figure 5.3 Intensity-duration of storms causing failure in the Pacific Northwest .....	83
Figure 5.4 Estimated intensity-duration envelope curves for the Pacific Northwest...	84
Figure 6.1 Injection test results from clear-cut site Well 2 .....	87
Figure 6.2 Injection test results from clear-cut site Well 3 .....	87
Figure 6.3 Injection test results from clear-cut site Well 4 .....	88
Figure 6.4 Injection test results from clear-cut site Well 8 .....	88
Figure 6.5 Results of salt injection test in Wells 2 and 3 at the old growth monitoring site .....	90
Figure 6.6 Soil moisture retention curves .....	92
Figure 6.7a Gravity drainage test results for old growth samples.....	94
Figure 6.7b Gravity drainage test results for clear-cut samples.....	94
Figure 6.8a Clear-cut groundwater monitoring site time series.....	97
Figure 6.8b Clear-cut groundwater monitoring site time series (cont.).....	98
Figure 6.9a Old growth monitoring site time series.....	100
Figure 6.9b Old growth monitoring site time series (cont.).....	101
Figure 6.10 Pre-storm saturation level versus time lag in response for the clear-cut monitoring site .....	104
Figure 6.11 Pre-storm saturation level versus time lag in response for the old growth monitoring site .....	106
Figure 6.12 1 hour intensity versus maximum response rate for Russ4 .....	109
Figure 6.13 3 hour intensity versus maximum response rate for Russ4 .....	109
Figure 6.14 Histogram of estimated daily snowmelt during the study period .....	113
Figure 7.1 Rainfall and temperature for Storm 93S28.....	116
Figure 7.2 Rainfall and temperature for Storm 93S29.....	118
Figure 7.3 Rainfall and temperature for storm 93S24 .....	119
Figure 7.4 Rainfall and temperature for storm 94S1 and 94S2 .....	121
Figure 7.5 Algorithm for modeling saturation level response to rainfall and snowmelt inputs .....	123
Figure 7.6 Groundwater modeling for storm sequence 93S24 and 93S25 .....	128
Figure 7.7 Groundwater modeling for storm sequence 93S26, 93S27, and 93S28 ...	129

Figure 7.8 Groundwater modeling for storm 93S29 .....	131
Figure 7.9 Groundwater modeling for storm sequence 94S1 and 94S2 .....	132
Figure 7.10 Groundwater modeling for storm 93S3 .....	134
Figure 7.11 Groundwater modeling for storm 94S16 .....	135
Figure 8.1 Location of failures during the study period.....	139
Figure 8.2 January 1993 failure .....	140
Figure 8.3 Rainfall time series for storm 93S3 .....	142
Figure 8.4 March 1994 open slope failure .....	144
Figure 8.5 Rainfall and temperature time series for storms 94S6, 94S7, and 94S8 ..	145
Figure 8.6 October 1994 failure .....	147
Figure 8.7 Rainfall and temperature time series for storm 94S16 .....	148
Figure 9.1 Intensity-duration envelope curves applicable to the Pacific Northwest..	152
Figure 9.2 Schematic for an early warning system .....	161

## LIST OF TABLES

Table 2.1	Typical coastal hillslope form.....	9
Table 2.2	Reported rainfall intensity and duration thresholds .....	11
Table 2.3	Antecedent conditions determined to be important for landsliding.....	14
Table 2.4	Slope and soil factors that influence the groundwater system .....	20
Table 2.5	Values of selected parameters from the literature.....	22
Table 2.6	Summary of links between rainfall, groundwater, and landsliding .....	31
Table 3.1	Tsitika watershed sub-basins .....	37
Table 3.2	Textural summary of Russell Creek soils .....	44
Table 3.3	Soil porosity at the monitoring sites .....	51
Table 3.4	Study rain gauge location and elevation .....	55
Table 4.1	Basis for separation of precipitation record into storm events.....	58
Table 4.2	Variables used in groundwater analysis.....	65
Table 5.1	Storms during the study period .....	76,77
Table 5.2	Size and temperature classification of observed storms .....	77
Table 5.3	Storm interval intensities for storm season storms .....	78
Table 5.4	Average characteristics of rainstorms in the Tsitika Valley .....	79
Table 5.5	A.E.S. rainfall intensity return periods for the Tsitika basin .....	81
Table 5.6	Classification of storm intensities into return periods .....	82
Table 6.1	Results of injection tests at the clear-cut monitoring sites.....	89
Table 6.2	Calculated values of hydraulic conductivity for tested wells.....	89
Table 6.3	Available time series for the groundwater monitoring sites .....	96
Table 6.4	Relation of lag time and pre-storm saturation level.....	105
Table 6.5	Estimated snowmelt frequency classes .....	112
Table 7.1	Recession rates for groundwater modeling.....	125
Table 7.2	Summary of model storm characteristics for modeled storms.....	127
Table 9.1	Return period of 1, 6, 12, 24 hour rainfall intensities for storms with failures .....	156
Table 9.2	Rainfall limits for the Interfor Shutdown System.....	157
Table 9.3	Shutdown criteria for the Dry and Wet Coastal Shutdown Systems .....	159

## Chapter 1 Introduction

In this thesis, I examine the linkages between rainfall, groundwater response, and landslide events. Previous studies have focused on linkages between rainfall and landsliding or rainfall and groundwater response without attempting to link the three components (Caine 1980, Cannon and Ellen 1985, Harp et al. 1990, Hogan and Schwab 1991). This study was recommended by two coroners reports that called for further research into the linkages between rainfall and landsliding following several fatalities in the logging industry during large rainstorms in the early 1990s on Vancouver Island.

When the size of the primary resource extraction industries operating on or near potentially unstable slopes is considered, the importance of examining linkages between rainfall and landsliding becomes obvious. This is emphasized by large storms in 1978 and 1990 that produced numerous landslides in forested and harvested terrain in the Pacific Northwest.

Cyclonic storms are common occurrences during winter months in the Pacific Northwest and the frequency of storms is controlled by large-scale synoptic features over the Pacific Ocean and the western portions of North America. In mountainous terrain of the Pacific Northwest, the period October to March contains most of the frequent and intense storms, and also is the period of most intense landsliding VanDine (1985). The combination of long, steep hillslopes with shallow soils and abundant rainfall means large areas of potential slope instability.

Groundwater levels are a response to inputs of water from rainfall and snowmelt and have been used to illustrate the responsiveness of the soil hydrologic system to rainfall inputs (Mosley 1979, McDonnell 1990a). Under conditions of high water input, soils respond rapidly: the time from the start of groundwater rise to the groundwater peak is typically short (Buchanan 1990). On slopes where the groundwater system is influenced by macropores, this response may be almost instantaneous, as water bypasses the unsaturated soil matrix en route to the saturated zone. Depending on the drainage rate of the soil, it may take several days for the groundwater table to recede to pre-storm levels. The antecedent conditions at a site prior to a storm therefore become important in that, if the soil has not drained completely from a preceding storm, groundwater levels will be higher than expected under the succeeding storm water input. This memory of the hillslope hydrologic system accounts for the non-linear response of groundwater to rainfall inputs.

Conventional stability analysis predicts that fluctuations in pore pressure will trigger slope instability by reducing the factor of safety of a slope to unity. Studies by Sidle (1992) and Buchanan and Savigny (1990) have shown that slope failures are triggered by peak pore pressures related to maximum groundwater levels. The maximum groundwater level, in turn, is related to previous history of rainfall and snowmelt inputs to the soil and soil properties. Thus, landsliding is usually associated with peak groundwater levels which in turn are related to the rate of input of water to steep hillslopes as well as to antecedent moisture conditions.

To conduct a study of rainfall conditions conducive to slope failure, it was necessary to find an area with steep, planar slopes with a previous history of

landsliding, and representative of terrain conditions in the forest-harvested belt of coastal British Columbia. Two areas with suitably steep slopes were considered for study. The area around Quatsino Sound on northwestern Vancouver Island was rejected as the area had a discontinuous soil cover, and was too remote to allow ease of access during the winter months. The Tsitika Valley on north-central Vancouver Island was eventually selected for study as the soils in the area were fairly continuous and the valley could be reached in less than 4 hours from Nanaimo, B.C. As well, logistical support was available from the Eve River Division of MacMillan Bloedel and a record of precipitation data and streamflow data was also available.

### **1.1 Study objectives**

The principal objectives of this study are:

1. to examine the relations between the precipitation and groundwater time-series on steep forested hillslopes and to compare responses between clear-cut and unlogged slopes.
2. to document the occurrence of landsliding during periods of extreme rainfall.
3. to assess the critical sequence of rainfall events required to destabilize steep forested slopes typical of coastal British Columbia.
4. to calibrate a groundwater model to predict periods of probable slope instability under rainfall-recharge conditions.

The four aspects listed above have been examined separately in a number of previous studies; however, here I attempt to show how all four aspects need to be considered in slope instability. Once the relations between the individual components

have been identified, it follows that periods of probable slope instability could be recognized from a knowledge of antecedent and actual rainfall conditions. This then outlines the intent of the thesis. The remaining discussion in this chapter describes the layout of this thesis.

In Chapter 2, I separate the research into three separate modules and examine relevant literature in each of the three components. Information on each of the components, and the controlling parameters in each component, is discussed. Findings from previous studies are used to develop linkages between rainfall episodes, groundwater fluctuations and landslide events.

The physical descriptions of the study area and monitoring sites are presented in Chapter 3. The results of analysis of sediment samples collected during field work are used to characterize the soils on slopes monitored during the study. The importance of lithology and hydrology in the Tsitika and Russell basins is also discussed. Chapter 3 also includes a discussion of the field installations.

Chapter 4 contains analysis of three types of data collected, namely rainfall records, groundwater records, and landslide event reports. The results of the rainfall and groundwater analyses are presented in Chapters 5 and 6, respectively. In each chapter, linkages between the measured component and reported landslide events are discussed. The rainfall discussion focuses on differences between storms during which failure was observed and storms with no observed failures. The groundwater results emphasize both the rapidity and magnitude of water level responses to observed rainfall and snowmelt inputs.

Chapter 7 deals with modeling of groundwater time series for the clear-cut monitoring site using rainfall data from a nearby tipping bucket rain gauge. The results of watertable modeling are presented and discussed in the first portion of the chapter. In the second portion, modeling results are discussed on a storm-by-storm basis.

Chapter 8 examines the storms known to have initiated instability. A discussion of the failure locations and the climatic conditions at the time of failure are presented. In Chapter 9 a synthesis of the preceding three results chapters is provided to achieve an integrated discussion of the links between rainfall, groundwater levels, and landsliding, and the attempts to model groundwater responses. Having examined these linkages, a discussion of the implications of the study findings to the issuing of public warning systems is presented. The discussion of landslide warning systems also includes an examination of two current systems for the shutdown of logging operations currently in use on Vancouver Island.

Chapter 10 summarizes the conclusions of the study and makes recommendations based upon these conclusions. The recommendations of the study are broken into operational and research-oriented categories. The intent of the operational recommendations is to suggest steps that could be taken to better monitor precipitation and landslide events for the purpose of reducing risk in the forest industry.

## Chapter 2 Study outline

### 2.1 Overview

In this chapter I provide a framework for the analysis of the three types of data dealing with the interrelations between rainstorms, groundwater fluctuations and landslide events in the Tsitika Valley, Northeastern Vancouver Island. The three components were examined as follows:

A) Rainfall-Landsliding B) Rainfall-Groundwater C) Groundwater-Landsliding

The term landsliding is subject to liberal usage in publications. For this study, landslide only applies to translational failures occurring in, or at the base of, shallow morainal or colluvial soils. Given the large number of papers dealing with shallow-layer landslides, emphasis in the literature review was placed on studies of climatically forced landslides involving a perched water table.

The failures considered may be analyzed using the Mohr-Coulomb failure criterion and the infinite slope model (Buchanan 1988). Figure 2.1 shows the stresses acting on the base of a typical soil block. The parameters, except slope angle ( $\beta$ ), are dependent on soil type and water inputs at a given site. The assumptions of the infinite slope that must be met are that the ratio of the soil thickness to both slope length and width is small, and that groundwater flow is roughly parallel to the slope.

The Coulomb factor of safety of a soil block may be expressed algebraically as shown in Eqn. 2.1. Soil cohesion ( $c'$ ) and root cohesion ( $\Delta c$ ) and the internal friction angle of

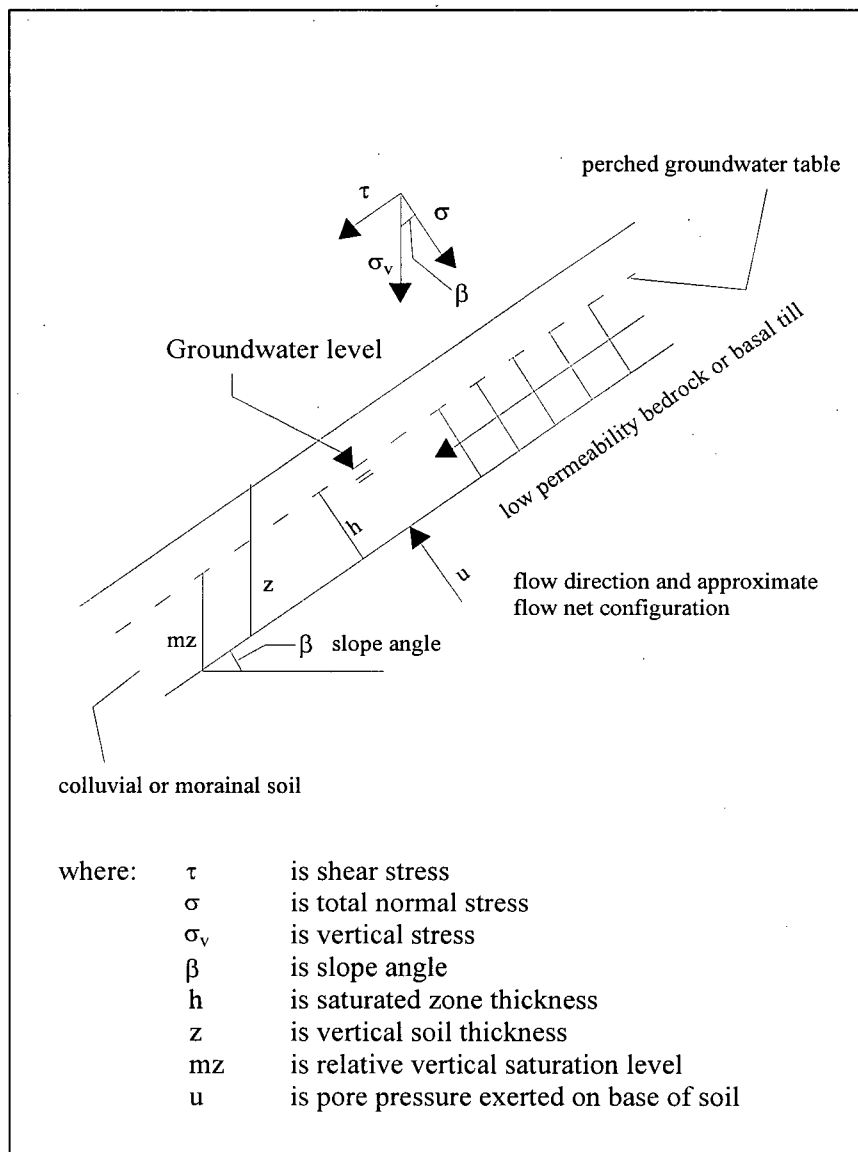


Figure 2.1 Schematic showing stresses acting on a soil block with a perched watertable.

particles ( $\phi'$ ) are all factors that act to stabilize hillslopes. Failure is assumed to occur when Eqn. 2.1 is equal to 1.0. Vegetative surcharge is included in the shear stress term of the equation. The relationship between pore pressure and the thickness of the saturated layer is shown by Eqn. 2.2. It is evident that pore pressures increase linearly with an increase in the relative saturation level of a soil described by parameter  $m$  in Eqn. 2.2. This is the ratio of the saturated zone depth to the total soil depth (Figure 2.1).

$$\text{F.S.} = \frac{c' + \Delta c + (\sigma - u) \tan \phi'}{\tau} \quad (\text{Eqn. 2.1})$$

$$u = \gamma_w m z \cos^2 \beta \quad (\text{Eqn. 2.2})$$

Examination of the variables involved in the factor of safety stability relation reveals that, over short time scales, only pore water pressure  $u$  fluctuates. Slope stability studies often make detailed measurement of parameters in Eqn. 2.1 to determine stability at a specific location; however, this is not feasible over areas of several square kilometers. Despite the spatial variability of soil strength parameters in Eqn. 2.1, it is generally agreed that groundwater pressures trigger most slope failures, and thus temporal changes in strength parameters  $c'$ ,  $\Delta c$ , and  $\phi'$  can be ignored over the time span of this study (2 years).

The typical configuration of a hillslope in forested mountainous terrain is listed in Table 2.1. The importance of mid-slope segments was identified by Rollerson (1992) who found that 417 out of 760 landslides in seven clear-cut areas on the Queen Charlotte Islands originated in middle slope segments. This study showed that the midslope segment is the most important in terms of groundwater and slope stability. Given that slope length is much greater than soil depth, a reasonable assumption is that the pore

pressure model in Figure 2.1, and described by Eqn. 2.2, applies to the steep forested slopes in the study area.

Table 2.1 Typical coastal hillslope form

- |   |
|---|
| <p>a) Very steep upslope segments (<math>&gt;35^{\circ}</math>). These sections often extend above 800 m elevation limit for rain-on-snow effects during winter and represent an accumulation area for snow. These steep sections are the starting zones for snow avalanches and rockfall onto lower slope sections. There is often only patchy soil in these sections and water not entering the bedrock flow system is rapidly drained to the midslope segments.</p>  |
| <p>b) Steep gradient midslope segments (<math>20-35^{\circ}</math>). These sections range in length from 100 metres to more than several hundred metres. Rain-on-snow is an important process on these midslope segments. These sections are transport zones for failures from upslope sections and are starting zones for debris flows. The timber resource on these sections is high, and since many of the floodplains and low gradient section of hillslopes were logged earlier in this century, they are currently being harvested intensively.</p> |
| <p>c) Lower gradient valley flat sections (<math>&lt; 20^{\circ}</math>). The length of lower slope segments is not as great as those in the midslope areas, ranging from tens of metres to about 200 m. These sections represent depositional areas for failures originating upslope and are too low gradient to be sites for initiation of failures. As mentioned in b, many of these areas have already been harvested and many are reforested and re-stabilized following earlier phases of logging.</p>  |

## **2.2 Relations between rainfall and landslide events**

Much of the annual precipitation in the Pacific Northwest falls during the period October to April (VanDine, 1985). In steep mountainous terrain, uplift and funneling of air by topographic confinement can result in intense localized rainfall (Givone and Meignien 1990, Church and Miles 1987). Intense precipitation can also result from convective cells of 1-5 km in diameter embedded within frontal storms (Houze, 1981), although this situation is more common at the study site during the summer months. Landslide activity has been observed to be associated with periods of intense rainfall in many mountain areas (O'Loughlin 1972, Eisbacher and Clague 1981, Sidle and Swanston 1982, Church and Miles 1987, Buchanan and Savigny 1990). The return period for storms causing landslides has been estimated to be 2-5 years for the Lower Mainland and Vancouver region (Eisbacher and Clague, 1981) and less than 2 years in the Queen Charlotte Islands (Hogan and Schwab, 1991). The low return period of these events suggests that storms with sufficient rainfall to cause landsliding are very common events in the Pacific Northwest. However, such estimates of storm return periods are based on short-term (24 hr.) summations only, and do not consider the precipitation history prior to cycles of slope failure.

### **2.2.1 Rainfall intensity-duration studies**

The term extreme rainfall is often encountered in the literature, whereas a definitive description of the term is not common. In this study I seek to establish a definition of extreme rainfall for the Tsitika basin based on the rainfall intensity (I) and duration (D) characteristics of observed storms and on the findings of other studies. Previous research

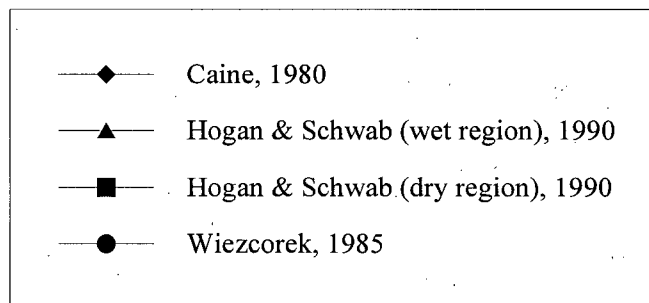
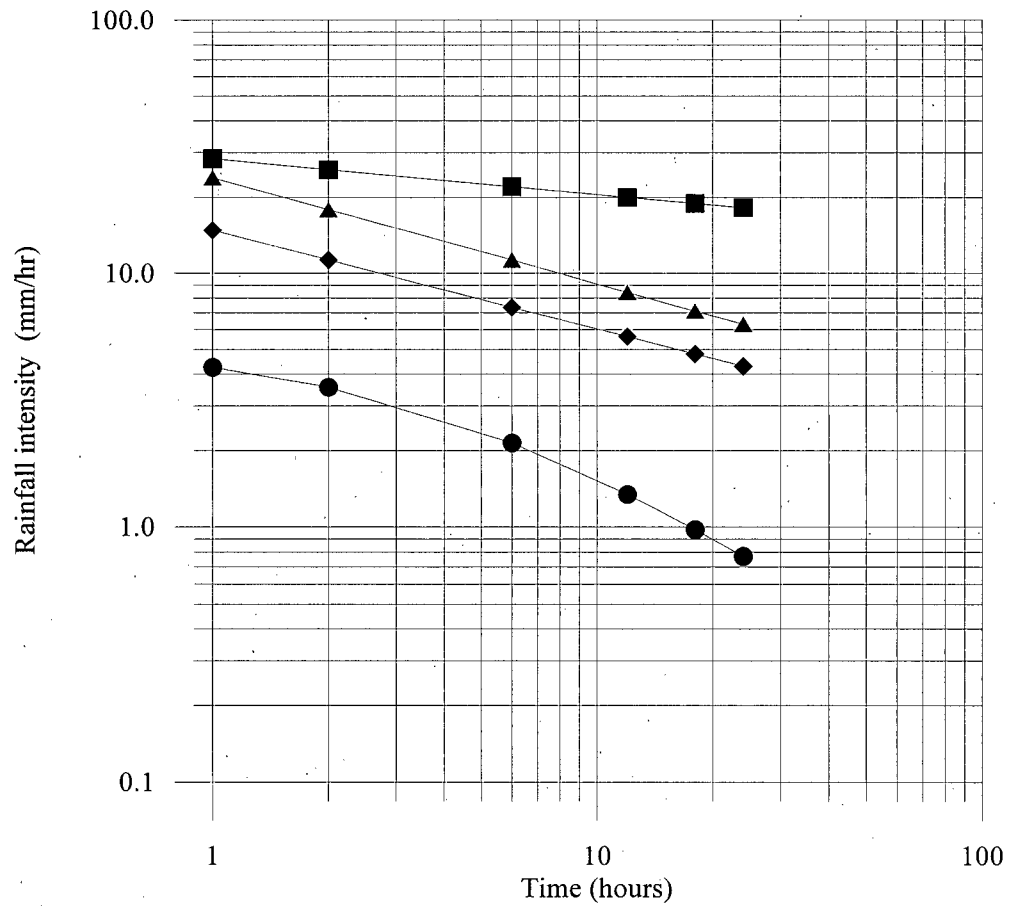
on the incidence of landsliding has identified threshold rainfall intensity-duration relations above which landsliding is likely to occur (Table 2.2). The existence of such a link between rainfall and landsliding has important implications, because if one can determine such a threshold for a specific area, steps can be taken to reduce the risk to personnel working in potentially unstable terrain during periods of heavy rainfall.

Table 2.2 Reported rainfall intensity-duration thresholds

Reference	Study location	Functions
Caine (1980)	world-wide data	$I = 14.82 D^{-0.39}$
Hogan and Schwab (1991)	Queen Charlotte Islands	$T_w = 6.3 D^{0.42}$ (wet) $T_d = 18.2 D^{0.14}$ (dry)
Wieczorek (1983)	California	$I = 0.9 / (D + 0.17)$

Intensity-duration relationships developed by Caine, Hogan and Schwab, and Wieczorek, as well as the range of estimated extreme annual rainfall totals for various durations in the study area from the Rainfall Frequency Atlas of Canada, are shown in Figure 2.2. The Caine threshold (Caine, 1980) was developed using extreme rainfall data corresponding to 73 events in a wide variety of climates. This relationship, though based in some cases on data of questionable quality, clearly shows a general relationship between rainfall intensity-duration and landsliding. Hogan and Schwab (1991) determined that two thresholds could be defined in the Queen Charlotte Islands depending on antecedent conditions classed as “wet” and “dry”, respectively. These two thresholds were only distinct so long as storm durations were less than 3 days. In that study, what they termed the  $T_w$  threshold represents the threshold for storms with wet antecedent conditions, while the  $T_d$  threshold is for rainfall following dry antecedent

Figure 2.2 Reported intensity-duration envelopes  
for triggering instability



conditions. The definition of wet or dry antecedent conditions is based on cumulative departures of daily rainfall from mean rainfall at a station determined for a 10 day period preceding the storm. The Wieczorek relationship was developed in the San Francisco Bay area of California, which differs geologically and climatically from the study area, but is included for comparison.

The envelopes drawn in Figure 2.2 show that rainfall thresholds vary regionally, due to factors such as topography, surficial materials, land use, and climate. The determination of a threshold for one region does not ensure transferability to other regions. Church and Miles (1987) concluded that the Caine threshold did not apply to failures in southwestern British Columbia, though two points may have influenced their findings. The first is that their data were climate-day values (fixed recording period) and intense rainfall is often spread over successive days. In order to properly assess whether the rainfall intensity-duration approach will work, it is necessary to use extreme values based on storm summations, not climate-day values. The second point is that the rainfall data in their study were imported from stations at low elevations and probably did not adequately reflect the climatic conditions at landslide failure sites.

### **2.2.2 Antecedent moisture conditions**

This section contains a discussion of antecedent conditions considered to be important in preconditioning hillslopes to failure. Conditions found to be important in landsliding are listed in Table 2.3. The list is not exhaustive, and not all of the conditions may apply at a particular location.

Table 2.3 Antecedent conditions determined to be important in landsliding

Reference	Study location	Antecedent condition(s)
Church and Miles (1987)	Fraser Valley	Snowmelt and thawing ground
Hogan and Schwab (1991)	Q.C.I.	Antecedent monthly and weekly rainfall
Cannon and Ellen (1985)	California	Seasonal Rainfall
Sidle and Swanston (1981)	Alaska	Pre-storm groundwater level
Sidle (1992)	Alaska	Two-day antecedent rainfall

The principal mechanisms for pore pressure increase on slopes in the Tsitika study area are rainfall recharge and rain-on-snow. Much less is known about the latter mechanism. Church and Miles (1987) identified its probable importance in triggering failures. During spring, as snowpacks ripen, a rainfall event can produce rapid melting of snow, thereby increasing the volume of infiltration water. The elevation range for rain-on-snow events has been identified as 300 to 800 m by the Coastal Watershed Assessment Procedure Guidebook (1995). Figure 2.3 is a nomograph developed by Church (1988) using a parameterization of the U.S. Army Corps of Engineers (1960) snowmelt equations. This nomograph shows how, for given climatic conditions, the ratio of snowmelt to precipitation varies with 24 hr rainfall. Temperature and wind speed are both important factors in determining the amount of snowmelt, but so is first-hand information on the actual snowpack. The use of such a nomograph without any firsthand information on rain-on-snow meltwater production is not recommended.

There is general agreement that peak streamflows are increased by rain-on-snow, though the results of studies vary due to the influence of timber harvesting on peak flows.

One attempt to investigate the influence of timber harvesting on rain-on-snow peak flows has been the development of an empirical model, ROCMOD, by the B.C. Forest Products Ltd. Resource Planning Group (hereafter known as the Resource Planning Group)

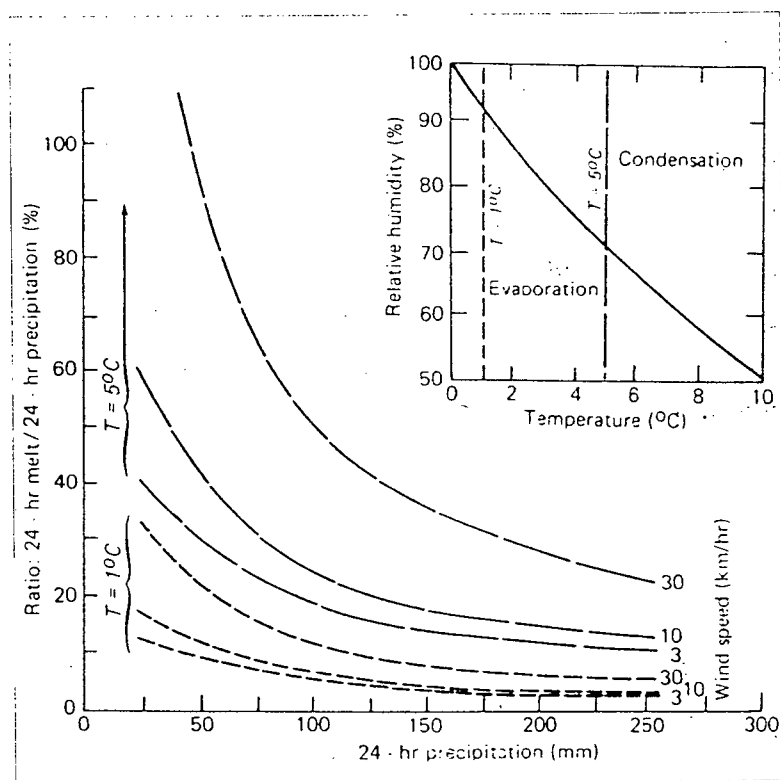


Figure 2.3 Nomograph showing effect of rain on snow for different temperatures and wind speeds (Church, 1988).

(Chatterton et al., 1985; Chatterton and Willington, 1987). The model incorporates snowmelt in a watershed by dividing the watershed into elevation bands and using the U.S. Army Corps. of Engineers (1960) equations to estimate melt within each band. Based on earlier research by the Resource Planning Group, the water retention ability of

the snowpack is assumed to reach zero when the density of the snowpack without rainfall and snowmelt input achieves a value of  $500 \text{ kg/m}^3$ . After this point, all water input is assumed to be transmitted to the soil below. Information on snowpack density and areal distribution of snow depth are necessary for the model to operate properly. When these data are lacking the operator is required to enter the elevational range of the snowpack and an initial density for the pack. The model then uses relationships derived from the work by Fitzharris (1975) to estimate snowpack depth and density within each elevation band. The latest version of the model, ROCMOD3, was calibrated using data from Carnation Creek, B.C., and this enabled prediction of most flow magnitudes to within  $\pm 10\%$  for that basin.

### **2.3 Definition of the rainfall-groundwater relation**

Before proceeding it is useful to define the term groundwater in the context of this study. Groundwater refers to the water within the soil matrix that exists in a state of positive pressure. The term groundwater table refers to a seasonal or transient, upper boundary of the saturated zone at which pore pressure is zero. Prior to the start of the storm season, many hillslopes are in a drained state. No saturated layer is present and water in the soil matrix is held in a state of tension. Initial water inputs to the soil system fill up available pore spaces and reduce the negative pressures within soil pores. Positive porewater pressures develop when all available space within the soil matrix is filled with water. Once a saturated layer develops, gravity driven movement of the water through the porous medium is governed by Darcy's Law (Eqn. 2.3) where  $q$  is the volumetric flow

rate per unit area,  $K$  is hydraulic conductivity of the soil,  $\partial h$  is the change in hydraulic head, and  $\partial l$  is distance.

$$q = -K \frac{\partial h}{\partial l} \quad (\text{Eqn. 2.3})$$

The term  $\partial h/\partial l$  in Eqn. 2.3 represents the hydraulic gradient and can be replaced by the term  $\nabla h$  reducing Eqn. 2.3 to a vector equation. The volumetric flow per unit area term,  $q$ , should be considered in terms of flow through connected pore spaces as determined by the porosity of the soil,  $n$ . The flow celerity can then be derived from:

$$c = \frac{q}{n} = \frac{K}{n} \nabla h = \frac{K \sin \beta}{n} \quad (\text{Eqn. 2.4})$$

where, for the purposes of infinite slope analysis the hydraulic gradient,  $\nabla h$  is approximated by sine  $\beta$  given that flow is roughly parallel to the soil surface (Figure 2.4a). Flow celerity is then a product of one slope parameter and two soil parameters.

The logical starting point for any discussion of groundwater response to rainfall is water movement through the unsaturated zone. The unsaturated layer is a zone through which water is transmitted roughly vertically to the underlying saturated zone at a rate dependent upon the moisture content of the layer. Buchanan (1988) found that drained moisture contents did not appear to change with depth for soils in Whatcom County, Washington. Tischer (1986) also found that there was little variation in initial moisture contents with depth at a site in the UBC Research Forest near Haney, B.C. Based on these observations it will be assumed that, within an individual soil horizon, soil is fairly homogeneous with respect to matrix water content. Short-circuiting, or bypassing, of the unsaturated zone as a result of flow through low-resistance paths, or macropores, is discussed in section 2.2.3.

Figure 2.4a. Flownet for undisturbed hillslope.

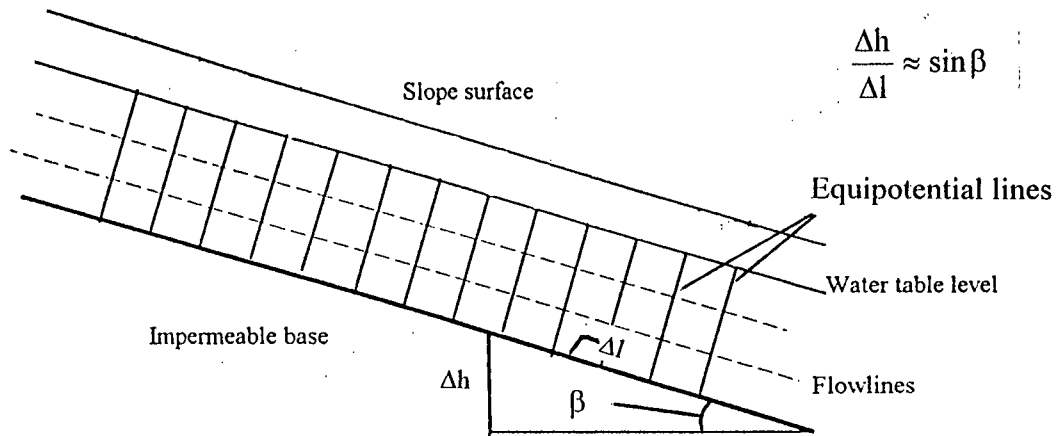
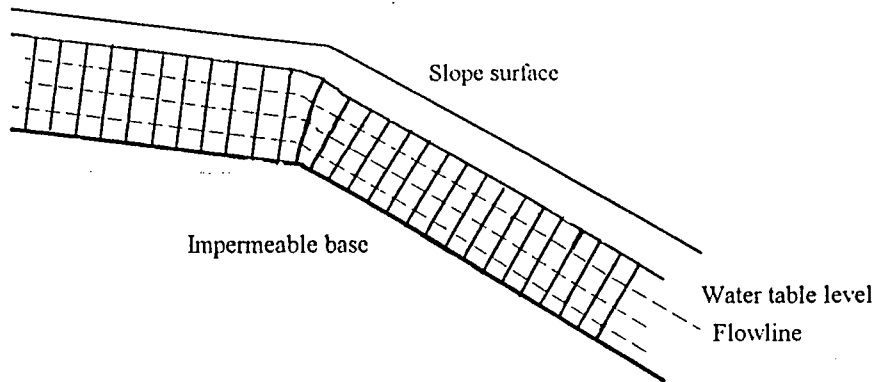


Figure 2.4b. Flow net showing changes in saturate layer thickness associated with slope breaks



Soils in the study area are assumed to have been previously wetted prior to the start of most storms. Support for this assumption is the frequent occurrence of rainstorms in the study area during the storm season, the presence of a continuous snowpack above 300 m between November and March, to provide recharge over much of the storm season, and evidence from field based studies conducted on similar soils. Soil water potential curves from deVries and Chow (1978) in Seymour basin show that, during the wetting phase, steady-state flow through the unsaturated zone was achieved usually within an hour of the start of sprinkler irrigation. Thus, frequent rainstorms can reasonably be assumed to maintain a field water content close to "field capacity" throughout the unsaturated zone. This means that the saturated zone can respond fairly rapidly to further inputs of rainfall. An example of this is shown by McDonnell (1990a) who found in New Zealand that when pre-storm moisture conditions were high, input to the soil-water system rapidly filled available storage spaces and a perched saturated layer rapidly developed. This is discussed in the analysis of the groundwater records in Chapter 6.

### **2.3.1 Influence of static variables on the groundwater system**

The storm-response hydrograph for groundwater at a site depends on slope factors, soil properties, and meteorological conditions. This section deals with the influence of slope factors and soil parameters on the typical groundwater responses. The explanations are based largely on theoretical considerations; however, values of parameters from other studies are included in Table 2.4 for reference, and are discussed later this section.

The slope factors and soil parameters deemed important in this study are listed in Table 2.4. Mountainous terrain in the Pacific Northwest is a complex assemblage of

Table 2.4 Slope and soil factors that influence the groundwater system

Slope factors	Soil parameters
1. slope convergence (hollows)	1. soil structure (layering)
2. slope angle	2. porosity
3. slope breaks	3. effective porosity
4. slope profile	4. hydraulic conductivity
	5. grain-size
	6. macroporosity of soil

convergent and divergent slope segments. Infilled hollows act as zones of convergent groundwater flow while a saturated layer is present. Dunne and Black (1970) found that zones of convergent flow exhibit higher groundwater levels and longer recession times relative to zones of divergent flow. Since hydraulic gradient is approximated by slope angle, slope angle increases cause hydraulic gradient and flow celerity increases. It follows that slope breaks are important for the groundwater table configuration so long as they are reflected in an associated break in the basal boundary of the soil. Figure 2.4a and Figure 2.4b show hypothetical flownets for hillslope drainage during rainfall input. Figure 2.4a shows the classic infinite slope model with flow parallel to the slope. Figure 2.4b shows the influence of topographic breaks on the groundwater configuration. The resulting changes in the saturated layer thickness result in variable factors of safety against sliding in a downslope direction.

Slope angle reduction results in a bulge in the groundwater table due to a decrease in the hydraulic gradient, slope steepening causes the opposite to occur. A lower slope angle acts to increase the stability of a slope segment, but if this sequence of breaks is

repeated many times over the length of a hillslope, then the most likely initiation zone of a failure should be at point A where concavity of the slope occurs. At point A, slope angle decreases and a thick saturated layer develops.

Soil structure is important in that it influences the values of other soil parameters in Table 2.4. Layering, the presence of a high or low conductivity zones within the soil profile, can significantly affect groundwater flow. Studies by Sidle, Pearce and O'Loughlin (1985) and Tischer (1986) showed measured differences in saturated conductivity,  $K_{sat}$  between A and B horizons of soils.

Of the other parameters listed in Table 2.4, effective porosity is perhaps the most important. Effective porosity,  $n_e$ , represents the proportion of the void space not water occupied. Thus,  $n_e$  is a useful measure of the pore space available for rainfall recharge. In the dry state,  $n_e = n$ , the full porosity value. However, when recharge events are closely spaced in time,  $n_e \ll n$ , and consequently small recharge events are able to saturate the soil matrix and cause large changes in saturated zone thickness.

Effective porosity typically varies from 0.005 to 0.45 (Table 2.5). Low values show that soils were close to saturation at the time of observation. Higher values, determined by Tischer, (1986) and Wu, McKinnell, and Swanston, (1979) represent cases where the soil column was unsaturated prior to a storm.

Hydraulic conductivity,  $K$ , represents the ability of a soil to transmit water under a specified hydraulic gradient. Hydraulic conductivity is often referred to as either  $K_{sat}$  or as  $K_{bulk}$ , depending on whether observed conductivity refers to the soil matrix or the matrix plus macropores. Values of  $K_{sat}$  for the studies listed in Table 2.5 have a

Table 2.5 Values of selected parameters from the literature

1. Porosity		
Buchanan (1988)	Cascades, U.S.A.	0.481
Tischer (1986)	Coast Mtns., B.C.	0.63
O'Loughlin (1972)	Coast Mtns., B.C.	0.548
2. Effective porosity		
Jackson and Cundy (1992)	Washington, U.S.A.	0.005
Tischer (1986)	Coast Mtns., B.C.	0.23-0.45
Wu and Swanston (1980)	Alaska, U.S.A.	0.08, 0.32
3. $K_{sat}$ ( $10^{-5}$ ) [m/s]		
Buchanan (1988)	Washington, U.S.A.	4.5 (in-situ)
Buchanan (1988)	Washington, U.S.A.	0.36 (till)
Tischer (1986)	Coast Mtns., B.C.	80
Wu et. al. (1982)	Alaska, U.S.A.	0.5-5 (in-situ)
Sidle, Pearce, and O'Loughlin (1985)	Listed as for typical forested soils	69 for A1 28 for B2
Jackson and Cundy (1992)	Washington, U.S.A.	6-41
O'Loughlin (1972)	Coast Mtns., B.C.	4.0 (in-situ)
4. $K_{bulk}$ ( $10^{-5}$ ) [m/s]		
Megahan and Clayton (1983)	Idaho, U.S.A.	16.0 – 33.0
O'Loughlin (1972)	Coast Mtns., B.C.	12.0 (in-situ)

range  $0.5-5 \times 10^{-5}$  m/s for coarse sandy soils considered comparable with Tsitika basin materials. The value of  $8.0 \times 10^{-4}$  m/s from Tischer (1986) represents the conductivity of the upper soil horizon including the high conductivity forest floor layer. Sidle, Pearce, and O'Loughlin (1985) estimate  $K_{sat}$  of an A1 horizon (equivalent to Ah) to be  $6.9 \times 10^{-4}$  m/s. These two studies show that there may be differences in  $K_{sat}$  of up to an order of

magnitude between soil layers. Parameter  $K_{\text{sat}}$  was found to be less than  $K_{\text{bulk}}$  by as much as a factor of 20 by Mosley (1979). The difference is explained by the enhanced conductivity of macropores. Megahan and Clayton (1983) determined that  $K_{\text{bulk}}$  was greater than  $K_{\text{sat}}$  by a factor of 10 - 20 using tracer tests in Idaho. In reviewing the literature values of hydraulic conductivity it was important to first determine which hydraulic conductivity the study had used to avoid improper assumptions.

Grain size is important in that the amount of fine-grained silts and clays control average pore sizes, and hence resistance to flow. Since fine-grained soils often have smaller porosities and hydraulic conductivities than do coarse grained soils, the recession curve of the groundwater table will be longer in finer soils, thereby increasing the importance of antecedent conditions. This means that the 'hydrologic memory' of a slope is greater in finer grained soils.

The influence of macropores on groundwater flow is well documented. One of the first reported insights as to the importance of root channels was made by Schumacher in the mid 19th century (cited in Tischer, 1986). Macropores are effective in downslope transport of water in the following two cases:

- a) the saturated layer has risen to a level above the entrance to the macropore. (Prior to that condition, water in the macropore would be lost to the unsaturated soil matrix below).
- b) the rate of water supply to the macropore is greater than the seepage losses to the surrounding soil matrix.

The connectivity of the macropore system is important in the second case. If the system is well connected then water can be drained rapidly downslope, thereby increasing slope

stability. If the system is not well connected, or if macropores are locally closed, then water may be delivered downslope to the closed end of a macropore resulting in pore pressures above those predicted by Eqn. 2.2. This effect has been documented as a cause of hillslope failures (Pierson, 1983; Brand et al., 1986).

A final point examined with respect to flow through macropores is the relative proportion of groundwater that bypasses the soil matrix. McDonnell (1990b) cites a 1979 New Zealand study by Pearce and McKercher that estimated 65% of total runoff and 39% of total annual rainfall was converted to quickflow through macropores. Chatterton and Willington (1987) determined empirically that 70% of water input is routed through macropores following a rainfall rate of 1mm/hr being exceeded for two hours, and that at input rates greater than 15 mm/hr, almost all water input is routed through macropores. If the first flow proportion value of Chatterton and Willington is accepted, then macropore flow routing should be the dominant subsurface flow process during even low intensity storms. The Pearce and McKercher study was for a series of small catchments with short slopes (<50m) in New Zealand, and it is not known how readily transferable their proportions are to larger basins with longer slopes. Clearly, the topic of proportional macropore flow routing is one that requires more study.

Macropores are also effective in increasing the infiltration rate of a soil. Chamberlin (1972) found that mountain soils of western British Columbia were anisotropic due to the presence of subsurface channels (now referred to as macropores). These channels may be formed by decayed roots, soil piping, or through the activities of biological organisms such as mice or worms. DeVries and Chow (1978) examined the infiltration of water into a forested soil under artificial recharge conditions. They found non-uniform wetting of

the soil, attributed to macropore-assisted infiltration. The latter was at a maximum during the non-steady-state response phase of the simulated rainfall event, and then decreased as a steady-state flow condition was approached. An excellent review of the importance of macropores for infiltration and for the generation of subsurface stormflow is provided by Beven and Germann (1982). In that review, macropores were shown to be effective in increasing the infiltration of "macroporous" soils, relative to soils lacking macropores.

Studies cited here have examined the effect of rainfall intensity upon flow in macropores. Clay-rich soils with desiccation cracks required an intensity of 1mm/hr to initiate flow. On agricultural lands, a threshold intensity of 5-8 mm/hr was required to initiate flow. McDonnell (1990), in a study in the MaiMai catchment of New Zealand, found that rates of vertical infiltration exceeded rates of lateral water transmission because of flow "short-circuiting" through macropores. Greater vertical infiltration rates produced transient peaks in the groundwater table that are of particular interest in stability studies. In this context, it is seen that conduits of higher conductivity can achieve more rapid delivery of water to the saturated zone, thus causing a soil to respond more quickly to surface water inputs. However, such conduits also allow more rapid lateral flow of water, which prevents the development of thick saturated zones. It is conceivable that the first effect could be offset by the second. This underscores the need for the local, empirical approach adopted here.

### **2.3.2 Groundwater studies**

The previous section contained information on how both slope factors and soil parameters influence the groundwater system. In this section I will examine the results of

some relevant studies in an effort to discuss the nature of the linkages between rainfall and groundwater recharge. The goal is to show that in shallow steepland soils the groundwater system response is closely related to rainfall duration and intensity.

Beven (1981, 1982) showed the ability of the kinematic-wave equation (Eqn. 2.5) to predict the steady-state water table profile when values of  $\lambda = 4 i \cos \beta / (K_{\text{sat}} \sin^2 \beta)$  were less than 0.75, where  $i$  = the rainfall intensity and  $\beta$  = the hillslope angle. The equation represents a combination of the continuity equation with the extended Dupuit-Forscheimer equation. The main assumptions of the kinematic-wave model are:

$$n_e \frac{\partial h}{\partial t} = - K_{\text{sat}} \sin \beta \frac{\partial h}{\partial x} + i \quad h = f(x,t) \quad (\text{Eqn. 2.5})$$

- a) The water table rises roughly parallel to the basal impermeable layer.
- b) Recharge to the groundwater system is spatially uniform and occurs at rate  $i$  over a given time step.
- c) The coordinate system used sets  $x=0$  as the top of the slope and  $x$  increases downslope.
- d) Flow is non-turbulent and follows Darcy's Law.
- e) Soil parameters ( $n_e$ ,  $K_{\text{sat}}$ ) are constant and uniform at all points in the soil.

As shown in Figure 2.4, Eqn. 2.5 represents a coordinate system where  $x$  is the distance from the crest of the hillslope,  $h$  represents the thickness of the groundwater table measured orthogonal to the slope, and  $t$  is time. Figure 2.5 shows, at great vertical exaggeration, the groundwater configuration as a series of slices of thickness  $i$  that are stacked on a slope with angle  $\beta$ , and length  $L$ . Each slice represents a contribution to the water table thickness during an individual time step. As each slice is added to the slope it

travels downslope from the divide at flow celerity,  $c$ . The next slice is added to the slope at the base of the preceding slice yielding the configuration shown in Figure 2.5. The slope of the groundwater table downslope of the divide is equal to  $i/cn_e$  up to the point  $x^* = ct^*$ . All recharge slices to the slope have moved as far as point  $x^*$  during the accumulated time period  $t^*$ . Downslope of  $x^*$ , the groundwater table runs parallel to the slope rises parallel to the slope.

A solution method for the kinematic-wave equation, known as the “method of characteristics”, was used by Tischer (1986) as a means of modeling 2-D groundwater responses during simulated rainfall tests. In essence, this method provides a Lagrangian

The thickness of each slice is equal to the input of water,  $i$  for that interval

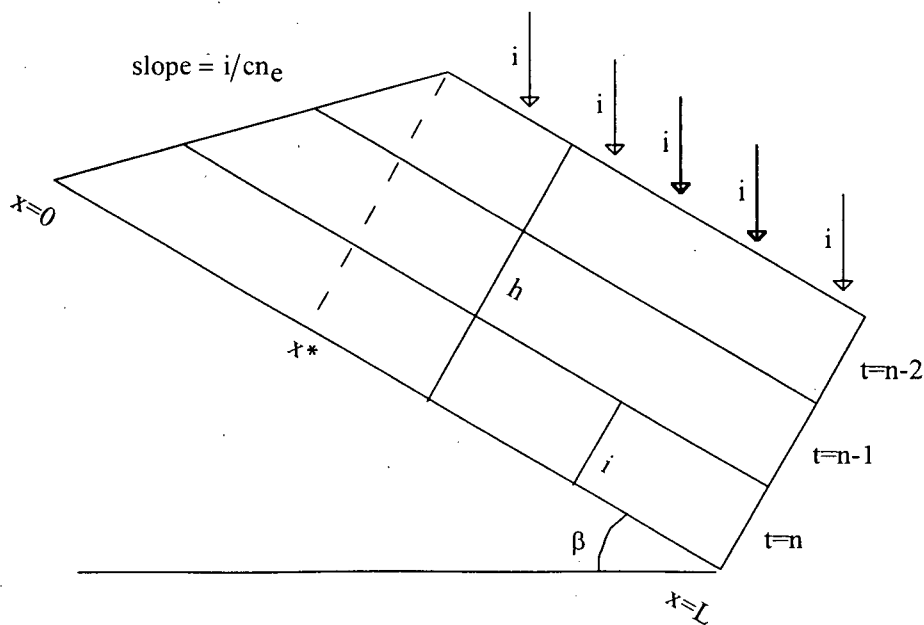


Figure 2.5 Representation of the groundwater configuration as a series of slices

solution for Eqn. 2.4 for “observers” moving downslope with flow celerity  $c$ . This reduces a partial differential equation to an ordinary differential equation allowing a variables separable solution to  $h=f(t)$  at various points on the slope. Jackson and Cundy (1992) also used the kinematic-wave equation as the basis for 3-D groundwater modeling during actual storms. These field-based studies showed that kinematic-wave equations can be effectively used to model transient groundwater flow.

Examination of groundwater time series in several of the studies mentioned above shows that water level response typically occurs within 6 hours of the occurrence of periods of heavy rainfall. The rate and magnitude of rise in a piezometer has be related to both the rainfall intensity and the effective porosity of the soil (Jackson and Cundy 1992, Haneberg 1991, Okimura 1982). Given that the term  $\delta h/\delta x$  is of the order of 0.01 or less for typical hillslopes, and  $K_{sat}$  is on the order of  $10^{-3}$ - $10^{-4}$  m/s, Eqn. 2.5 can be reduced to the total differential form shown in Eqn. 2.6. This equation defines the relationship between groundwater table rise at a point, the rainfall intensity,  $i$ , and the effective porosity,  $n_e$ . The underlying assumption is that all available water infiltrates and contributes directly to groundwater recharge. Eqn. 2.6 was found by Jackson and Cundy (1992) to work for planar slopes, but in complex topography provided only an approximation to water table change because of flow convergence and divergence.

$$\frac{dh}{dt} = \frac{i}{n_e} \quad (\text{Eqn. 2.6})$$

## 2.4 The groundwater-landslide relation

Studies examining the linkage between groundwater and landsliding can be divided into two general groups. The first group uses detailed analysis of the forces involved in failure to back-calculate the groundwater configuration at failure for a particular site. The second group makes use of actual measurements of pore pressure at the time of known failure using sites at or near the landslide initiation zone. Of these two groups, the bulk of the literature falls into the first group. Discussion of the first group is brief here, since such studies do not offer any fundamentally new insights into the basic link between rainfall events and landsliding.

Back-calculation of groundwater conditions at failure can be done by re-arranging Eqn. 2.1 to solve for pore pressure,  $u$ , at  $F.S.=1.0$ . This requires that measurements, or reasonable approximations, be made for the values of other parameters in the equation. Buchanan (1990) used slope stability analysis to back calculate the critical groundwater table at nine headscarps in Whatcom County, Washington, as a check on modeled water table profiles. Other studies have quantified the critical pore pressure required to initiate failure on a given slope in the manner described above (Sidle, 1985; Keefer et. al. 1987). Drawbacks to these types of studies are that they tend to be site specific and have to make broad assumptions about soil properties to allow for back calculation of pore pressure.

The following two studies examined pore pressure changes directly prior to the occurrence of failure. Harp et. al. (1990) instrumented three hillslopes in Utah and California to monitor pore pressures and shear displacements during failure induced by irrigation of test plots. It was found that pore pressures increased following infiltration until 5 to 50 minutes prior to the initiation of failure, at which time a drop in pressure was

observed. This was explained by piping of fines and by the dilation of the soil mass in the initial stages of failure. The latter in particular would cause a transient increase in  $K$  because of dilation.

The second study was conducted by Okimura (1982) in the Mt. Rokko district of Japan. Here, the role of the rate of increase in the groundwater table on the incidence of failure was investigated using numerical simulation and a conceptual "tank" model. Under application of differing rates of groundwater rise, failure occurred at a similar peak groundwater level for all applied rates. It was also noted that the occurrence of failures was 2 to 3 hours after the attainment of the maximum rainfall rate. This finding agrees with reported observations of typical lag times for groundwater response by Haneberg (1991). The findings of Okimura and Harp are important because they illustrate the linkage between peak groundwater levels and the occurrence of landsliding.

#### **2.4 Summary of the links between rainfall, groundwater, and landsliding**

In this chapter the inter-relations between rainfall and landsliding, rainfall and groundwater, and groundwater and landsliding have been discussed. A summary of the key linkages is given in Table 2.6. The linkages between rainfall and landsliding are clear: the above discussion has shown that intensity-duration relationships may be of use in general predictions of slope instability periods so long as antecedent conditions are taken into consideration. This approach is best suited to area-wide warnings, and cannot claim to forecast failures on individual hillslopes. In the Pacific Northwest, where rain-on-snow processes are an important source of water input to the soil during many winter storms, there is a need for increased information on rainfall and snowpack characteristics

Table 2.6 Summary of important linkages between rainfall, groundwater, and landsliding

Linkage	Important relationships
A) Rainfall-landsliding	<ol style="list-style-type: none"> <li>1. Intensity-duration thresholds can be applied to warn of impending probable instability over areas where failure is a result of intense rainfall.</li> <li>2. Antecedent conditions are important in pre-conditioning a hillslope for failure and may result in destabilization of slopes under rainfall intensities lower than the threshold intensity.</li> </ol>
B) Rainfall-groundwater	<ol style="list-style-type: none"> <li>1. Groundwater table response to rainfall is rapid under conditions of high water input, and very small lag times are observed between rainfall and groundwater peaks.</li> <li>2. Under high water input rates, water can bypass the unsaturated zone through macropores and be delivered to the saturated layer at a rate greater than that of matrix flow.</li> </ol>
C) Groundwater-landsliding	<ol style="list-style-type: none"> <li>1. The onset of failure is closely associated with peaks in porewater pressure.</li> </ol>

during periods of slope instability.

The response of the groundwater system to rainfall is conditioned by a combination of soil and slope parameters, but is primarily a function of the input rate of water to the system. During the storm season, soils usually exist in a pre-wetted state due to antecedent rainfall. Under conditions of high water input to the soil, macropores permit bypassing of the unsaturated layer and thus deliver water rapidly to the base of the soil profile. This leads to the development of transient peaks in pore pressures that are documented to affect slope stability. However, macropores also accelerate downslope drainage of a soil mass, which must somewhat offset the more rapid recharge.

The linkage between peak groundwater and pore pressure levels and landsliding is predicted by conventional slope stability analysis in the Mohr-Coulomb equation. Field studies have substantiated the theoretical assumptions, and the limited observations of

pore pressure increase up to the time of failure show that these pressures are responsible for initiating instability.

## Chapter 3 Study Sites

### 3.1 Overview

The study area is located in Tsitika River basin, a 39,490-hectare area, on the eastern side of Vancouver Island (Figures 3.1,3.2). Elevation varies from sea level, at the basin outlet, to approximately 1700 m in some of the steeper sub-basins. Land use in Tsitika basin consists of logging, recreational fishing, and hunting in the winter. Logging is conducted by MacMillan Bloedel (Eve River Division) and Canadian Forest Products (Engelwood Logging Division). Access to most sections of the watershed is possible via two networks of logging roads maintained by these companies. In 1990, Tsitika basin was the site of a public protest due to proposed logging in the lower sections of the watershed. Killer-whale rubbing beaches exist near the basin outlet at Robson Bight, and the impact of sediment produced by forest harvesting upon the texture and gradation of rubbing beaches was not known. This resulted in a logging moratorium and the initiation of a geomorphic study program. The Tsitika has been the focus of a large body of research [see B.C.F.S. Technical Background, (1990) for more information]. Current geomorphological research under the supervision of Dr. Robert Hudson (B.C.F.S.) focuses upon temporal and spatial characteristics in sediment transport and their relationship to precipitation events.

### 3.2 Climate

The Tsitika basin is located in the drier hydrologic region of Vancouver Island

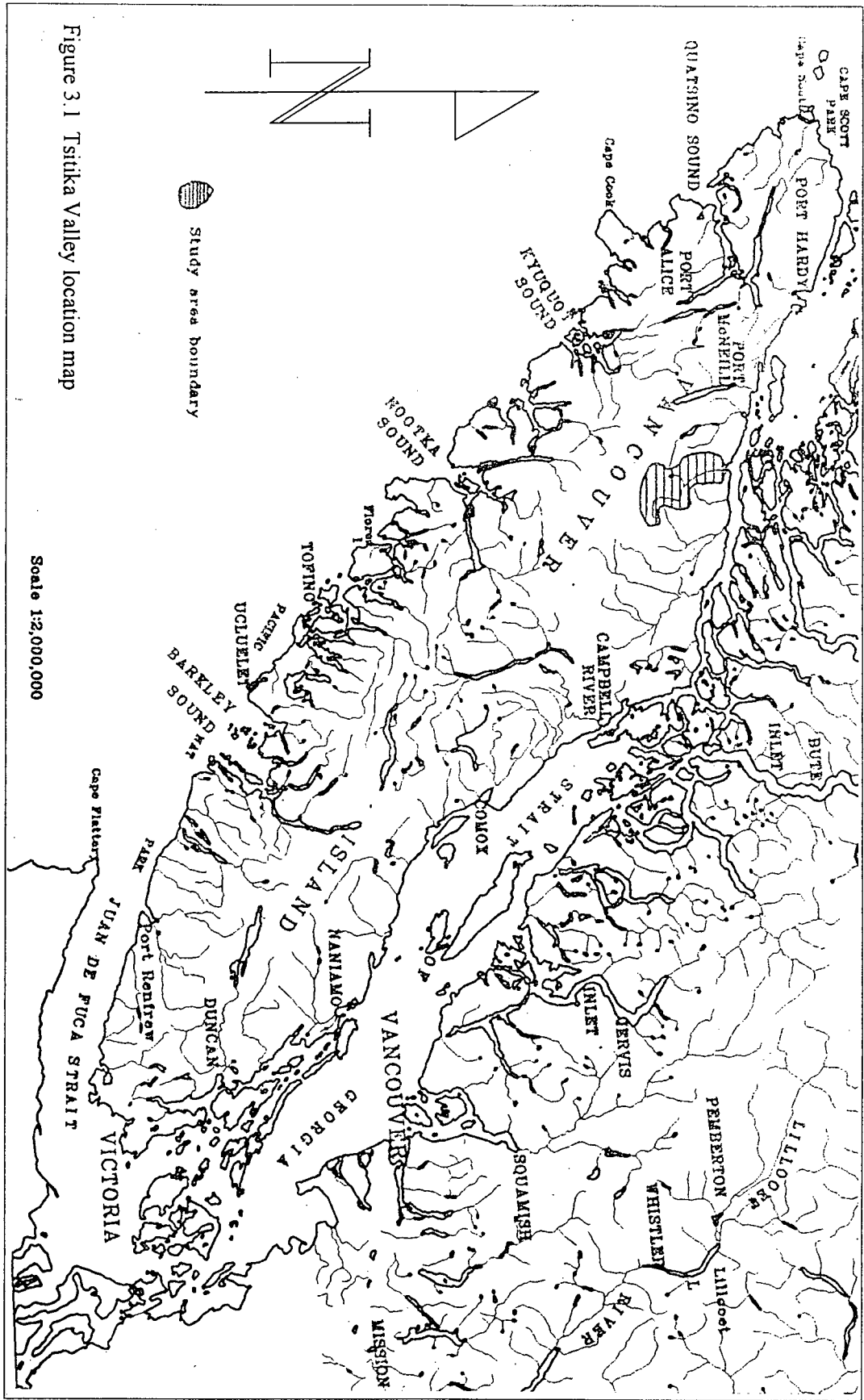
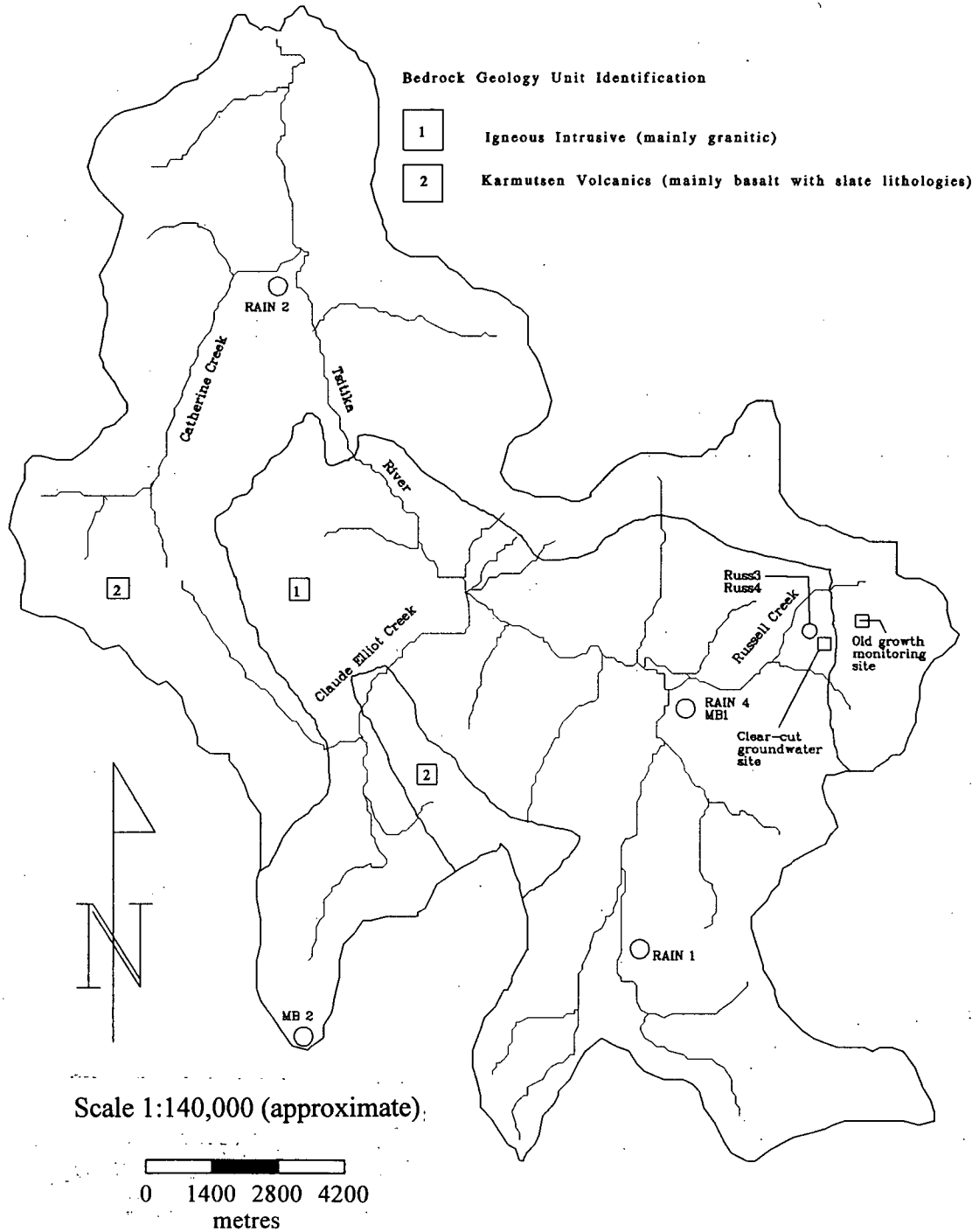


Figure 3.1 Tsitika Valley location map



Scale 1:140,000 (approximate)

Figure 3.2 Tsitika basin map showing geology and monitoring site locations (geology taken from Sterling, 1997)

(Howes, 1981), and exhibits lower rainfall intensities than the west coast of the island. Tsitika basin receives approximately 2000 mm of total precipitation with much occurring as snow during the winter months. Precipitation is augmented by orographic lifting, especially when moist air masses approach from the east.

The snowpack in the Tsitika basin is transient during October, but by the middle to end of November there is usually a continuous cover at the higher elevations. During winter months the area below 750 m may have a transient snowpack. Given the maritime influence on weather systems, rain-on-snow events are common at the lower to middle elevations in winter.

### 3.3 Hydrology

The hydrologic regime for Tsitika basin could be described as “flashy”, which is typical of steep mountainous systems. Low flows ranging from 0.8 to 4.0 m<sup>3</sup>/s typically occur in August or September, while peak flows ranging from 140 to 620 m<sup>3</sup>/s occur from October to January (Karanka, 1990). Following major rain-on-snow storms, stage in the main channel may increase by several metres within 24 hours, demonstrating the rapid response of the system.

Tsitika basin comprises 16 sub-basins listed in Table 3.1. Within each sub-basin there are a number of major tributaries and countless small gullies that drain individual hillslopes. At the hillslope scale, response in small drainages is rapid with peak flows occurring within twelve hours precipitation peaks. Nistor (1996) found that peak flows in two small streams monitored in the Russell Creek basin occurred during winter rain-on-snow storms. Most of the small drainages have no surface flow during the late summer

Table 3.1 Tsitika watershed sub-basins (from Hogan and Chatwin, unpublished.)

Basin I.D.	Stream order	Total area (km <sup>2</sup> )	Area of sub-basin >250m and <750m	Area >750m (km <sup>2</sup> )	Mean slope (°)
1	5	11.45	6.3	4.65	25
2 Catherine Cr.	3	48.75	29.25	18.55	28
3	4	18.1	14.16	3.55	31
4	3	18.19	6.41	3.43	29
5 Derby Cr.	3	3.64	2.94	0.75	35
6	3	1.35	0.72	0.56	36
7	3	8.6	4.99	3.46	28
8	3	2.25	1.67	0.53	33
9	3	2.97	1.88	1.05	38
10 Claude Elliot Cr.	3	58.96	28.4	30.55	29
11	4	7.15	5.44	1.7	28
12	3	18.64	8.03	2.6	28
13 Akan Cr.	4	20.89	10.48	10.26	28
14 Russell Cr.	4	29.08	16.12	12.95	24
15	3	19.45	5.78	13.6	28
16	3	15.64	9.94	5.7	19
Tsitika River		400	164 (41 %)	204 (51 %)	27.7

and remain that way until the first winter storms in September or October. In the sub-basins of the Tsitika River the annual peak flow may be the result of rain-on-snow events, such as occurred in 1992 and 1993, when the peak flows on Russell Creek occurred on October 23rd and December 4th respectively.

### 3.4 Bedrock Geology

Bedrock in Tsitika basin consists of the "Island Intrusives" and the Karmutsen Formation (Figure 3.2). The Island Intrusives, consisting of quartz diorite, quartz monzonite and granodiorite, are of Jurassic age. The older Karmutsen Formation is a series of basaltic lava flows, pillow lava, limestone and breccia formed in the Upper

Triassic. Pillow lava and columnar basalt are the most frequently encountered Karmutsen rocks in Tsitika basin. Figure 3.2 shows the approximate boundaries between the two main bedrock types. Island Intrusives outcrop in the upper parts of the watershed. Mountains formed in the Karmutsen Formation have high relief and are subject to rockfall and avalanching, while the Island Intrusives tend to form more rounded, lower relief hills (Figures. 3.3, 3.4).

### **3.5 Quaternary Geologic Setting**

Tsitika basin has experienced multiple glaciations including the Fraser Glaciation (Howes, 1981). Several tributary hanging valleys enter the trunk valley in the central portion of the watershed. During the Fraser Glaciation, valley glaciers merged in the main valley before flowing northward toward Johnstone Strait. Glacial and de-glacial sediments were identified by Maynard (1991) as having originated in the upper portions of the watershed where glaciers eroded the coarse-grained granitic materials. Ablation and basal tills deposited during the last glaciation mantle most slopes in the basin and have a predominantly sandy texture. Clastic material of igneous origin found within the basal till represents approximately 10-20% of the till matrix. Ablation till has a similar component of clastic material, but clasts of both igneous and basaltic material are present. Colluvial soils derived from granitic bedrock have a sandy matrix containing large blocks. Soils derived from volcanic bedrock may have a more silty matrix depending on the activity levels of rockfall on the hillslope.

Detailed study of the basin by Maynard (1991) showed the importance of rockfall on the soil matrix of some slopes. Rockfall from pillow lava outcrops has been an active



Figure 3.3 Typical Karmutsen Formation mountain form



Figure 3.4 Typical island intrusive mountain form

process since deglaciation of the valley. Where rockfall layers are close to the surface, large voids are common. In the soil profile, this void layer is 30 - 40 cm in thickness and is found buried under an organic layer 10 cm - 20 cm thick. The large void spaces allow water to drain rapidly off the slope when the water table reaches the level of the voids.

### 3.6 Basin morphometry

The watershed was divided into 16 sub-basins of stream order 3 which branch off the main channel (Hogan and Chatwin, unpublished). Table 3.1 shows the sub-basin areas as well as the percentage of each sub-basin within the 250 - 750 m elevation band.

Morphometrically, the sub-basins may be divided into two types: large, broad, upper sub-basins (e.g. Russell Cr.), and small, narrow sub-basins (e.g. Derby Cr.) in the lower sections of the watershed. The average slope angle of the 16 sub-basins is  $28^{\circ}$  due to the basaltic cliffs present in most drainages. From Table 3.1 it can be seen that approximately 40% of the watershed is within the rain-on-snow zone mentioned in Chapter 2.

### 3.7 Vegetation

Tsitika Valley lies within the Coastal Western Hemlock and Mountain Hemlock biogeoclimatic zones (Meidinger and Pojar, 1991). Dominant tree species include western hemlock (*Tsuga heterophylla*), western red cedar (*Thuja plicata*), yellow cedar (*Chamaecyparis nootkatensis*), and Douglas fir (*Pseudotsuga menziesii*). In clear-cuts, shrub vegetation consists of a mix of blueberry (*Vaccinium spp.*), huckleberry (*Vaccinium spp.*), fireweed (*Epilobium angustifolium*), and seedlings of the typical coniferous species

listed above. In certain restricted areas of the Tsitika, lodgepole pine (*Pinus contorta*), red alder (*Alnus rubra*), and willow (*Salix spp.*) may be found.

### **3.8 Russell Creek sub-basin**

#### **3.8.1 Overview of Russell Creek sub-basin soils**

Russell Creek is a 30 km<sup>2</sup> sub-basin located in the southeast portion of tsitika basin (Figure 3.5). Geologically, the basin contains pillow lava and columnar basalt of the Karmutsen Formation at higher elevations and diorites and granodiorites of the Island Intrusives at lower elevations. The approximate boundaries between the two lithologies is shown in Figure 3.5. Soils range in thickness from 0.3m, on upper slope segments, to 2m in hollows and on the lower hillslope segments. Soil depths were determined by drilling, soil pits, and examination of road cuts.

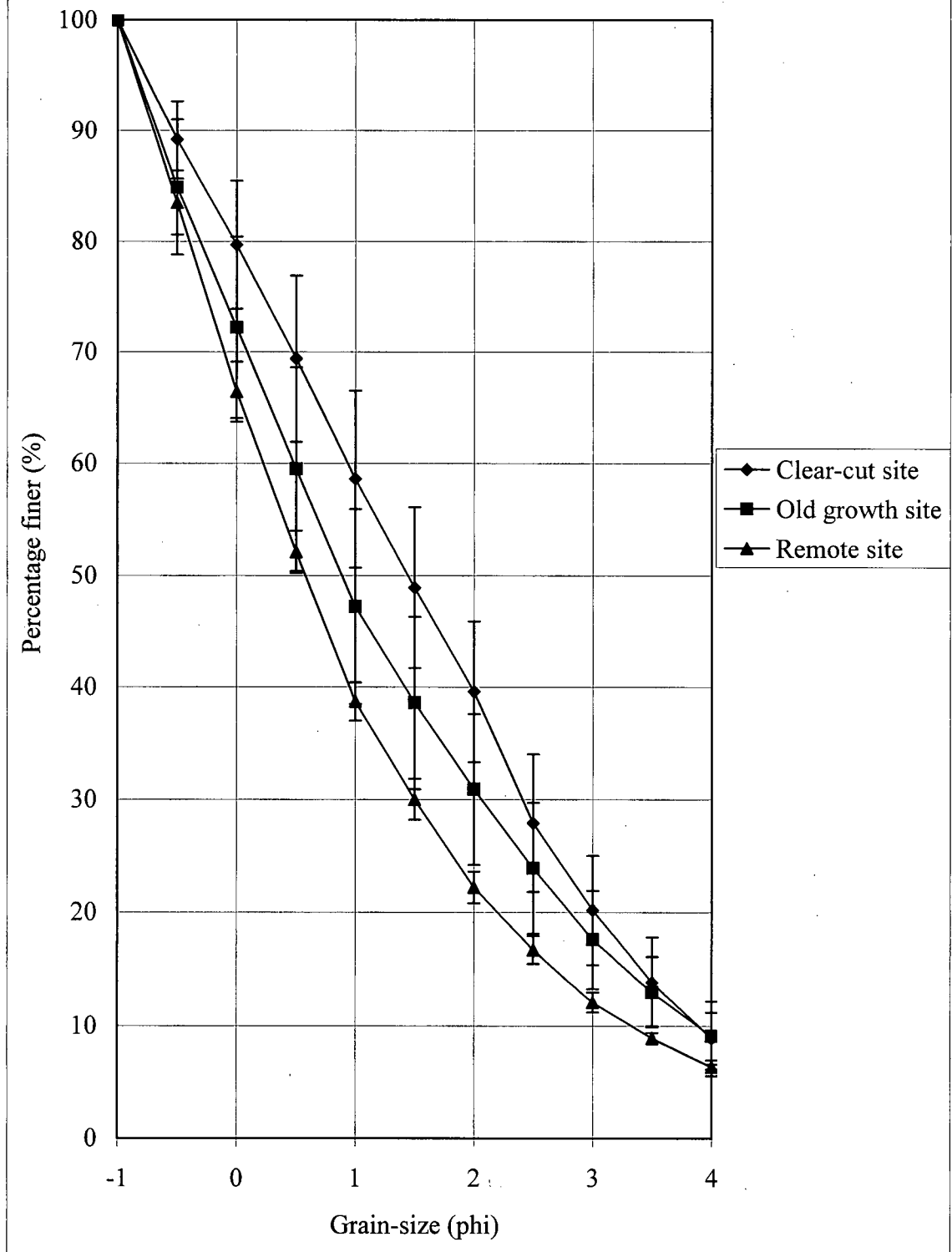
##### **3.8.1.1 Grain-size distribution of Russell Creek soils**

Average grain-size distribution curves for study area soils are shown in Figure 3.6. The error bars on the distribution curves represent  $\pm 1$  standard deviation. It is important to note that the number of samples from each of the three listed sites were not the same. The clear-cut distribution is based upon 11 samples, the old growth curve is based upon the 16 samples, and the remote site is based upon only three samples. Sieve analysis was done on the sand portion of the matrix. Summary results of the sediment analysis are contained in Appendix A.

The textural composition of soils was shown in Table 3.2. The soil had an overall sandy matrix with clay contents generally below 3% by weight. The soils were classified



Figure 3.6 Grain-size distribution summary curves for Russell Cr.



as sands based on their texture, although sample Shear3 was close to a sandy loam. The stone content (> 2 mm.) of the soils within the sub-basin ranged from 30-80%, by volume based on visual estimates from road cuts and soil pits. The clastic component tended to be greatest in the lower soil horizons. No Atterberg Limit tests were conducted on the soils because of the predominantly non-plastic nature of the soils.

Table 3.2 Textural summary of Russell Creek soils

Clear-cut site	% sand	% silt	% clay
CC1	93.9	5.1	1.0
CC2	94.8	4.5	0.7
CC3	89.7	8.6	1.7
Oldgrowth site	% sand	% silt	% clay
OG1	91.1	7.5	1.4
OG2	91.3	7.4	1.3
OG3	89.3	7.4	3.3
OG7	87.9	10.4	1.7

### 3.8.1.2 Soil profiles from pits and road cuts

To gain understanding on the nature of Russell Creek soils, four pits were excavated at each of the groundwater monitoring sites. Supplemental information on soils covering a wider area of the basin was obtained from examination of soils exposed by road cuts near the two monitoring sites. The profiles from the soil pits are shown schematically in Figures 3.7 to 3.14.

The soil stratigraphy at the clear-cut monitoring site, as determined by soil pits, is as follows: a surface debris and litter layer that varies from 0.1-0.4 m. in thickness, an Ah layer 0.4-0.7m. thick, and a Bm layer 0.6-0.7 m. thick. A black charcoal layer was present at the base of the Ah layer in all pits which is evidence of a forest fire on this hillslope at some time. Roots observed in the soil pits were primarily, though not exclusively, found in the Ah horizon. Macropores examined in the soil horizons were

Figure 3.7 Soil Profile for Pit CC1

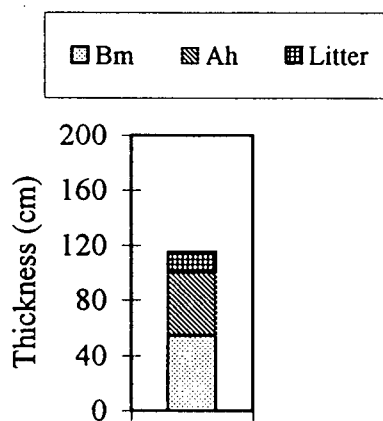


Figure 3.8 Soil Profile for Pit CC2

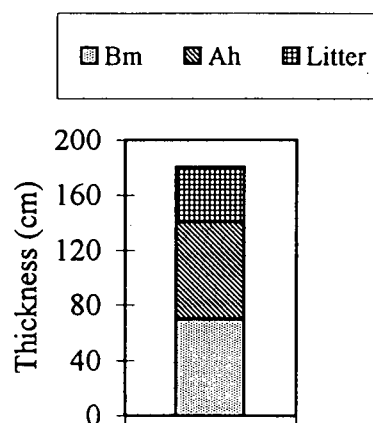


Figure 3.9 Soil Profile for Pit CC3

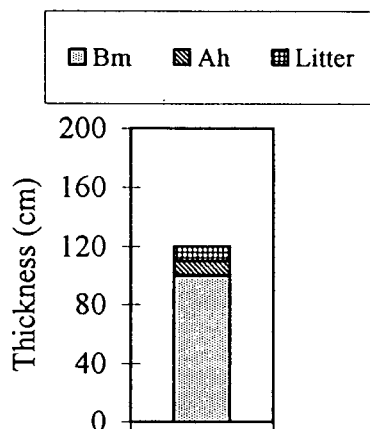


Figure 3.10 Soil Profile for Pit CC4

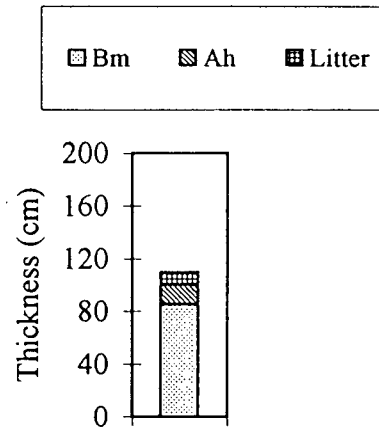


Figure 3.12 Soil Profile for Pit OG2

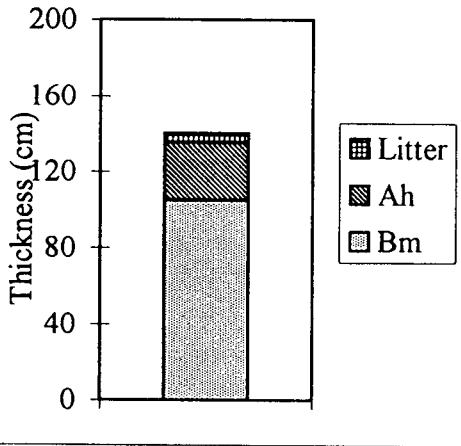


Figure 3.11 Soil Profile for Pit OG1

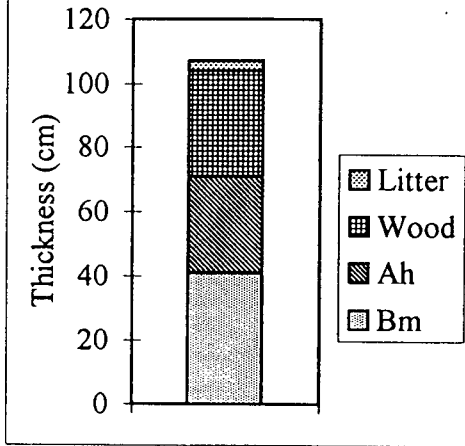


Figure 3.13 Soil Profile for Pit OG3

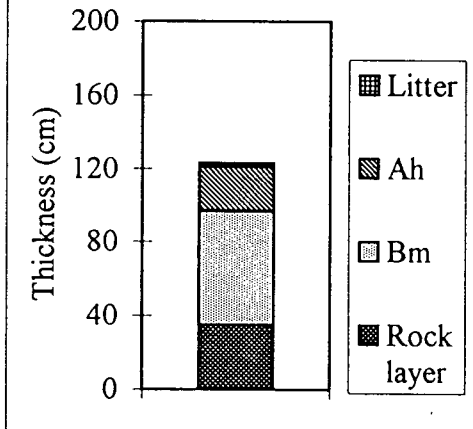
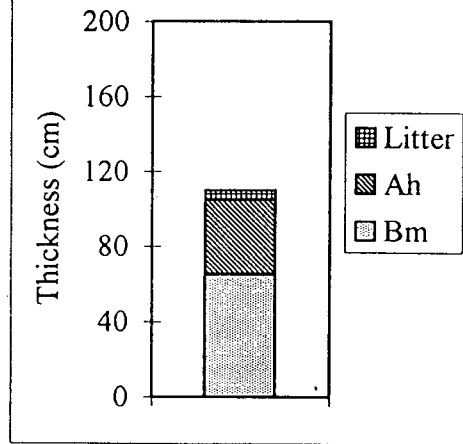


Figure 3.14 Soil Profile for Pit OG4



distributed apparently at random throughout the entire soil profile at this site.

The soil stratigraphy for the old-growth soils, based on soil pit examination, is as follows: 0.02-0.1 m. litter layer, a 0.2-0.4 m Ah horizon, and a 0.6-1.0 m Bm horizon. Large voids are found in the upper portions of the soil profile where large clasts interlock without a soil matrix. Macropores derived from organic materials and micro-organisms are distributed throughout the soil profile. Clastic material tends to be pre-dominantly basaltic in origin. A buried rockfall layer, excavated near the base of the Bm horizon, (Figure 3.13 Pit OG3) contained open voids due to bridging of clasts. During periods following precipitation, seepage was observed from this layer.

Figure 3.15 shows a roadcut from below the clear-cut monitoring site. The distance between pins 30 and 32 in the photo was 44.5 cm and the total soil thickness is 90 cm in this profile. Macropores formed from decayed roots are visible as dark brown patches contained within the soil matrix. In this profile it is evident that there is a large concentration of macropores near the soil/till interface. The diameters of macropores in this profile ranged from 2 mm to a maximum of 30 mm.

The soil profile in Figure 3.16 was taken from a roadcut below the old growth monitoring site. The distance between pins 30 and 31 in this photograph was 19.5 cm with the total soil thickness equaling 55 cm. The upper layer of the soil contains many roots and was looser than the lower soil layer (based on ease of insertion of pins into the soil). There appears to be a seepage band between the two soil horizons just above pins 30 and 31 that probably reflects a difference in the porosity of the layers.

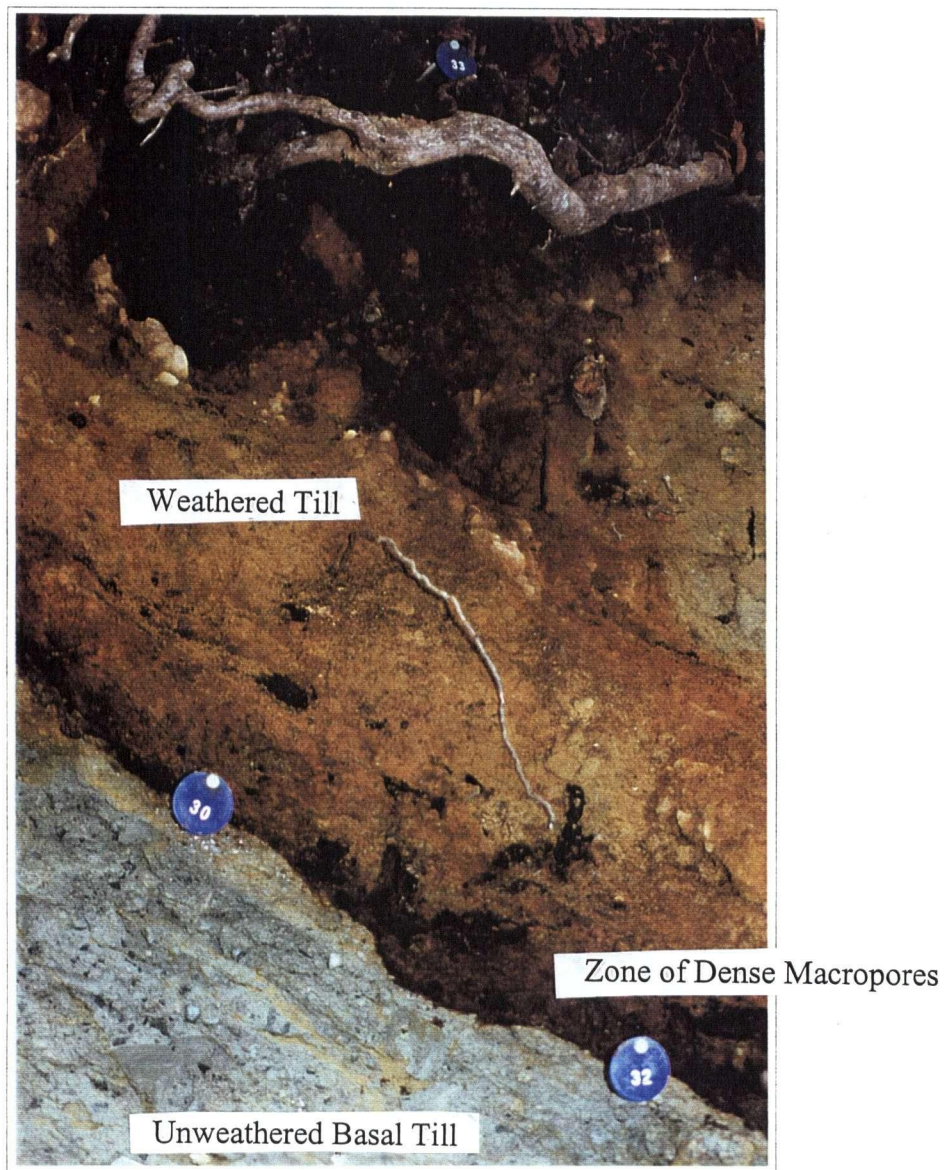


Figure 3.15 Road-cut into soils near the clear-cut monitoring site



Figure 3.16 Road-cut into soils near the old growth monitoring site

### **3.8.1.3 Clay content of study area soils**

The results of clay content determinations is shown in Table 3.2. The average clay content of samples from the clear-cut site was 1.1%, while the old-growth soil samples averaged 2.0%. These averages are based on few measurements of the clay content which varies over short distances and thus may not be representative of other soils in the wider Tsitika basin. The low values suggest that clay content does not significantly influence groundwater conditions in the sandy soils of Russell Creek basin (It should be noted that in some of the sub-basins close to Catherine Creek (Figure 3.2) there are deposits of glacial lacustrine sediments that have much higher silt and clay contents than those listed in Table 3.2).

### **3.8.1.4 Soil porosity determination**

Porosity of the clear-cut and old-growth soils was determined from constant volume samples taken from the Bm Horizon of the soil pits. Table 3.3 shows the final results of the porosity determination. From the samples analyzed, the clear-cut site has a lower average porosity of 0.47, although, the averages of both sites are within one standard deviation of each other. The average porosity values in Table 3.3 are above those of a coarse sand, 0.4, which is probably a result of either, or both, of two factors. First, during excavation of the constant volume samples, some disturbance may have occurred causing internal fragmentation. Second, the activities of micro-organisms and roots effectively increased the porosity of the sample above the value for a coarse sand.

Table 3.3 Soil porosity at the monitoring sites

Sample #	Clear-cut site	Old growth site
1	0.57	0.50
2	0.47	0.52
3	0.58	0.41
4	0.42	0.43
Average	0.51	0.47
Std. deviation	0.08	0.05

### 3.8.2 Clear-cut study site

The location of the clear-cut groundwater monitoring site within Russell Creek is shown in Figure 3.17 (see Figure 3.5 for location). The hillslope is segmented by logging spur roads that run both above and below the monitoring site effectively serving as drainage divides for the lower slope sections. The angle of this hillslope varies from 25°-30° with the steeper section occurring in the middle segments of the slope. The site is at an elevation of 650 m and has a northwesterly aspect (Figure 3.17). Logging of the instrumented section of slope was conducted in 1987 by MacMillan Bloedel. Several open slope failures have occurred on the study slope since logging was completed. These failures are thought to have been associated with the November 1990 rain storms that caused widespread slope instability in coastal British Columbia.

The site is located within the Island Intrusives but is within 200 m of the Karmutsen Formation boundary. Basaltic pillows found during excavation of soil pits at this site suggest that the soil is derived from ablation till deposited by retreating glaciers. Soil thicknesses on this hillslope average 1.3 m in depth.

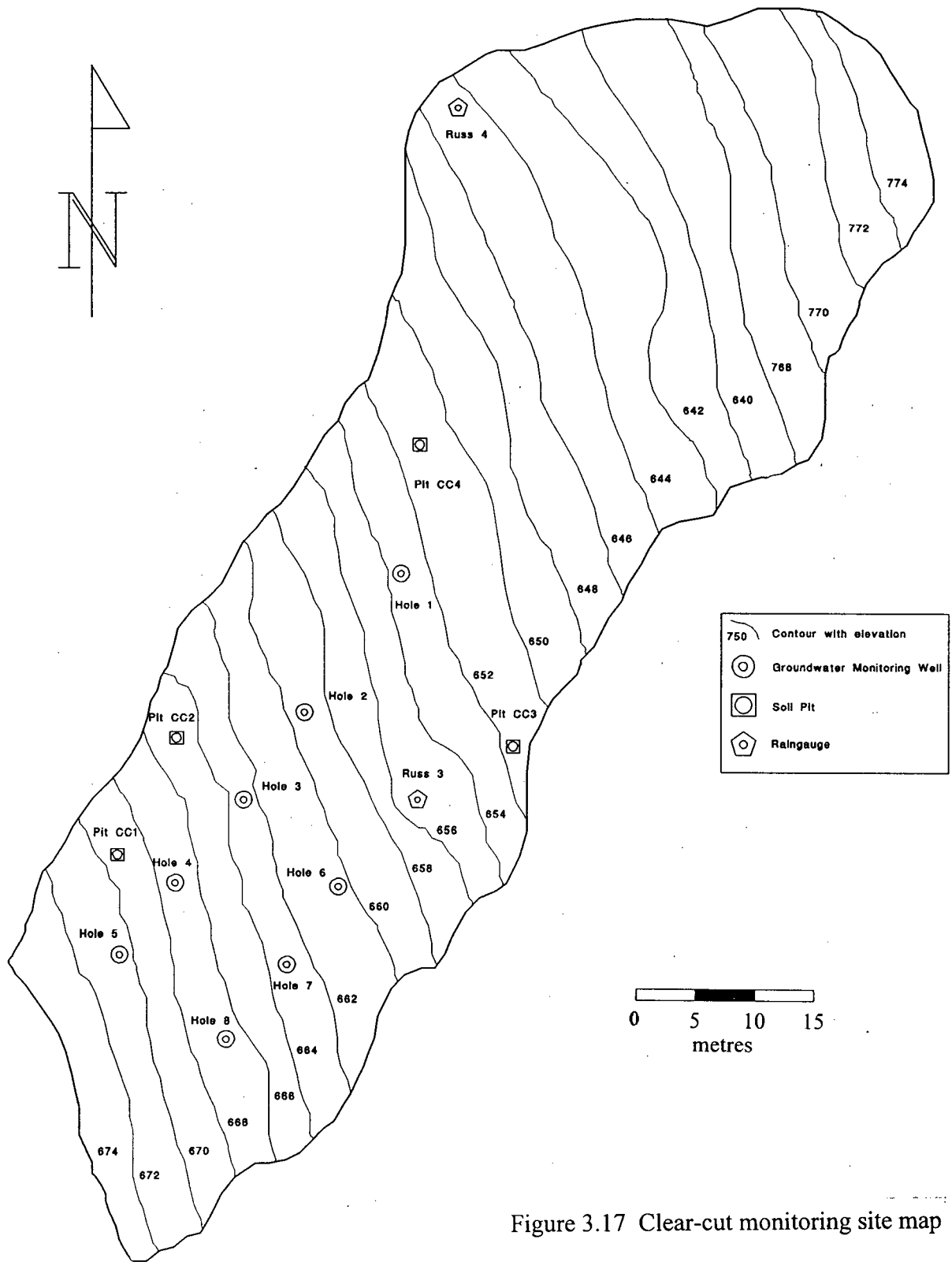


Figure 3.17 Clear-cut monitoring site map

### **3.8.3 Old-growth study site**

The old-growth study site is located near a saddle feature in the upper portion of the Russell Creek sub-basin (see Figure 3.18). The site lies within the Karmutsen Formation which plays an important role in the texture of the soil on this hillslope. The site is situated at an elevation of 750 m. and has a north-northwesterly aspect (see Figure 3.18). Slope angles at this site average  $32^{\circ}$  with some sections directly below large trees having angles up to  $36^{\circ}$ .

Based upon map and air photo analysis, the hillslope extends to an elevation of approximately 1000 m. with numerous rock bluffs. Bluffs of pillow lava are found 65 m. and 92 m. upslope of the monitoring site. The uppermost bluff is approximately 15 m. in height and cuts off ground access to higher sections of the hillslope. It is not known what impact these bluffs have on the hydrology of the monitoring site. Soil thicknesses at the study site average 1.2 m. in thickness and groundwater is present most months of the year due to discharge from upslope.

## **3.9 Field instrumentation**

### **3.9.1 Rain gauges**

Rainfall data were collected using a network of 1.0 mm resolution Sierra Misco tipping bucket rain gauges connected to Unidata portable data loggers. Figure 3.2 showed the location of the rain gauges in the watershed. The rain gauge elevations and slope aspects are listed below in Table 3.4. The array of stations located near the test site in

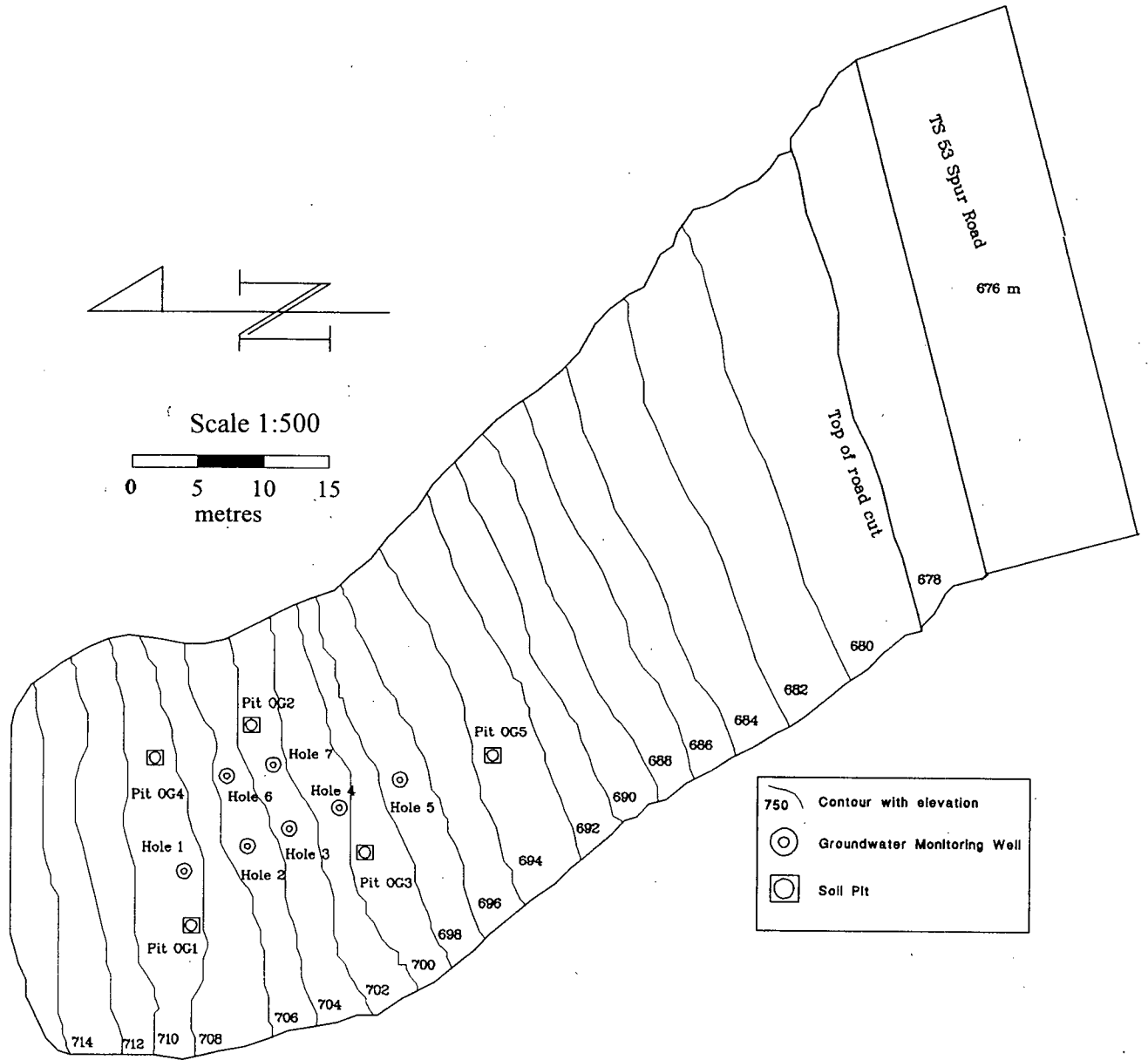


Figure 3.18 Old growth monitoring site map

Table 3.4 Locations and elevations of rain gauges

Guage ID	Location	Elevation (m)
Rain1	Russell Creek outlet	400
Rain2	Catherine Creek outlet	200
Russ2	Below road TS120	560
Russ3	Above road TS120C	630
Russ4	Above road TS120C	650
MB1	On spur road M366	440

Russell Creek was intended to give good resolution of the spatial distribution of precipitation near the groundwater monitoring sites. Each rain gauge site was equipped with a thermistor to measure air temperature. Other gauges in Tsitika basin provided rainfall data over a wider area beyond the two instrumented slopes to provide regional precipitation estimates should slope failures occur elsewhere in Tsitika basin. The last station listed in Table 3.4 was operated by MacMillan Bloedel. The data at this site are daily totals based on 1200h daily measurements.

### 3.9.2 Groundwater installations

Groundwater wells were hand augered using a 3.5" continuous flight auger. Figure 3.19 shows a schematic view of a typical groundwater installation. Three slots were cut in the 2" ID ABS pipe at a spacing 5 cm to allow water to enter the pipe. A fine gravel and sand backfill was used around the pipe to provide a fill with greater hydraulic conductivity than that of the soil matrix. If the conductivity of the fill were less than the conductivity of the soil, there would be a hydrostatic lag between the occurrence of groundwater fluctuations and their recording within the pipe (Hvorslev, 1951). End caps were placed on the bottom of the pipes to prevent intrusion of matrix fines.

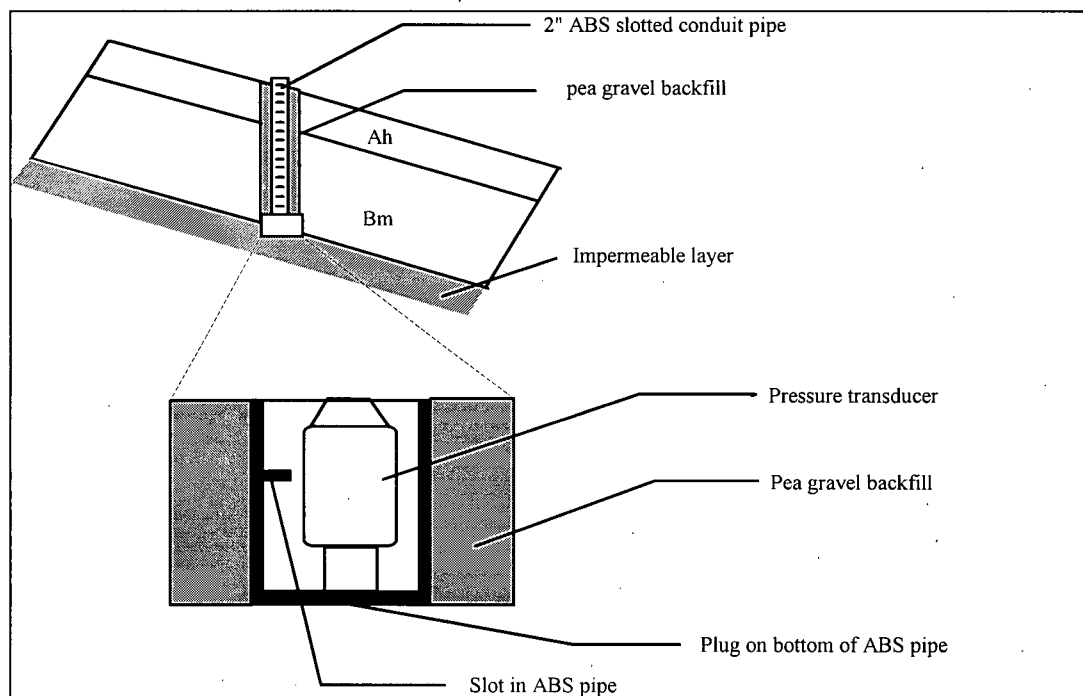


Figure 3.19 Schematic drawing of a groundwater well.

### 3.9.3 Data loggers

Two different types of data loggers were used during the study. The groundwater monitoring sites were instrumented with Campbell Scientific CR-10 data loggers with SM192 storage modules. The data loggers were programmed to record groundwater levels on a 15 minute interval. Information on the storage modules was downloaded during field visits to a laptop computer.

The tipping bucket rainfall sites were connected to Unidata 6004 data loggers. These data loggers were programmed to record data on a 15 minute interval. The information stored on the data logger was downloaded during field visits directly to a laptop computer using a RS-232 interface cable. The Unidata data loggers were found to be ideal for rainfall monitoring sites due lower costs as compared with the Campbell scientific data loggers.

## Chapter 4 Methods of analysis

This chapter contains analysis of the available rainfall and groundwater time series. Analysis first focuses on the rainfall data and examines characteristics of individual storms observed over the study period. This is followed by an analysis of the groundwater time series and its relations with the rainfall record.

### 4.1 Rainfall records

The goal of this analysis is to provide insight into the questions below:

1. How frequent are large rainstorms and rain-on-snow storms?
2. How do rainstorms causing failure compare with other observed storms?
3. How important are conditions such as antecedent rainfall and rain-on-snow for the storms that trigger instability?
5. Can a rainfall intensity-duration approach be applied to the occurrence of slope failures in the study area?

Establishing a link between rainfall levels and slope instability events requires reliable records of rainfall close to landslide initiation sites. Many studies published to date do not meet this basic requirement. The record at each rain gauge must be examined for errors such as undercatch and if possible corrected using relations with adjacent stations. Examination of station records for errors is compounded by several factors in Tsitika basin. The first factor is lack of a lengthy period of record which would permit rigorous consistency checks ( Most of the stations had been in existence for only for 1 or 2 years at the time of the study). The second factor is that most rain gauge records contain missing data. These gaps resulted from either overflow of the datalogger buffer, or

systematic failure of the station, such as battery failure, frozen tipping bucket, or frozen delivery funnel.

To account for different patterns of rain and snowfall, individual storm events were first separated into “warm”, “mixed” and “cold” types using the criteria in Table 4.1. “Warm” events are storms during which the average air temperature was greater than 2 °C during the entire event. “Mixed” events involve fluctuations in the air temperature above and below 2 °C. “Cold” events have average air temperatures lower than 2 °C throughout the event. An average event temperature of 2 °C represents the value above which precipitation occurs primarily as rainfall (U.B.C. Watershed Model Manual, 1994).

Between 0 °C and 2 °C precipitation tends to be a mixture of rain and snow. At air temperatures below 0 °C all precipitation is assumed to occur as snowfall.

Table 4.1 Basis for separation of precipitation record into storm events

<u>Classification basis:</u>	
	1. temperature
<u>Classes</u>	<u>Criterion</u>
“Warm”	Average air temperature greater than 2 °C
“Mixed”	Average air temperature fluctuates above and below 2°C during storm
“Cold”	Average air temperature below 2 °C
	2. rainfall
<u>Classes</u>	<u>Criterion</u>
Large	24 hr rainfall exceeding 60 mm
Medium	24 hr rainfall between 20-60 mm
Small	24 hr rainfall less than 20 mm

The second criterion for precipitation event classification was the 24-hour intensity.

Table 4.1 shows the values used to define each class. These intensity values are the same

as those used by Loukas (1991) to analyze storms in Capilano Watershed, British Columbia. Only storms falling into the medium and large classes were subjected to further analysis, since regional literature suggests that the precipitation threshold for landsliding is well above 20 mm./day (Hogan and Schwab, 1991).

#### **4.1.1 Analysis of synoptic-scale characteristics of storms**

To determine synoptic similarities between storm types influencing the study area, surface weather maps were examined for the source of the air mass (maritime Arctic, maritime Polar, maritime Tropical), the type of atmospheric instability (single front, multiple fronts, occluded front, trough), the storm track, average pressure gradients, and the location of the quasi-stationary Arctic front. The synoptic maps were also used to determine whether prolonged periods of rainfall represented a single or multiple storm event, thereby allowing for the definition of the storm event duration.

#### **4.1.2 Analysis of averaged storm values**

The analysis of averaged storm values was based on rainfall, temperature, and storm duration from four rain gauges in the Tsitika network. Averaged storm values were used to determine the frequency of significant rainfall and rain-on-snow storms during the study period. Total rainfall catches in a given storm were examined for elevation trends using regression analysis. If a significant elevational trend was not found, a spatially averaged storm precipitation was obtained by taking the mean of the observed rainfall totals. If a significant elevation trend was detected, the average precipitation value at the median watershed elevation was determined from regression of rainfall against elevation.

Average storm temperature was also examined to determine if snowfall had occurred at higher elevations during periods of rainfall at the lower elevation gauges.

#### **4.1.3 Analysis of rainfall intensity and duration**

Rainfall intensity-duration analysis is a standard method for analyzing the severity of individual storms, and was used to determine if the storms with the potential to cause slope failures were representative of storms during which no slope failures were recorded. The second purpose was to see if a rainfall intensity-duration threshold for landsliding could be established over the study area to establish the representativeness of storms known to have caused slope failures, the intensity-duration of these storms were compared with storms having similar total rainfall amounts. Extreme rainfall intensities for durations of 1,3,6,12, and 24 hours were calculated from the Rainfall Frequency Atlas for Canada (1985). As described in the Rainfall Frequency Atlas for Canada (1985), a correction factor was used to adjust the mapped extreme value rainfall maps for use with partial-duration series. Since the number of rain gauges operating during any given storm was not constant, it was assumed that the most extreme rainfall recorded during each storm was representative of the maximum rainfall intensity for all points in the watershed. This assumption was based on an observation of the recorded maximum storm rainfalls at each of the operating rain gauges. The observed peak storm rainfall intensities during the study period were not specific to any one rain gauge. A storm was considered representative if other storms of similar magnitude had similar intensity rankings over the different storm durations examined.

The existence of a general rainfall threshold for the study area was more difficult to determine given that only three storms were observed to have caused failures during the study period. A decision was made to supplement the database on rainfall-landsliding by using values of rainfall from other studies conducted in the Pacific Northwest. Data in this analysis were gathered from published rainfall records for storms in terrain similar to that of Tsitika basin. The data were plotted to allow for the identification of a regional rainfall intensity-duration threshold.

#### **4.2 Groundwater analysis**

The goal of the groundwater analysis was to understand the response characteristics of the saturated zone to rainfall and snowmelt recharge. Of particular interest was modeling vertical changes in groundwater level over time for mid-slope locations. Given the variability in soil parameters over even small distances, interpretation of groundwater records was based on site-averaged values for both response magnitude and time lag. As noted in Chapter 2, variations in the horizontal thickness of the groundwater table on planar slopes is often on the order of  $10^{-2}$  m/m. If a consistent model for the characteristic response of the groundwater table to rainfall input could be developed then it could have the potential to be applicable at any point on the midslope segment.

Groundwater data are available at two sites over the period September 1993 to March 1994. Pressure transducer readings were taken every 15 minutes until January 17th, 1994 at 1700h, after which the sampling interval was changed to one hour due to the uncertainty in the scheduling of field trips for the remainder of the project. Groundwater pressures measured in wells were converted to an equivalent groundwater thickness,

measured orthogonal to the impermeable basal till boundary, relative to the total soil profile thickness. This ratio,  $m$ , is referred to hereafter as the relative saturation level of the soil. It approximates the pore-pressure ratio of conventional soil mechanics, defined by the ratio of groundwater pressure,  $u$ , to total vertical stress,  $\gamma z$ .

#### 4.2.1 Soil parameter determination

As the groundwater table response is controlled by several measurable or calculable parameters, the methods for determining these parameters is outlined. Parameters measured or calculated during this study include; clay-content, grain-size distribution, hydraulic conductivity, porosity, unit weight, and soil thickness. Some of these have already been presented. The method used for grain-size analysis distribution of soil samples is similar to that in Craig (1994). Samples were air dried and, prior to sieving, moisture and organic material samples were taken for correction of the retained sieve weights. Grain-size analysis used a one-half phi sieve increment. Plots of the grain-size distributions for the collected samples were discussed in Chapter 3.

The silt/clay component was examined with the Sedigraph 5100 x-ray diffraction machine. Analysis of samples for this study were done using the approved technique outlined in the users manual for the machine. Copies of the outline covering the procedure followed during analysis may be obtained by contacting the Department of Geography at U.B.C.

Water was determined from Eqn. 4.1. Small ( $\sim 50$  gm) samples taken from the main sample at the time of sieving were oven dried for 24 hours at  $105^\circ\text{C}$  to obtain  $W_{\text{dry}}$ .

Eqn. 4.2 can be re-arranged to solve for the weight of solids. The weight of the solids

may also be expressed as the volume of solids multiplied by the specific gravity of the solids and the unit weight of water as shown in Eqn. 4.3. Clastic fragments from the soil samples were gathered and using displacement theory specific gravity,  $G_s$ , of the material was determined to be 2.7. The last value to be determined for the sample is the volume occupied by the solids which may be obtained using Eqn. 4.4. Having determined  $V_s$  the porosity,  $n$ , of the sample is determined using the relation  $n = V_v / (V_v + V_s)$ . Since  $V_v + V_s = V_t$  was known, porosity could be calculated.

$$\text{Water content} = w = \frac{W_{\text{wet}} - W_{\text{dry}}}{W_{\text{dry}}} \quad (\text{Eqn. 4.1})$$

$$\text{Sample weight} = W_t = W_s + W_w = W_s(1 + w) \quad (\text{Eqn. 4.2})$$

$$\text{Weight solids} = W_s = \frac{W_t}{(1 + w)} = V_s \times G_s \times \gamma_w \quad (\text{Eqn. 4.3})$$

$$\text{Volume solids} = V_s = V_t - V_v = \frac{W_s}{(G_s)(\gamma_w)} \quad (\text{Eqn. 4.4})$$

The hydraulic conductivity of soils at the clear-cut site was determined by slug tests (Domenico and Schwartz, 1990). For each test, a 5 litre volume of water was poured into the groundwater well and the time decay of saturated zone thickness was recorded using a pressure transducer set to a 1 second scan rate until the water level dropped to pre-test levels. A total of 10 tests were conducted on 5 holes at the clear-cut site. Light rainfall had occurred on the two days prior to the testing. The general relationship describing the change in water level with time following injection of a slug of water into a piezometer is shown in Eqn. 4.5. When the initial conditions,  $h(t) = h_0$  at  $t = 0$ , are applied to Eqn. 4.5, then  $T_0$  is equal to  $t$  when the left hand side of Eqn. 4.5 is equal to 0.37.

$$\frac{h(t)}{h_0} = e^{-t/T_0} \quad (\text{Eqn. 4.5})$$

The hydraulic conductivity was determined from Eqn. 4.6. For each slug test, two values of  $L$ , the length of intake area, were used to provide a range of calculated  $K$  values. This was considered necessary since the method being applied was designed for piezometers and not for groundwater wells which are slotted the entire length of the pipe. Efforts were made to seal the pipe above the groundwater table prior to each test. The two values used were the initial water height in the groundwater well and the maximum level of groundwater in the well. It is important to note that Eqn. 4.6 incorporates the shape factor of the intake of the groundwater well and is considered valid so long as  $L/r$  is greater than 8, where  $r$  is the radius of the borehole.

$$K = \frac{r^2 \ln\left(\frac{2L}{r}\right)}{8LT_0} \quad (\text{Eqn. 4.6})$$

#### 4.2.2 Analysis of groundwater hydrograph

Over the period of record, 27 groundwater peaks and associated rainfall events, were recorded at the two groundwater sites. Of interest in this study are the five relations listed below:

1. The time lag between onset of rainfall and the start of groundwater response.
2. Groundwater response sensitivity to peak rainfall intensities.
3. Influence of antecedent conditions on #2.
4. Hydrologic memory of the study area soils to storm inputs, defined as the time for soil water levels to recover to pre-storm water values.

5. The importance of snowmelt during the individual storm events.

To explain the first four relations, the eight pieces of information listed in Table 4.2 were recorded from each groundwater peak. The fifth point of interest is discussed in section 4.2.3 of this chapter.

Table 4.2 Variables used in groundwater analysis

- |  |
|--|
| <ol style="list-style-type: none"> <li>1) start time of rainfall</li> <li>2) time of maximum rainfall intensity</li> <li>3) maximum rainfall intensity</li> <li>4) average pre-storm relative saturation value, m.</li> <li>5) average start time of hydrograph rise</li> <li>6) maximum rate of groundwater rise</li> <li>7) time of groundwater peak</li> <li>8) recession characteristics of groundwater wells</li> </ol> |
|--|

Haneberg (1991), used Eqn. 4.8 as a method for calculating the maximum time lag,  $t_s$ , for the downward propagation of a pressure wave to the base of a soil layer. Comparison of predicted responses with the observed responses in several studies from Alaska, Ohio, and California revealed that the equation was capable of closely estimating the response times of the groundwater table.

$$t_s = \frac{n_e Z}{K} \quad (\text{Eqn. 4.8})$$

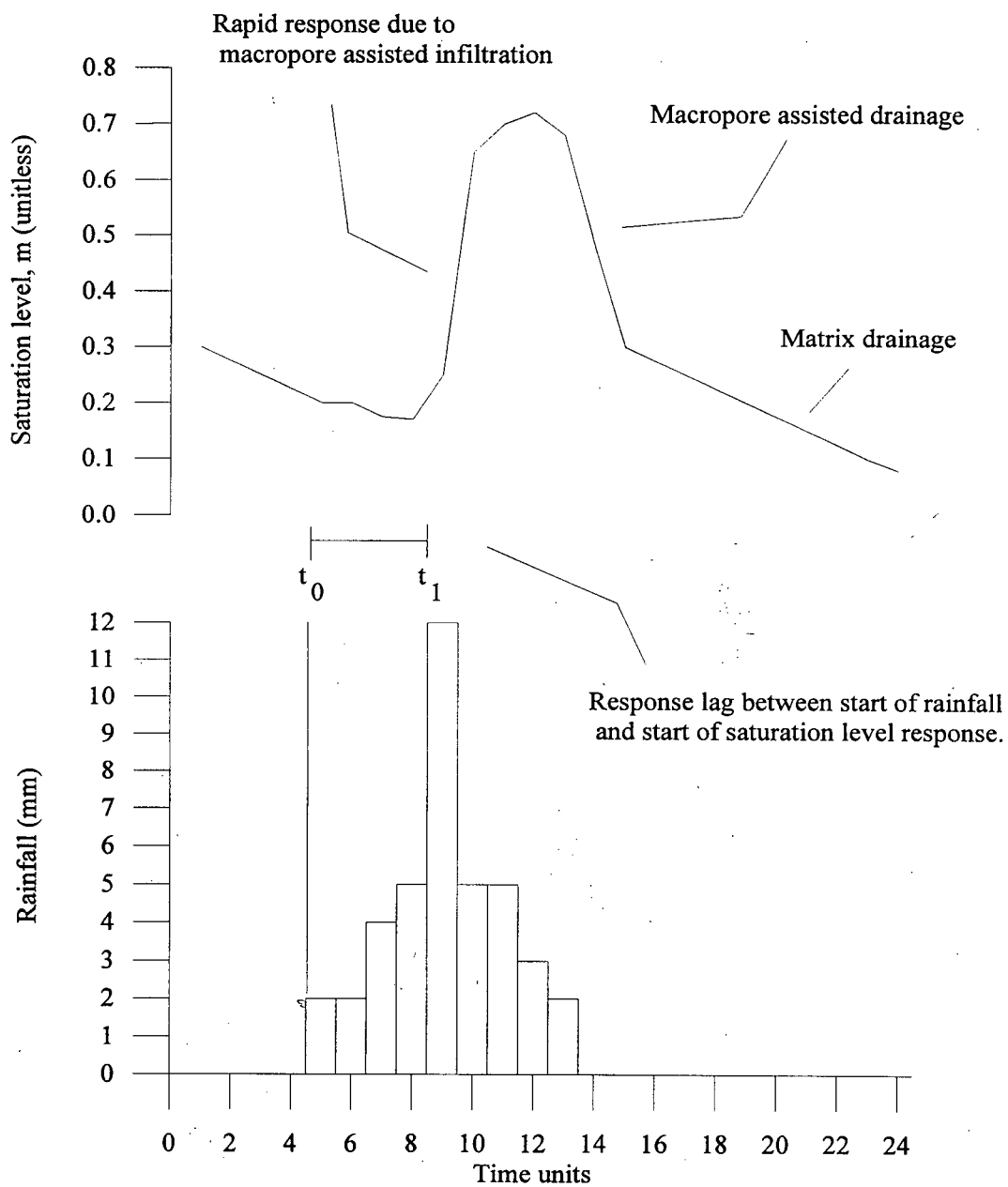
where  $z$  is depth to impermeable layer,  $n_e$  is effective porosity, and  $K$  is hydraulic conductivity

The relation between response lag (the time between the start of rainfall and the start of a rise in the groundwater table) is influenced by the saturation level and effective porosity of the soils prior to rainfall as well as the rainfall intensity (see Figure 4.1). If

the soil has had sufficient time to drain, the lag in start times  $\left(\frac{t_s}{2}\right)$  will tend to be longer unless the rate of water input to the system is great enough to trigger macropore assisted infiltration (see Figure 4.1). To determine the response sensitivity at a site, a lag correlation was sought between averaged groundwater responses and rainfall intensity. Regression was performed for durations of 1,3,6,12, and 24 hours, to determine which duration exerted the greatest influence on the groundwater hydrograph. The lag times between the maximum rainfall intensity and the maximum groundwater peak were then plotted against the average antecedent groundwater level. This allowed for graphical interpretation of the influence of antecedent moisture and rainfall intensities on the response of the groundwater system during a particular storm event.

To obtain estimates for the effective porosity of the soil, Eqn. 2.5 was re-arranged to solve for this term  $n_e = i * \frac{dh}{dt}$ . The assumptions of this method are that the time lag of the soil has a consistent relationship with antecedent moisture content, and that other influences such as interception and evaporation are not sufficiently variable between measurement periods to affect this relationship. Given that neither the ground cover nor the evaporative thermal regime exhibited notable changes over the period of groundwater measurement, these assumptions are considered reasonable. The first assumption allows the water input rate,  $i$ , to be determined, and then values for the effective porosity may be determined at several points during the rising limb of a storm hydrograph. Support for the second assumption is taken from Kimmins (1987), who estimates that interception during winter storms in humid environments is minimal due to saturation of the

Figure 4.1 Schematic diagram illustrating lag between precipitation and saturated zone response



interception storage capacity of the canopy and due to shaking of the vegetation by wind.

The recession rate of groundwater following a peak requires determination of the time over which antecedent rainfall conditions were important. Recession rates were determined by fitting a negative exponential curve to data recorded from boreholes that displayed non-flashy responses. The higher the recession rate of a soil, the more rapidly the soil would drain in the post-rainfall period, and therefore the less influence it would be able to exert on the rate or amount of groundwater rise during succeeding rainfall events. Figure 4.1 shows the two hydrograph phases common to coarse mountainous soils. The initial phases of rise and recession tend to be steep, attributed to macropore assisted drainage of the soil column. Eventually, as the saturation level decreases, drainage becomes matrix dominated and the recession phase becomes less steep. The length of the recession limb controls the hydrologic memory of the soil and hence the ability of antecedent conditions to influence future groundwater responses.

#### **4.2.3 Estimation of snowmelt and rain-on-snow inputs**

One unknown input to the groundwater hydrograph is meltwater produced by rain-on-snow events and thermal snowmelt. Rain-on-snow meltwater has already been shown to greatly influence the occurrence of landsliding during otherwise moderate storm events (Church and Miles, 1987). Due to the scant snowpack data available over the study period, it was necessary to estimate snowmelt input to groundwater at the Russell Creek monitoring sites. Estimates of daily snowmelt and rain-on-snow melt were obtained from the clear-cut slope,  $M_C$ , and forested slope,  $M_F$ , using the degree-day method from the U.B.C. Watershed Model (U.B.C. Watershed Model Manual v3.0, 1994). Equations 4.9 and 4.10 from the U.B.C. Watershed Model were used to calculate daily melt.

$$M_c = \left( T_{\max} + \frac{\left( T_{\min} + \frac{T_{\max} - T_{\min}}{1.0} \right)}{18 + \frac{T_{\max} - T_{\min}}{1.0}} \right) \times T_{\min} \times 5.0 \quad (\text{Eqn. 4.9})$$

$$M_f = \left( T_{\text{mean}} + \frac{\left( T_{\min} + \frac{T_{\max} - T_{\min}}{1.5} \right)}{18 + \frac{T_{\max} - T_{\min}}{1.5}} \right) \times \left( \frac{T_{\max} - T_{\min}}{1.5} + T_{\min} \right) \times 5.0 \quad (\text{Eqn. 4.10})$$

In addition, during periods of rainfall, Eqn. 4.11 was used to calculate the additional amount of melt resulting from rainfall alone.

$$\text{Rainmelt} = 0.0126 \times (T_{\text{mean}}) \times (\text{Rainfall}) \quad (\text{Eqn. 4.11})$$

The first term in Eqn. 4.9 and Eqn. 4.10 represents the temperature control on melt in open and forested areas. In open areas, melt is dependent on daily maximum air temperature, while in forested areas it has been found to depend more on the mean air temperature. The second term in Eqn. 4.9 and Eqn. 4.10 represents a partitioning of energy between snowmelt and sublimation. The factor of 1.5 in Eqn. 4.10 is used to simulate the reduction in daily temperature range by a forest canopy. Estimates of snowmelt obtained using these equations probably represent minimum values for snowmelt in open areas, since the effects of advective melt are ignored. During the study period only 12 checks of snow depth were conducted. Based on the limited first hand information on the snowpack and the importance of estimates of snowmelt during a particular storm, the use of these equations is justified.

## Chapter 5 Rainfall analysis

In this chapter I examine rainfall data collected over the 1992-1994 observation period. The first section describes rainfall conditions during October 1992 to October 1994. The second section contains the analytical results using the methods outlined in the previous chapter.

### 5.1 Overview of precipitation during the study period

This section contains a general synopsis of the weather conditions encountered during the study period. Figure 5.1 shows daily rainfall totals for rain gauges operating in the Tsitika network. Data from stations R1 and R2 start on 9/28/92. Russ2 and Russ3 gauges were established on 11/7/92, and data from gauge MB1 was available from 1/2/93 until 10/27/94. Figure 5.2 shows the average daily temperature, where available, for each of the rain gauges. While gaps exist in the data, at least one rain gauge was operating in the Russell Creek area during the entire study period. Gaps during the dry summer period are considered unimportant. The rain gauges are arranged according to elevation with the lowest rain gauge, R2, at the bottom and the highest rain gauge, Russ3, at the top (see Figure 3.2). Comparisons of the overlapping portions of the individual records shows that there is generally good agreement between stations during a given storm. This suggests that most of the storms influencing the study area are the result of frontal disturbances.

During winter 1992 there were two large storms during October and a two medium sized storms. Precipitation occurred at regular intervals until early January 1993,

Figure 5.1 Rainfall time series for the Tsitika basin

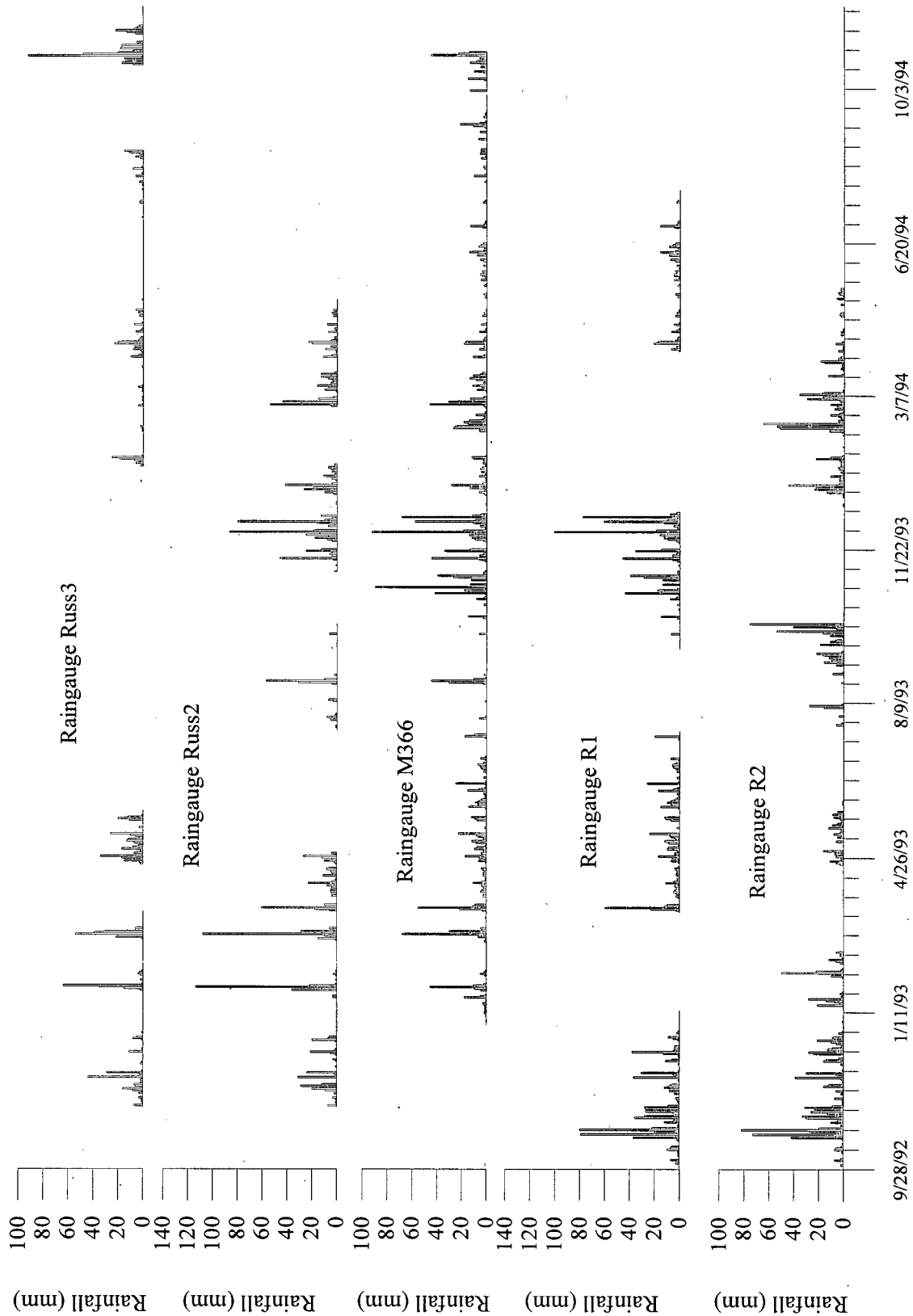
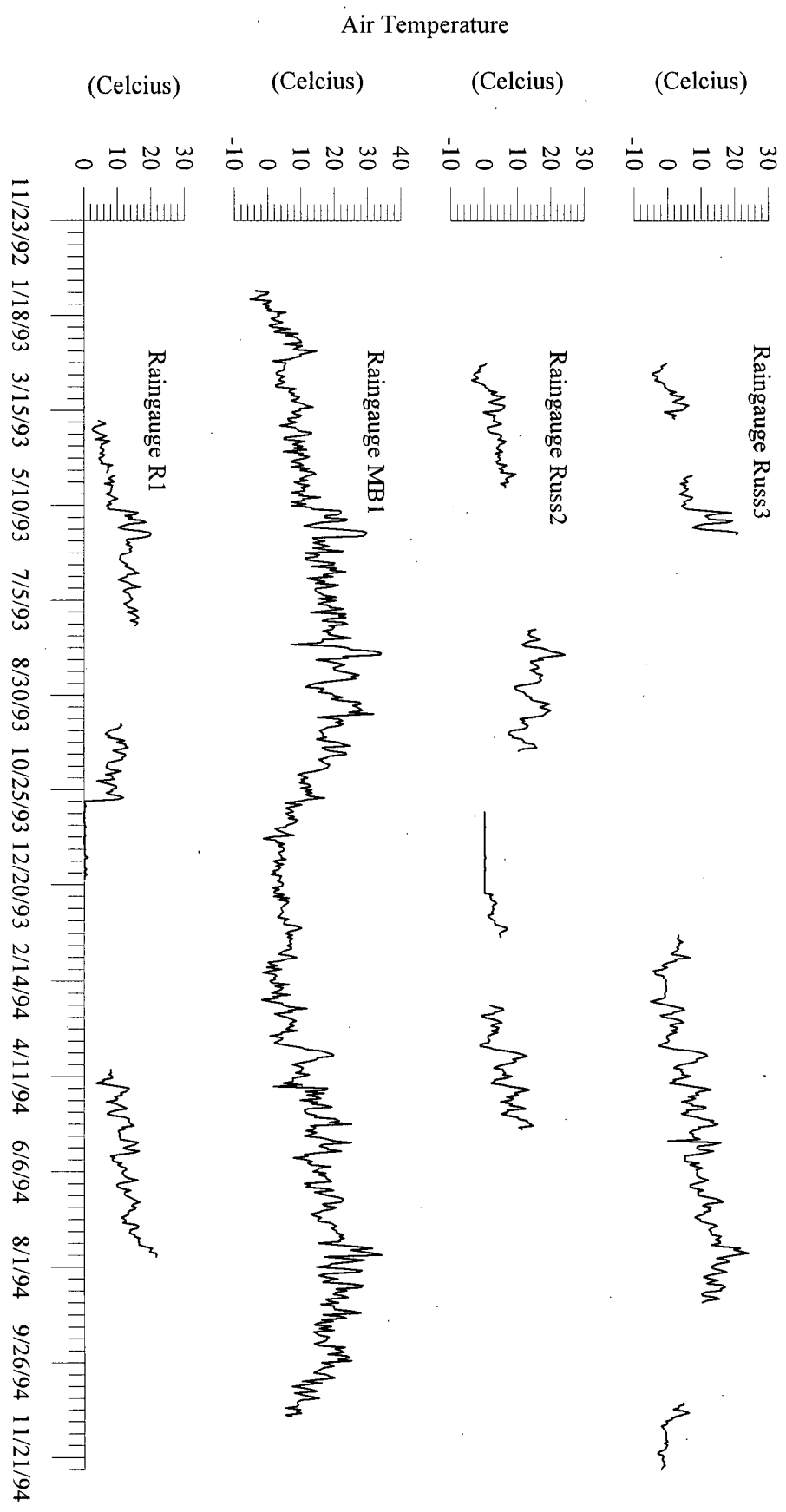


Figure 5.2 Temperature time series for the Tsitika basin



when a dry period of several weeks occurred. One major storm occurred in late January during which one failure is known to have been triggered in Russell Creek sub-basin. February 1993 was fairly dry in the Tsitika with only one large storm. March, April and May 1993 exhibited predominantly small rainstorms. Only one large storm occurred during the three month period. During this period, snowpack in the area was depleted. Summer 1993 featured little rainfall and only one large event during August. None of the events after January 1993 produced slope failures.

In late September 1993 there was considerable rainfall recorded at R2 while little was measured in the Russell Creek area. It is believed that small-scale convective, or orographically enhanced, precipitation was occurring in the lower portions of the watershed. October until mid-December 1993, featured almost daily rainfall in the watershed. During the first part of December three large storms deposited close to 300 mm. of rainfall on the valley. There was a dry period of approximately one week in December followed by another period of almost daily rainfall lasting until the end of January 1994. During this rainy period, much of the lower elevations of the watershed became snow-free and the snowpack in the Russell Creek sub-basin had thinned. A dry period of approximately two weeks at the beginning of February was followed by a almost daily rainfall lasting until the end of April 1994. During this period three failures are known to have been initiated in the Tsitika Valley as a result of storms at the end of February. The failures (two road related and one open slope) were located in the Upper Tsitika basin and in the Claude Elliot sub-basin not far from the instrumented slopes (see Figure 3.2). During the first part of this period snowpack increased in thickness and a

large storm at the beginning of March 1994 initiated three known failures in the Tsitika watershed.

During Summer 1994, the highest rainfall was in June with several small rainstorms occurring during the middle of the month. No subsequent slope failures occurred during this entire period of record.

The start of the third storm season was dry, with minimal precipitation occurring prior to October 20th, 1994. Continuous rainfall from this date occurred up to and for several days after a large October 25th storm that initiated a second slope failure in the Russell Creek basin. At the time of the failure a transient snowpack of approximately 30 cm. existed in the area but this was all melted during the storm. In the short period of record available from November 1994, there were several days of rain at the start of November followed by a two week dry period.

A summary of general weather conditions in Tsitika basin would be as follows. In fall there is almost daily rainfall in the valley with a number of large to medium rainstorms. The over-winter snowpack begins to establish itself towards the middle of November. The winter months feature a mixture of wet and dry periods during which the snowpack at higher elevations continues to accumulate while at lower elevations snowpack tends to behave inversely to the temperature during the wet periods. If wet periods are characterized by warm weather, snowpack will thin, while the opposite is true if the wet periods are associated with cold weather. During spring the watershed again receives almost daily rainfall and snowpack melts away as a result of warming temperatures and semi-continuous rainstorms.

## **5.2 Analysis of storm rainfall**

The classification of storms during the study period is shown in Table 5.1. A total of 53 medium to large storms were observed during the 24 months of this study. Discussion of the characteristics of the storms is broken into three sections. The first deals with storm-averaged values for total rainfall and duration. The second deals with the intensity-duration analysis of the observed storms. The intensity-duration analysis is concerned with determination of the representativeness of the three storms known to have caused failures and with attempts to determine a regional threshold for hillslope failure in the Tsitika basin.

### **5.2.1 Storm averaged rainfall analysis**

Of the 53 significant storms, 40 occurred during the main storm season September to March. Table 5.2 shows the breakdown of the storm season and non-storm season events into size and temperature classes. Fourteen of the 40 storms were classed as large events (see Figure 5.1), which shows that large storms are frequent events in Tsitika basin. The breakdown of each storm season event into temperature classes shows that the Warm and Mixed classes occur in nearly equal proportions. The occurrence of only two Cold class storms does not reflect the absence of this type of storm. The tipping-bucket rain gauges used in this study are not designed to record snowfall and are also subject to freezing during Cold class storms. The frequent occurrence of Warm class storms during the storm season is very important in that during these events both rainfall and snowmelt rates may be large. The importance of rain-on-snow events in the study area can be assessed using Table 5.1. During the period of study, a total of 33 medium and large

Table 5.1 Storms during the study period

Storm ID	Total Ave. rainfall (mm)	Duration (hours)	Start (yy/mm/dd hhmm)	Temp class	Size class	Rain-on-Snow?
92S1	26	54.5	92/12/17 1615	N/A	M	Y
92S2	40	60.8	92/11/20 1045	N/A	M	Y
92S3	39	20.5	92/11/26 1215	N/A	M	Y
92S4	29	21	92/11/29 0700	N/A	M	Y
92S5	26	35.8	92/12/13 0915	N/A	M	Y
92S6	26	24.3	92/12/22 0730	N/A	M	Y
93S1	24	24.1	93/1/14 2135	N/A	M	Y
93S2	28	16.8	93/1/18 1335	N/A	M	Y
93S3	150	91	93/1/24 0115	N/A	L	Y
93S4	73	61.2	93/2/5 0630	N/A	M	Y
93S5	21	17.6	93/3/1 0210	N/A	M	Y
93S6	145	91.4	93/3/3 0000	N/A	L	Y
93S7	103	106.7	93/3/19 1320	N/A	L	Y
93S8	48	56.1	93/4/23 0205	W	M	N
93S9	23	17.3	93/5/1 0315	W	M	N
93S10	21	54.8	93/5/7 0505	W	M	N
93S11	30	27	93/5/10 0230	W	M	N
93S12	32	86.5	93/5/19 0520	W	M	N
93S13	22	25.5	93/6/8 2000	W	M	N
93S14	27	50.3	93/6/13 0330	W	M	N
93S15	21	32.8	93/7/15 0245	W	M	N
93S16	42	12.3	93/8/5 0840	W	M	N
93S17	96	39.2	93/8/22 0325	W	L	N
93S18	26	26.5	93/9/4 1630	W	M	N
93S19	39	18.7	93/9/10 0120	W	M	N
93S20	75	51.1	93/9/24 0015	W	M	N
93S21	123	67.5	93/9/28 0850	W	M	N
93S22	77	53.8	93/10/21 1800	W	M	N
93S23	69	39	93/11/1 1230	W	M	N
93S24	50	22.7	93/11/14 0945	M	M	N
93S25	44	31.3	93/11/19 1200	M	M	Y
93S26	27	48	93/11/27 1450	W	M	Y
93S27	28	25.8	93/11/30 1845	M	M	Y
93S28	106	16	93/12/2 0800	M	L	Y
93S29	89	40	93/12/9 0800	M	L	Y
93S30	80	25.5	93/12/12 1215	C	L	Y

Table 5.1 Storms during the study period (continued)

Storm ID	Total Ave. rainfall (mm)	Duration (hours)	Start (yy/mm/dd hhmm)	Temp class	Size class	Rain-on-snow?
94S1	50	57.3	93/12/31 0745	M	M	Y
94S2	48	32.1	94/1/3 0940	W	M	Y
94S3	39	43.8	94/1/21 0615	W	M	Y
94S4	82	50.5	94/2/11 1200	M	L	Y
94S5	63	38.3	94/2/14 0330	M	L	Y
94S6	54	24.3	94/2/27 1215	W	M	Y
94S7	28	14.1	94/2/28 1940	W	M	Y
94S8	49	23	94/3/1 1940	W	M	Y
94S9	20	32.8	94/3/12 0145	M	M	Y
94S10	47	40.2	94/3/16 1210	M	M	Y
94S11	45	40.7	94/3/19 2255	M	M	Y
94S12	44	54.8	94/4/10 1730	W	M	Y
94S13	63	92.3	94/6/10 1530	W	M	N
94S14	20	44	94/6/30 0215	W	M	N
94S15	50	90.5	94/10/20 0115	M	M	Y
94S16	127	35.5	94/10/24 1115	W	L	Y
94S17	39	43	94/10/26 0730	W	M	N

Table 5.2 Size and temperature classification of observed storms

Size class	Storm season	Other months	Total
Large	14	2	16
Medium	26	11	37
Total	40	13	53
Temperature class	Storm season	Other months	Total
Warm	18	13	31
Mixed	14	0	14
Cold	2	0	2
Total	34	13	47

rain-on-snow events occurred. During the months September-April, 32 of the 40 recorded medium and large storms involved rain-on-snow.

The three storms during which slope failures are known to have occurred rank 1, 3, and 16 with respect to total storm rainfall (Table 5.3). The triggering of the failures

Table 5.3 Storm interval intensities for storm season storms (mm/interval)

Storm ID	Month	Interval										Slope Failures
		1 hr	Rank	3 hr	Rank	6 hr	Rank	12 hr	Rank	24 hr	Rank	
93S3	Jan	12	3	29	3	54	2	79	2*	116	1	Y
93S28	Dec	9	9*	23	7	41	5	79	2*	110	2	
93S6	Mar	14	2	38	1	69	1	88	1	108	3*	
94S16	Oct	15	1	35	2	49	4	72	5	108	3*	Y
93S29	Dec	10	6*	25	5	38	6	64	6	86	5	
94S5	Feb	8	14*	20	10*	33	9*	49	9	83	6	
93S30	Dec	6	23*	16	18*	29	15*	53	7	78	7	
93S21	Sept	11	4*	28	4	50	3	75	4	77	8	
94S4	Feb	8	14*	19	14*	31	12*	46	12	76	9	
93S7	Mar	8	14*	20	10*	31	12*	48	10*	62	10	
93S20	Sept	10	6*	24	6	37	7	52	8	58	11*	
94S8	Mar	6	23*	16	18*	29	15*	40	15	58	11*	
93S4	Feb	9	9*	20	10*	32	11	45	13	56	13*	
94S6	Feb	8	14*	19	14*	30	14	48	10*	56	13*	
93S23	Nov	8	14*	21	8*	33	9*	38	16	55	15	
93S24	Nov	5	29*	12	29*	21	20*	37	17	52	16*	
94S2	Jan	8	14*	15	20*	20	22*	36	18	52	16*	
94S7	Mar	9	9*	20	10*	24	18	28	23*	52	16*	Y
93S25	Nov	5	29*	11	31*	19	26*	34	19*	49	19	
93S22	Oct	9	9*	21	8*	35	8	43	14	47	20	
94S11	Mar	6	23*	13	28	20	22*	33	21	45	21	
92S3	Nov	5	29*	15	20*	25	17	34	19*	44	22	
93S19	Sept	9	9*	17	17	22	19*	29	22	39	23	
94S17	Oct	6	23*	14	23*	20	22*	25	25	34	24	
94S10	Mar	7	20*	14	23*	17	31	24	26*	32	25*	
92S2	Nov	5	29*	9	36*	12	37*	20	34*	32	25*	
92S4	Nov	6	23*	14	23*	21	20*	28	23*	32	25*	
93S27	Dec	11	4*	15	20*	19	26*	23	28*	32	25*	
94S1	Jan	10	6*	18	16	20	22*	23	28*	31	29	
94S3	Jan	5	29*	11	31*	16	32*	24	26*	28	30*	
93S2	Jan	4	38	7	39	14	35	23	28*	28	30*	
92S5	Dec	7	20*	14	23*	19	26*	22	31*	26	32*	
92S6	Dec	6	23*	14	23*	19	26*	22	31*	26	32*	
94S15	Oct	7	20*	9	36*	13	36*	20	34*	25	34	
92S1	Nov	5	29*	11	31*	16	32*	20	34*	23	35*	
93S1	Jan	5	29-	9	36*	15	34	21	33	23	35*	
93S26	Nov	5	29*	10	34*	12	37*	17	38	21	37*	
93S5	Mar	2	40	12	29*	19	26*	20	34*	21	37*	
93S18	Sept	5	29*	10	34*	12	37*	13	39	20	39	
94S9	Mar	3	39	5	40	8	40	10	40	18	40	

Note: Events are presented in rank order based on 24 hour interval.

during events 93S3 and 94S16 was most likely the result of intense rainfall, although a snowpack was present at the start of both storms. The failures during 94S7 are the result of warm temperatures, and rainfall onto a deep snowpack.

The average values of total storm rainfall and storm duration are shown in Table 5.4. The values have been determined for all storms, including all storm season events and other non-storm-season events. Based upon these data for Tsitika basin, the average storm event yields 53 mm of rainfall and has a duration of 42 hours. The greater number of events during the storm season heavily influences the comparison of all events, but if values for the main winter storm season and other non-winter events are compared, it can be seen that events during the winter season have a much larger magnitude and a slightly lower duration than non-winter events.

Table 5.4 Average characteristics of rainstorms in the Tsitika Valley.

	# storms	Ave. rainfall (mm)	Std. deviation.	Ave. duration (hours)	Std. deviation.
1. all storms	53	52.7	33.2	42.4	23.1
1a. large	16	95.1	28.1	56.2	26.7
1b. medium	37	34.4	10.9	36.5	18.8
2. storm season	40	57.6	36.3	41.4	24.6
2a. large	14	97.3	28.8	54.8	26.4
2b. medium	26	36.2	9.9	34.2	17.2
3. other storms	13	37.6	21.9	45.6	24.2
3a. large	2	79.5	23.3	65.7	37.6
3b medium	11	30.0	10.3	42.0	21.6

### 5.2.2.1 Storm rainfall intensity analysis

Analysis was restricted to events in the winter storm season, since these are the only storms likely to cause failures. Ranked results of the rainfall intensity-duration analysis are shown in Table 5.3. The storms during which failures were observed in Tsitika basin are indicated in Table 5.3. Examination of the rainfall intensity values for the four storms with 24 hour rainfall totals greater than 100 mm. shows that the 12 and 24 hour interval totals are of similar magnitude. For intervals less than 6 hours in duration, storm 93S28 ranks consistently lower than the other three storms, showing that during this event, rainfall was more evenly distributed over the course of the storm. The most intense 1 hour rainfall recorded was 15 mm during storm 94S16, the most intense 24 hour rainfall 116 mm during storm 93S3. It is interesting to note that storm 93S6 was the most intense storm observed over the 3, 6, and 12 hour intervals, yet no failures were observed within the study area. Reviewing Table 5.2 it appears that storms 93S3 and 94S16 are representative of storms with rainfall greater than 100 mm. in a 24 hour interval based upon examination of the interval-intensity totals. The third storm to initiate failure was 94S7, which consistently ranks in the low teens. Examination of the intensity totals of storms with similar 24 hour values shows that this storm is also representative of medium storms with similar rainfall intensities.

Estimated return periods for rainfall intensities of 1, 6, 12, and 24 hour duration are shown in Table 5.5. It should be noted that given the standard deviation associated with each duration, there is considerable overlap between return periods. An example of this is storm 93S3 which had a 24 hour total of 116 mm. of rainfall. This storm is close to the

average 25 year storm, but with a standard deviation of 18 mm. at this duration, the storm return period is between 10 and 50 years.

Table 5.5 A.E.S. rainfall intensity return periods for the Tsitika

Duration (hours)	Std. deviation. (mm.)	Return Period (years)						
		2	5	10	15	20	25	50
1	+ 4.2	14	17	19	20	21	22	24
6	+ 11	44	50	55	58	61	62	69
12	+ 16	68	76	84	88	92	95	103
24	+ 18	88	97	105	109	114	117	127

Observed storm intensities for all storms were compared with the average A.E.S. return periods from Table 5.5 and are shown in Table 5.6. The asterisks in the columns of this table identify storms causing failure in each class. Two asterisks in a column means that two storms known to have caused failure occurred in this class. Discussion of the intensity-duration relation for only the storms known to have caused failure is contained in Chapter 9. During the study period the most extreme observed storm was associated with at least one slope failure. Storm 93S3 had a 6 hour duration return period of 50 years and yet no failures were observed. Most important is the fact that failure was associated at all durations with at least one storm having a return period of less than 2 years. This shows that there can be no simple reliance upon rainfall totals alone in predicting periods of likely slope instability in Tsitika basin. This complies with the conclusions of studies on the relationship between rainfall and landsliding conducted elsewhere (Church and Miles 1987, Hogan and Schwab, 1991).

Table 5.6 Frequency of storm intensity-duration by return period for all storms

Duration	Return period (years) (from Hogg and Carr, 1985)						
	< 2	2	2-5	5	5-10	10	10-15
1	38**	1	1*				
6	36*		1*	1	1*		
12	35*		2*		2*		
24	36*						2*
Duration	Return period (years) (from Hogg and Carr, 1985)						
	15	15-20	20	20-25	25	25-50	50
1							
6							1
12	1*						
24		1		1*			

### 5.2.2.2 Regional rainfall intensity-duration thresholds

Given the lack of a consistent relationship between rainfall totals and slope failures, this portion of the analysis contains the determination of a regional rainfall intensity-duration threshold for failures based on published rainfall values for storms known to have caused failure. The data are drawn from studies in Alaska, the Cascades, the southern Coast Mountains and the three storms from the Tsitika basin. The data are summarized in Figure 5.3 and Figure 5.4 and also contain the thresholds computed by Hogan and Schwab (1991) and Caine (1980). The bold legend entries are for storms during which snowmelt was thought to be a major contributing factor. From Figure 5.3 it can be seen that the Hogan and Schwab thresholds from the Queen Charlotte Islands do not apply to the rest of the database. The thin soils, steep slopes, and logging

Figure 5.3 Intensity-duration of storms causing failure in the Pacific Northwest

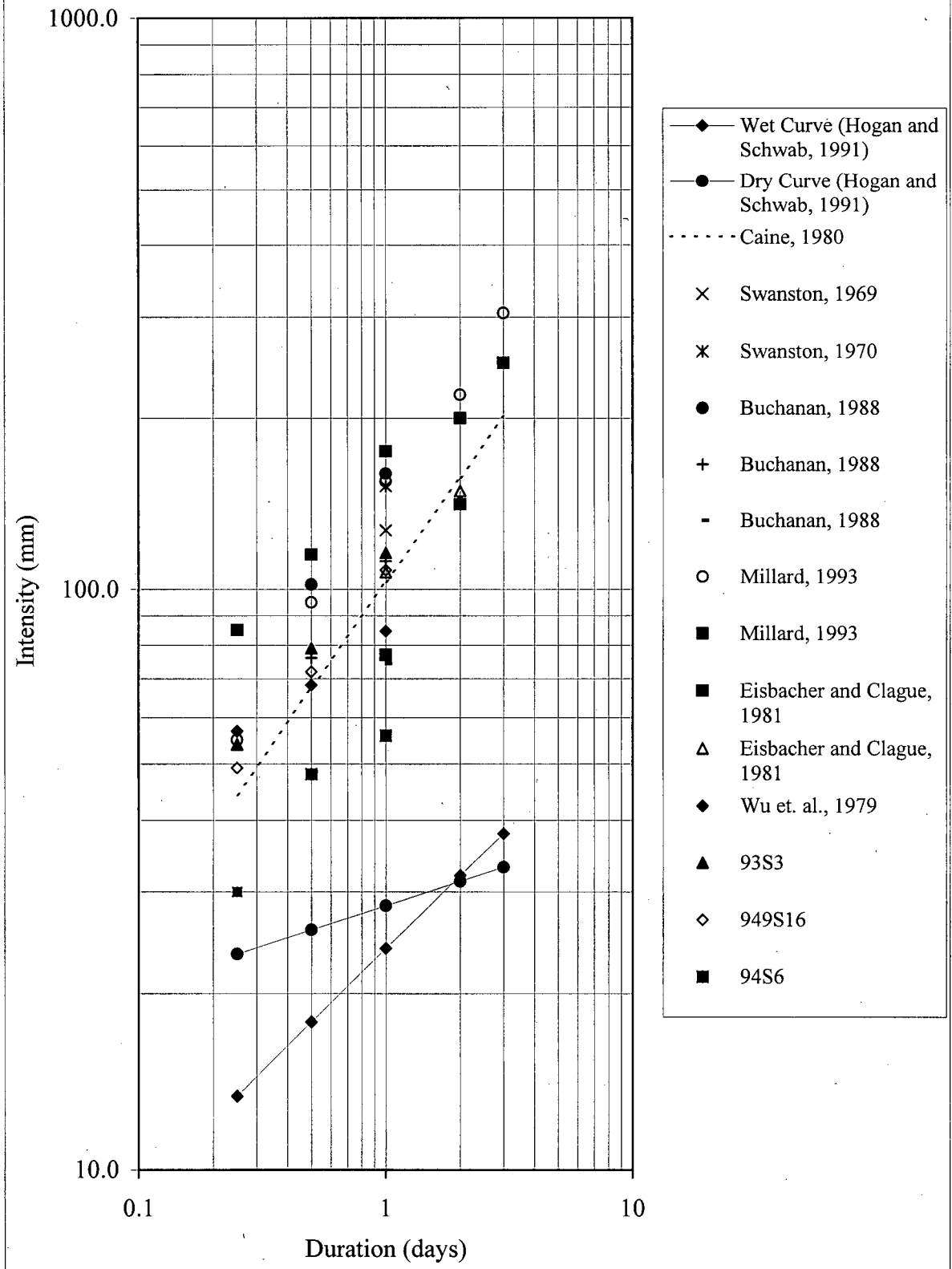
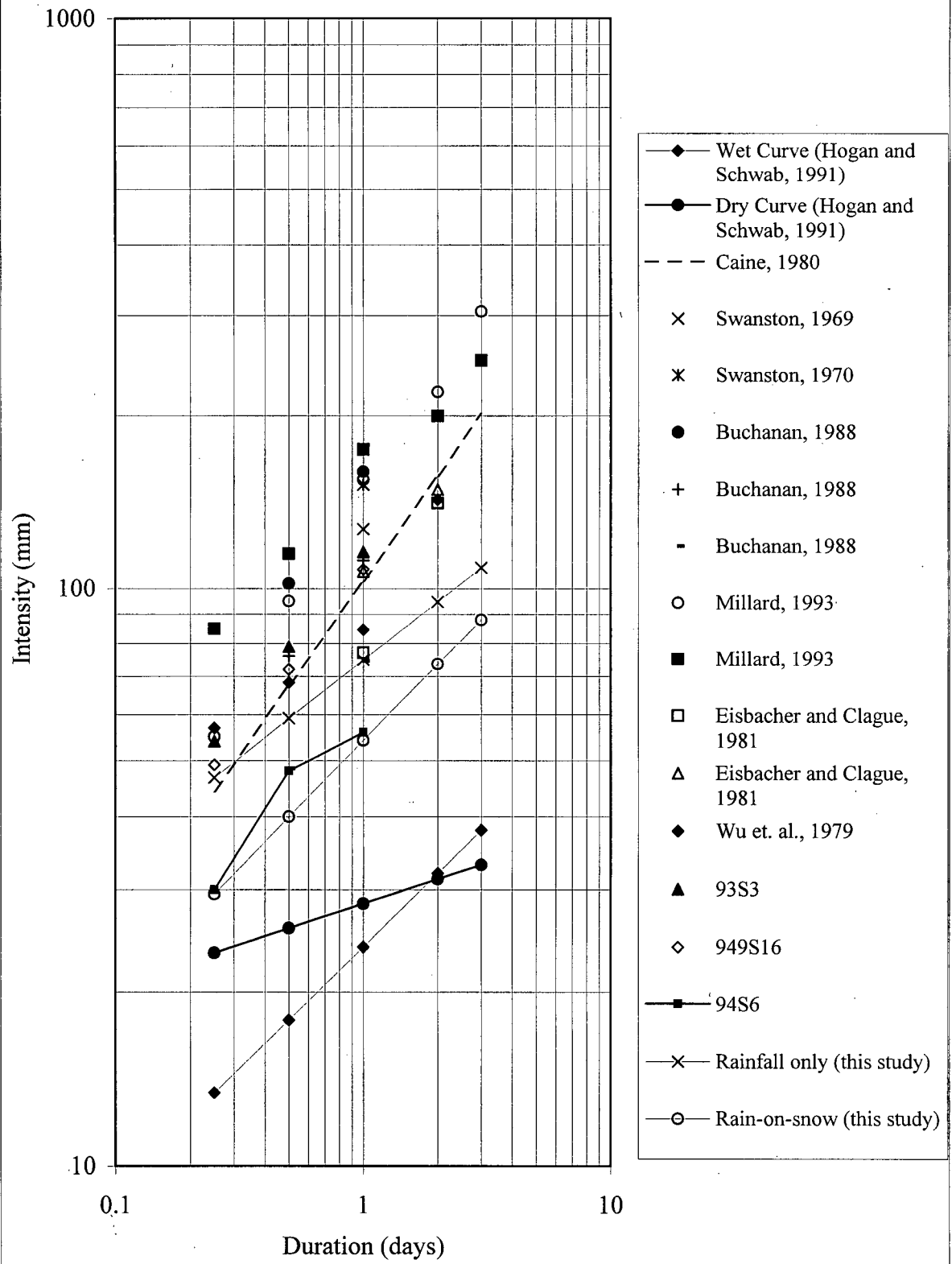


Figure 5.4 Estimated intensity-duration envelope curves for the Pacific Northwest



history of the Queen Charlotte Islands are the most probable explanation of the significantly lower precipitation thresholds of these two curves. The Caine threshold works for most storms but there are still many slope failures below this threshold. A possible explanation is that the Caine data included geographic areas greatly different in climate and terrain conditions from the Pacific Northwest. It must also be remembered that many slope failures documented in these studies had no climatic data taken close to the actual failure locations. Thus the precipitation rates at these locations were probably substantially higher than the values shown in Figure 5.3, given that most climate stations are located at lower elevations.

For the case where slope instability is associated with rainfall alone, it is possible to define a reliable envelope based on the 11 available data points. The rainfall only envelope is defined by  $I=25.4D^{0.34}$  (see Figure 5.4). For rain-on-snow storms causing failure, more data are needed before an effective envelope can be defined. However, based on the two storms during which snowmelt was a major factor, the relation  $I=13.4D^{0.44}$  is suggested (Figure 5.4).

## Chapter 6 Groundwater analysis

This chapter deals with the analysis of groundwater time series and its relations with principal storms in the study area. Modeling of groundwater time series is discussed in Chapter 7. Discussion of the results presented in this chapter is conducted in Chapter 8 of the thesis.

### 6.1 Saturated hydraulic conductivity

A principal requirement of groundwater analysis is knowledge of the hydraulic conductivity of soil materials, since this controls flow speed and the magnitude of pressure-head changes on a slope under specified rainfall inputs. The results of the slug tests from Eqn. 4.6 were plotted against time on semi-log paper (see Figures 6.1 to 6.4). A value of  $T_0$  was determined from each test at the clear-cut site when the L.H.S. equaled 0.37. Values of  $T_0$  for the individual tests shown in these figures at the clear-cut site ranged from 8 to 26 seconds (see Table 6.1). Well 2 in Figure 6.1 showed no consistency in  $T_0$  between tests and so a decision was made to exclude Well 2 from the calculation of saturated hydraulic conductivity, K values for the site as a whole. The  $T_0$  values were then used in Eqn. 4.7 to determine the value of K. The values of K determined by this method are shown in Table 6.2. From this analysis, an average K value of  $6 \times 10^{-4}$  m/s with a standard deviation of  $1.5 \times 10^{-4}$  was determined for soils at the clear-cut site using all holes. Exclusion of Well 2 from the analysis resulted in an average K value of  $7 \times 10^{-4}$  m/s with a standard deviation of  $8.4 \times 10^{-5}$  m/s. The difference between the two values determined for K was  $9 \times 10^{-5}$  m/s which represents approximately a 12%

Figure 6.1 Injection test results for clear-cut site Well 2

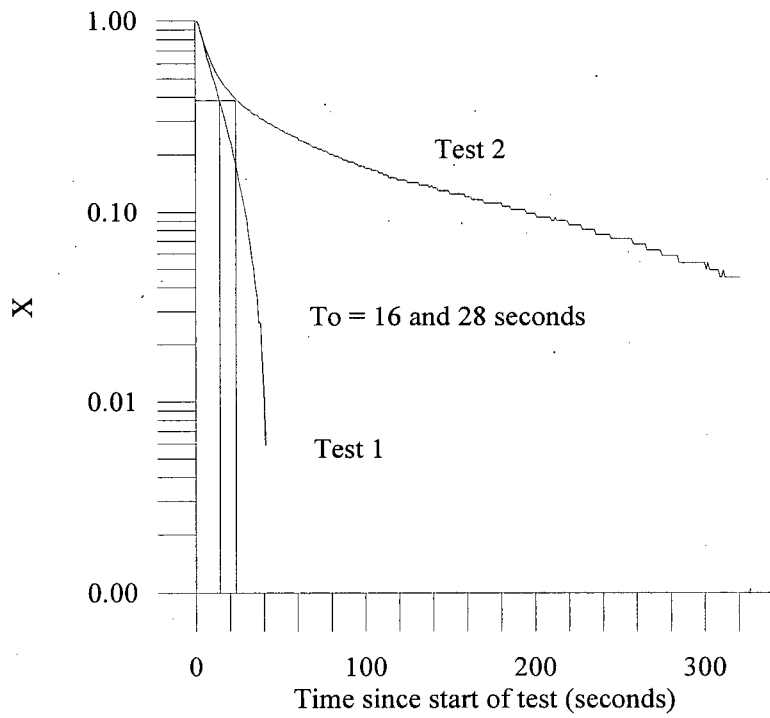


Figure 6.2 Injection test results for clear-cut site Well 3

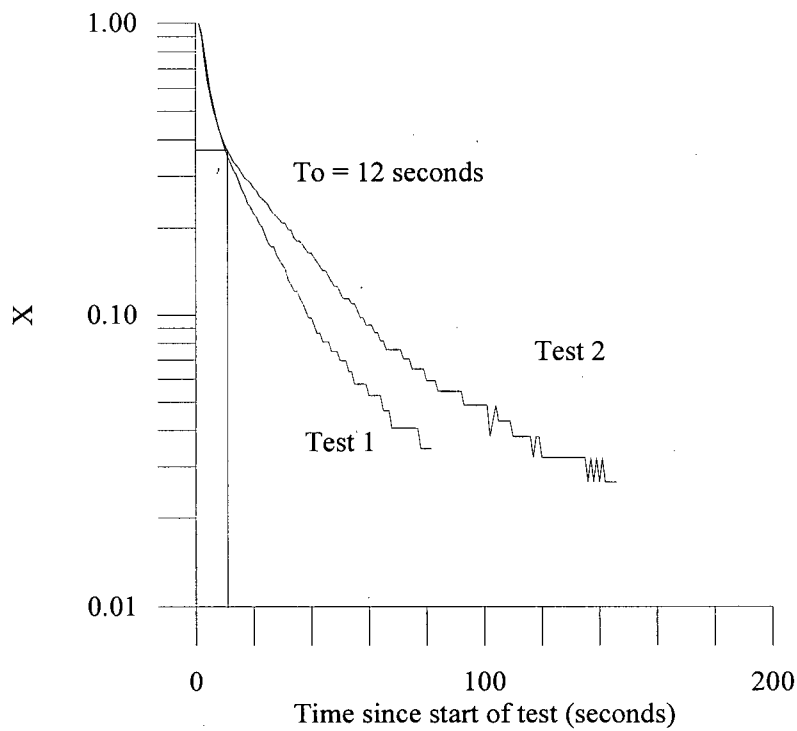


Figure 6.3 Injection test results for clear-cut site Well 4

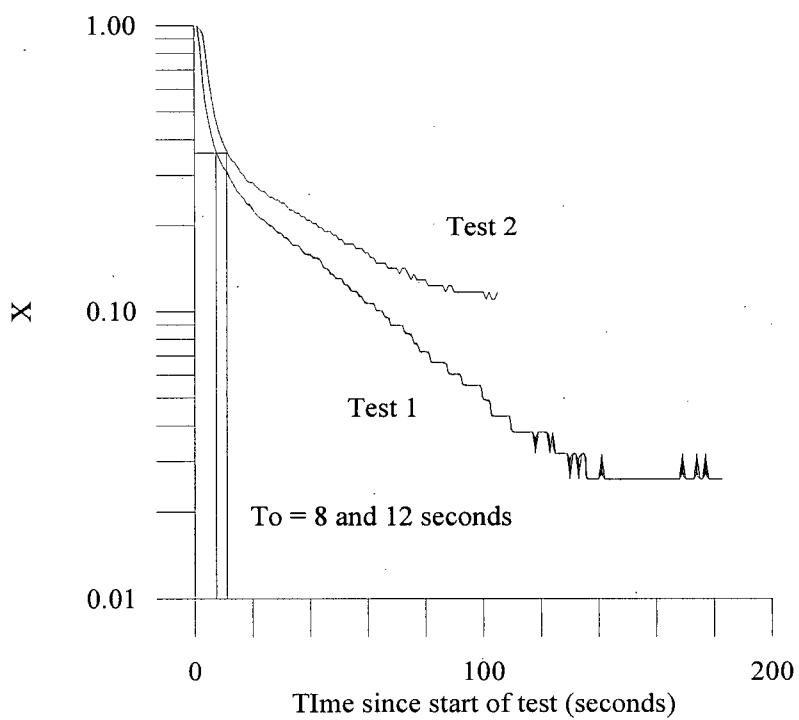
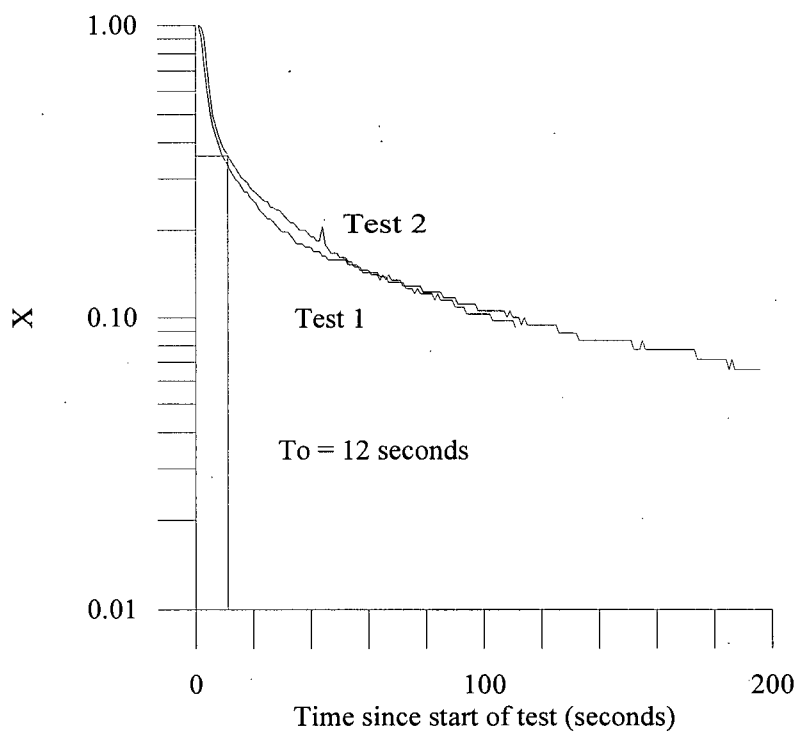


Figure 6.4 Injection test results for clear-cut site Well 8



difference in conductivity. Both values of K determined above seem reasonable when compared with other values listed in Table 2.5.

Table 6.1 Results of injection tests at the clear-cut monitoring sites

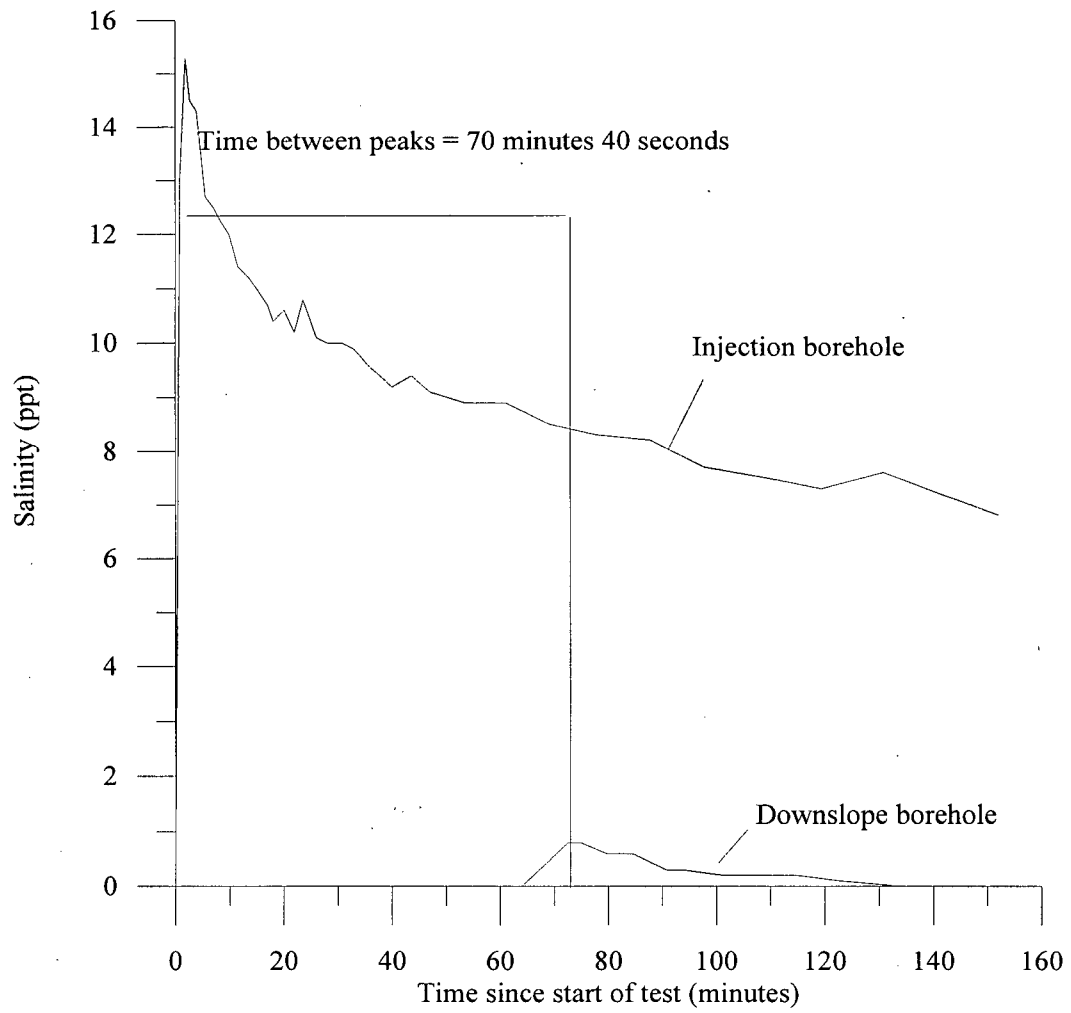
Hole	Test 1			Test 2		
	T <sub>o</sub>	H <sub>o</sub>	H <sub>max</sub>	T <sub>o</sub>	H <sub>o</sub>	H <sub>max</sub>
Hole 2	16	39.9	44.5	28	39.3	44.5
Hole 3	12	40.5	44.5	12	40.5	44.5
Hole 4	8	41.5	45.3	12	40.5	44.5
Hole 8	10	41.7	45.8	10	41.9	45.9

Table 6.2 Calculated values of hydraulic conductivity for tested holes

Hole	Test 1		Test 2	
	K1 (H <sub>o</sub> )	K2 (H <sub>max</sub> )	K1 (H <sub>o</sub> )	K2 (H <sub>max</sub> )
Hole 2	0.0004	0.0004	0.0004	0.0004
Hole 3	0.0008	0.0008	0.0008	0.0008
Hole 4	0.0008	0.0008	0.0008	0.0008
Hole 8	0.0007	0.0006	0.0007	0.0006

An injection test was conducted at the old-growth monitoring site during a large rainstorm as a method of determining the flow celerity. A salt solution was injected in an upslope hole and the salinity of groundwater in a borehole 2.9 m. downslope was monitored. This results of this test are shown in Figure 6.5. Based on the 0.4 m groundwater level at the time of the test and an elapsed time of one hour and twelve minutes until the solution was detected in the downslope borehole, the flow celerity at this site was determined to be  $7 \times 10^{-4}$  m/s. Using equation 2.3 with a slope angle of  $31^{\circ}$

Figure 6.5 Results of salt injection test in Hole 2 at the old growth site



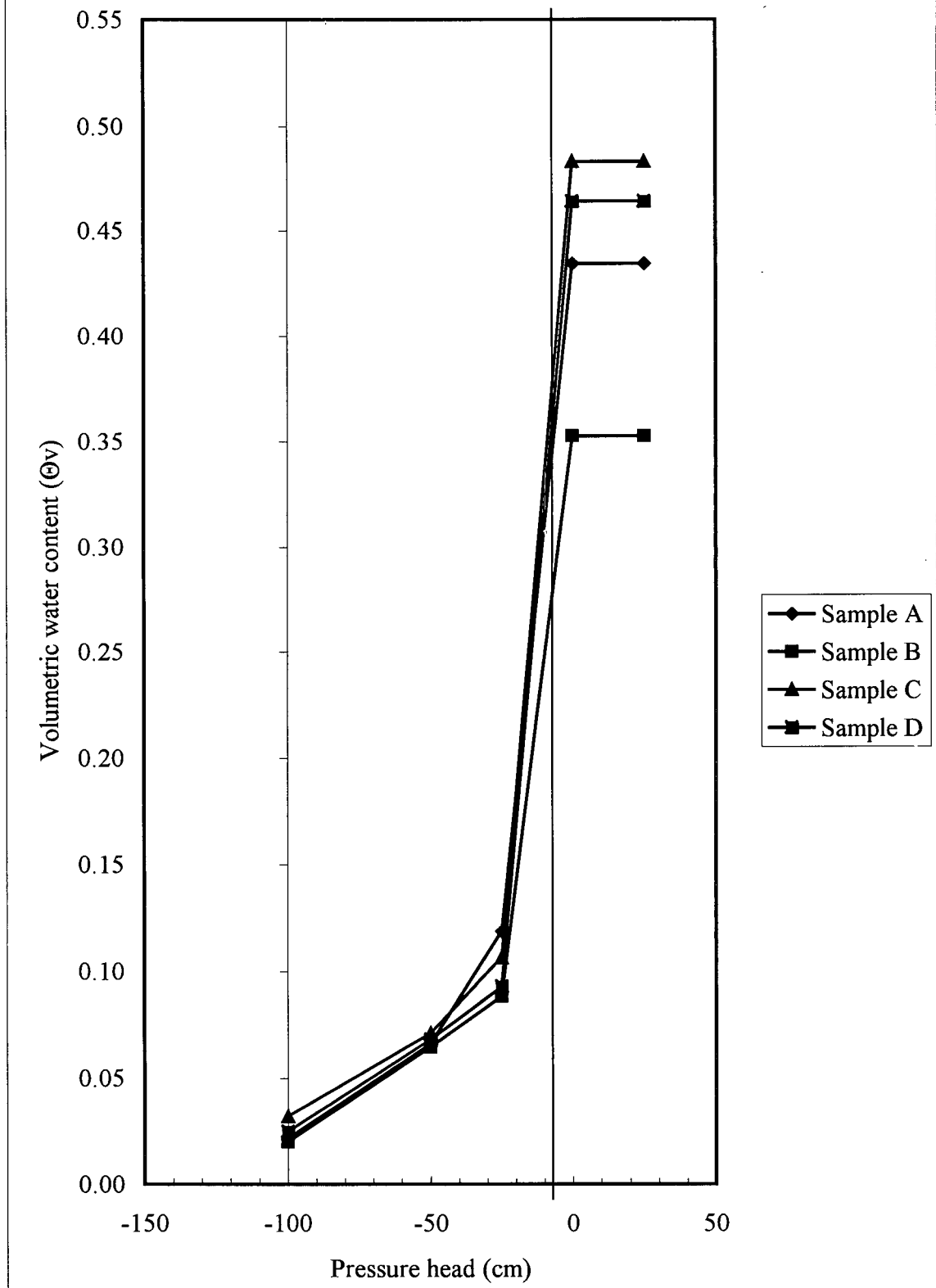
and a porosity of 0.3, the hydraulic conductivity of the soil was determined to be  $4 \times 10^{-4}$  m/s. The results of tests at the two monitoring sites show that the hydraulic conductivity values of soils at the sites are fairly comparable.

## 6.2 Soil moisture considerations

Attempts at measuring soil moisture characteristic curves in the laboratory were only partially successful. Due to the coarse-grained nature of the soils, at low moisture contents, samples tended to crumble during transfer to the scale for weighing. The results of the soil moisture retention curve determinations are shown in Figure 6.6. The sample porosities varied from 0.38 to 0.48. Figure 6.6 shows that the most rapid change in volumetric water content occurs at low negative pressures which is caused by the emptying of the largest soil pores. All four samples that were successfully tested lost approximately 80% of their volumetric water content once a negative pressure head of -25 cm. was attained. This shows that the study area soils drain rapidly at low suctions. All samples achieved fairly constant values of water content at around 2.5% at a pressure of -100 cm. During the storm season it is unlikely that soils have enough time to drain to this level. It is not known if the consistency of these values is a result of similar distributions of small pores in each sample or if the values reflect a control on the water content imposed by the organic contents of the samples.

To determine a lower limit for effective porosity during the storm season, it was necessary to know the drainage rate of the study area soils. The drainage rate was measured using gravity drainage of samples compacted to the original density of the soil

Figure 6.6 Soil moisture retention curves



and allowed to drain to field capacity. The volume of water in the sample at field capacity was then subtracted from the sample porosity to give a lower bound for the effective porosity. Soil samples were placed in a soil sieve and compacted, with care being taken to minimize any layering of the samples that would influence drainage. During these tests care was taken to minimize the effects of evaporation loss. The results of the gravity drainage tests are shown in Figure 6.7a and Figure 6.7b. The gravity drainage tests show that the study soils lost approximately 25% of their volumetric water content in the first 6 to 12 hours as large pores within the soil matrix drained. Following this time period, the soil drainage rate slows since large pores have drained.

For the clear-cut site the equation relating changes in the volumetric water content to time is  $\theta_v = -0.032 \cdot \log(t) + 0.46$  ( $r^2 = 0.89$ ). The effective porosity of the soil can be determined by subtracting the value of  $\theta_v$  from the soil porosity value. It should be noted that, despite the high  $r^2$  value of the relationship, the equation is based on relatively few samples and may not be representative of actual field conditions. The maximum effective porosity determined using this method would be approximately 0.2. The old-growth soil samples used for gravity drainage tests had been screened to remove stones greater than 2.83 mm and this is believed to result in the observed differences in the curves shown in Figure 6.7a and Figure 6.7b.

### **6.3 Groundwater response during storms**

The characteristics of groundwater response for the observed storms is discussed in the following two sections. The first section contains an examination of the general response of monitored boreholes during rainstorms. The second section contains the results of the

Figure 6.7a. Gravity drainage test results  
for old growth samples

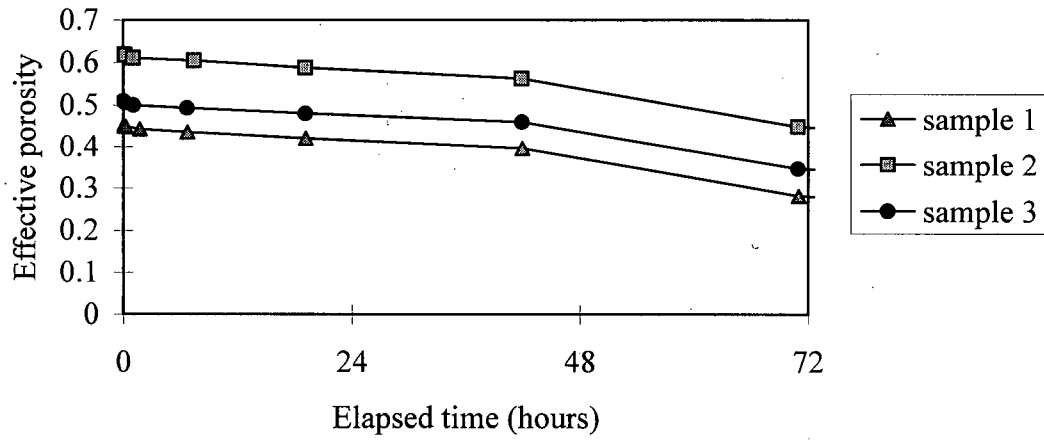
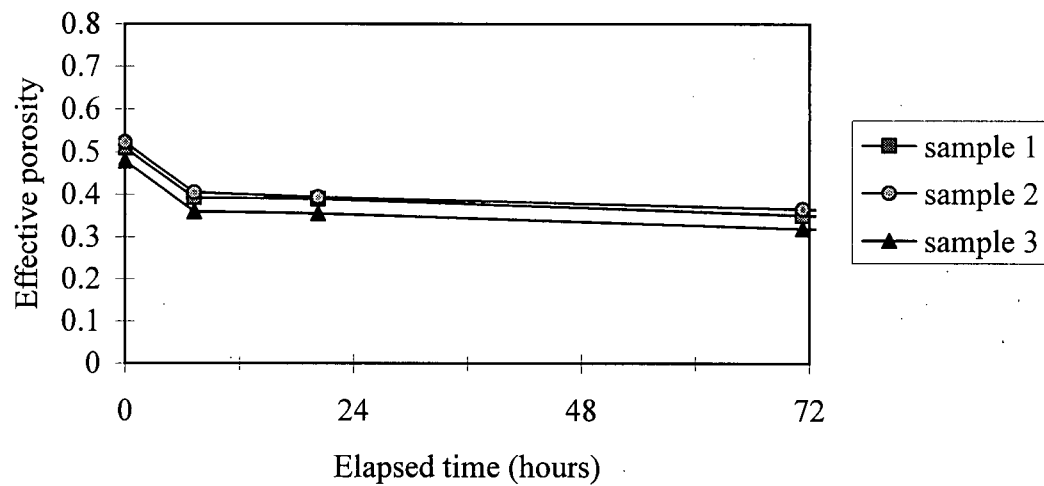


Figure 6.7b. Gravity drainage test results  
for clear-cut samples



analysis outlined in Chapter 4. At each site a discussion is presented of lag time calculations, effective porosity determinations, response rates, groundwater recession rates, and potential meltwater inputs to the groundwater system. All groundwater levels discussed in this section deal with normalized saturated layer thicknesses so that the proportion of the soil profile saturated at each borehole may be directly compared between adjacent boreholes. This normalization of data is justified since slope failure is dependent on pore pressure ratio,  $r_u = u/\gamma z$ , not simply pore pressure,  $u$ .

### **6.3.1 Observed groundwater responses during storms**

This section describes the available time series at the two groundwater monitoring sites. Some of the possible influences on the observed time series at individual boreholes are also discussed. Data gaps exist in the groundwater time series primarily as a result of equipment failure. Table 6.3 lists the available time series at the two monitoring sites. During the period of study access roads TS53 and TS120 were impassable by early December as a result of snowfall (see Figure 3.3 for road locations). The Tlatlos South mainline road was kept clear of snow by graders during the winter months allowing access into upper Russell Creek basin. As a result there are fewer gaps in the data record at the clear-cut monitoring site. As a result of these gaps, it is important to note that only one of the storms known to have caused failure has groundwater coverage and that the data for this storm is available only at the clear-cut monitoring site.

Table 6.3 Available time series at the groundwater monitoring sites.

Clear-cut site data record	Old-growth data record
September 12, 1993 1345 to October 24, 1993 1645. 15 minute interval	February 12, 1993 1220 to March 14, 1993 1745. 5 minute interval
October 27, 1993 1100 to December 20, 1993 1400. 15 minute interval	September 12, 1993 1715 to December 21, 1993 1500. 15 minute interval
December 22, 1993 1700 to January 17, 1994 1545. 15 minute interval	
January 17, 1994 1700 March 11, 1994 07:00. 1 hour interval	

The groundwater time series from the clear-cut site is shown in Figures 6.8a and 6.8b. Wells 1 and 2 develop a water table in early October 1993 but the steadily rising levels at Well 2 are questionable given the large variations shown in both the rising and falling of this early trace. All holes show the influence of the first large winter storm on October 21, 1993. At this time the seasonal water table develops and is sustained for the rest of the winter period 1993-94. The individual time series all show different trends in the average saturated layer thickness. For example, Well 2 shows the average saturated layer thickness to increase to a maximum in mid-January 1994 while the time series at Well 5 shows a fairly consistent average saturated layer thickness of around  $m=0.4$  to  $m=0.5$  up to mid-January. From the individual time series at this site it is apparent that the water table is highly variable over the array of monitoring wells. The peak value of parameter  $m$  (the ratio of saturated zone thickness to total soil thickness) attained a value of 0.92 at Well 7 on December 4, 1993. It should be noted that this peak in the groundwater level

Figure 6.8a Clear-cut site groundwater time series

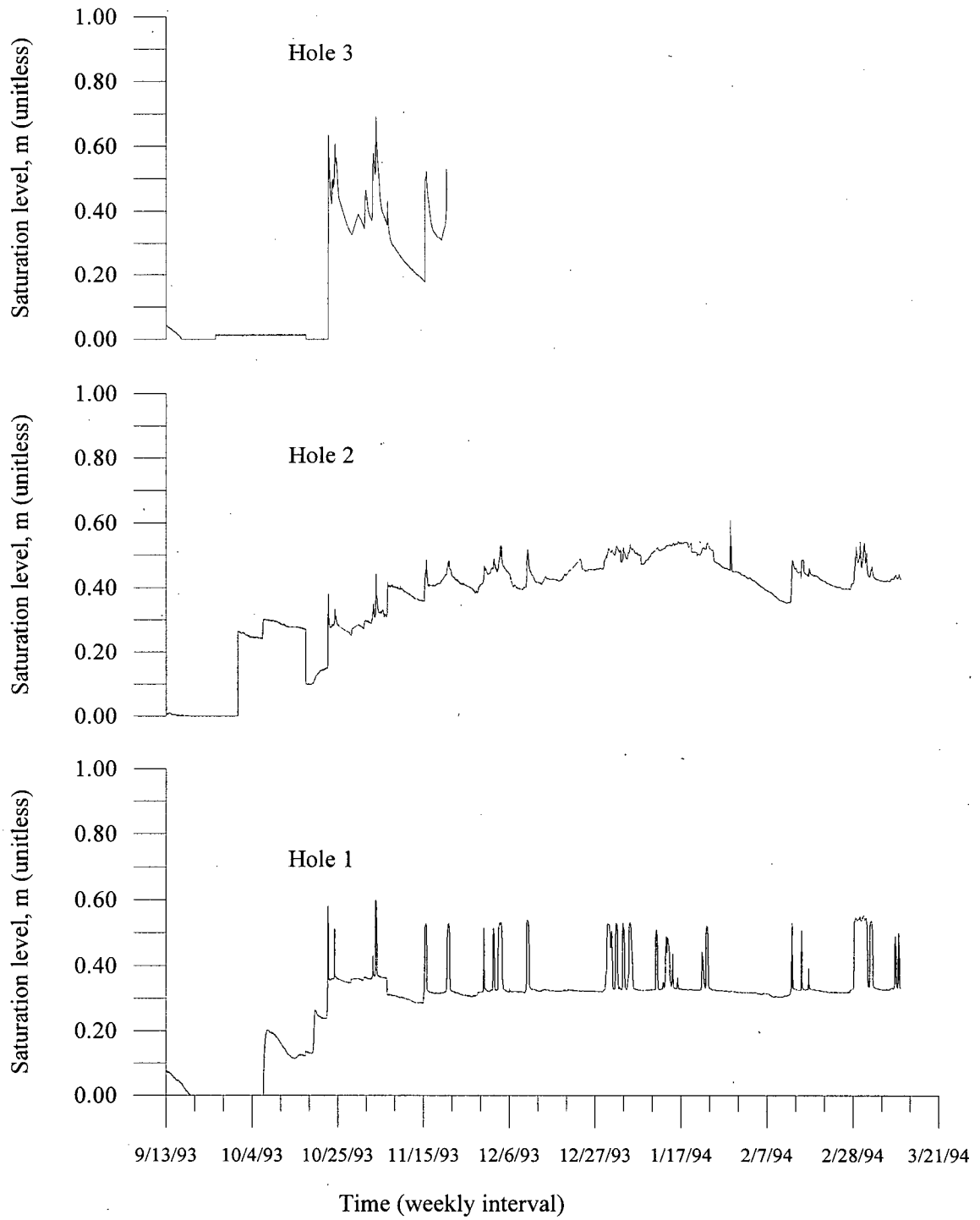
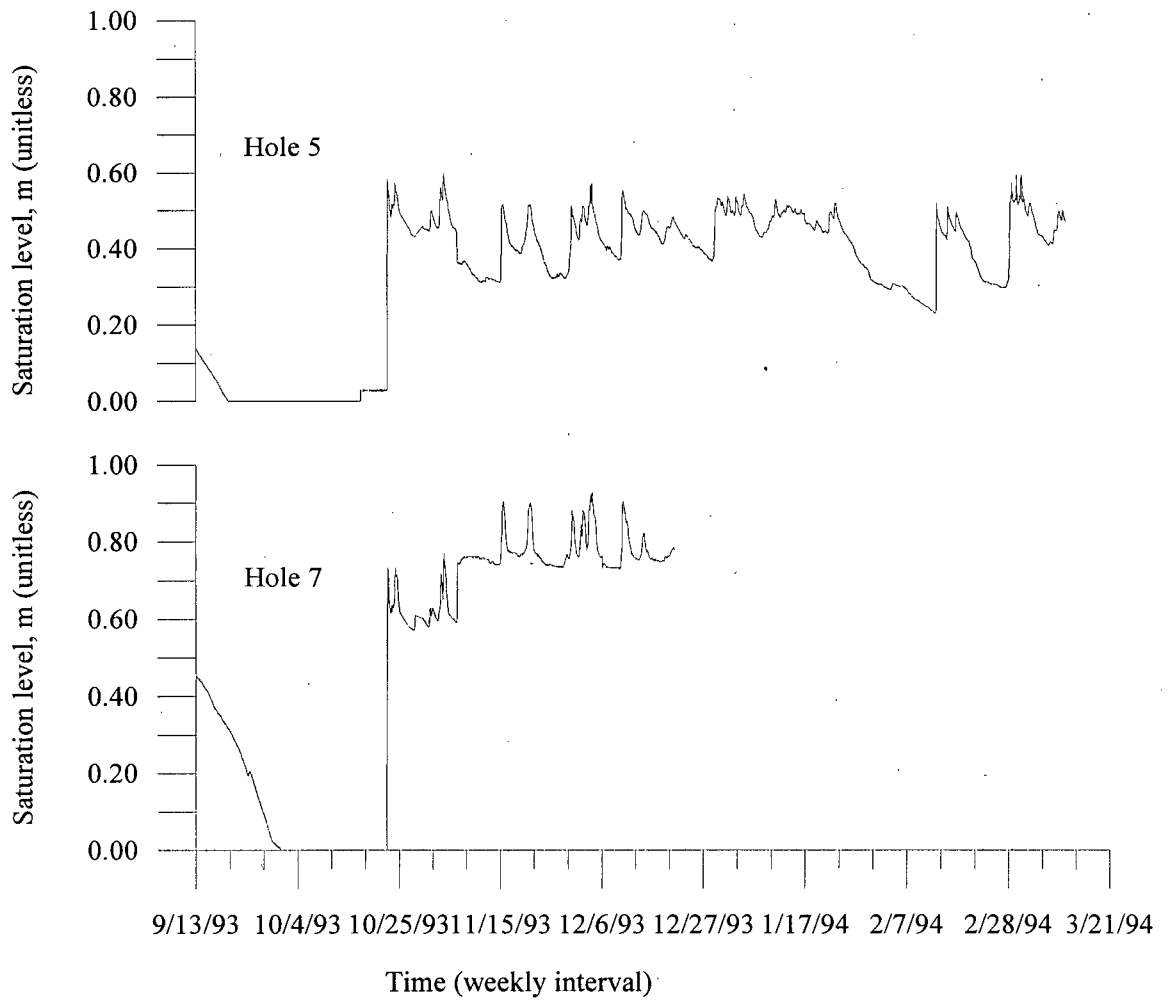


Figure 6.8b Clear-cut site groundwater time series



coincides with the 1993 peak streamflow on Russell Creek resulting from a large rain-on-snow event.

The time series from the wells all show close correspondence both in terms of the timing of groundwater peaks and the onset of the rises. It is the recession limbs of the hydrographs that shows the most variation. The most notable difference is the recession rate of Well 1 compared to the other wells. This well is believed to have drainage assisted by macropores. The time series at Well 3 is believed to be an example of both macropore and soil matrix drainage. The smaller recession rate, below  $m=0.4$ , at Well 3 reflects drainage of water through the soil matrix. The rapid recession rates at  $m$  values greater than 0.4 probably reflects the influence of drainage through macroporous cavities contained within the upper part of the soil profile.

The available time series for the saturated layer thickness at the old-growth monitoring site is shown in Figure 6.9a and Figure 6.9b. The time series in Figure 6.9a show a long recession during most of February, 1993. This corresponds with a period of approximately 2 weeks with no rainfall in Tsitika basin. The rise in the saturated layer thickness at the end of February 1993 is associated with the medium-sized storm 93S5 (Table 5.1). The second large rise in the saturated layer is associated with storm 93S6 in which 145 mm of rainfall were recorded at the Russell Creek rain gauge R2, including

Figure 6.9a Old-growth site groundwater time series

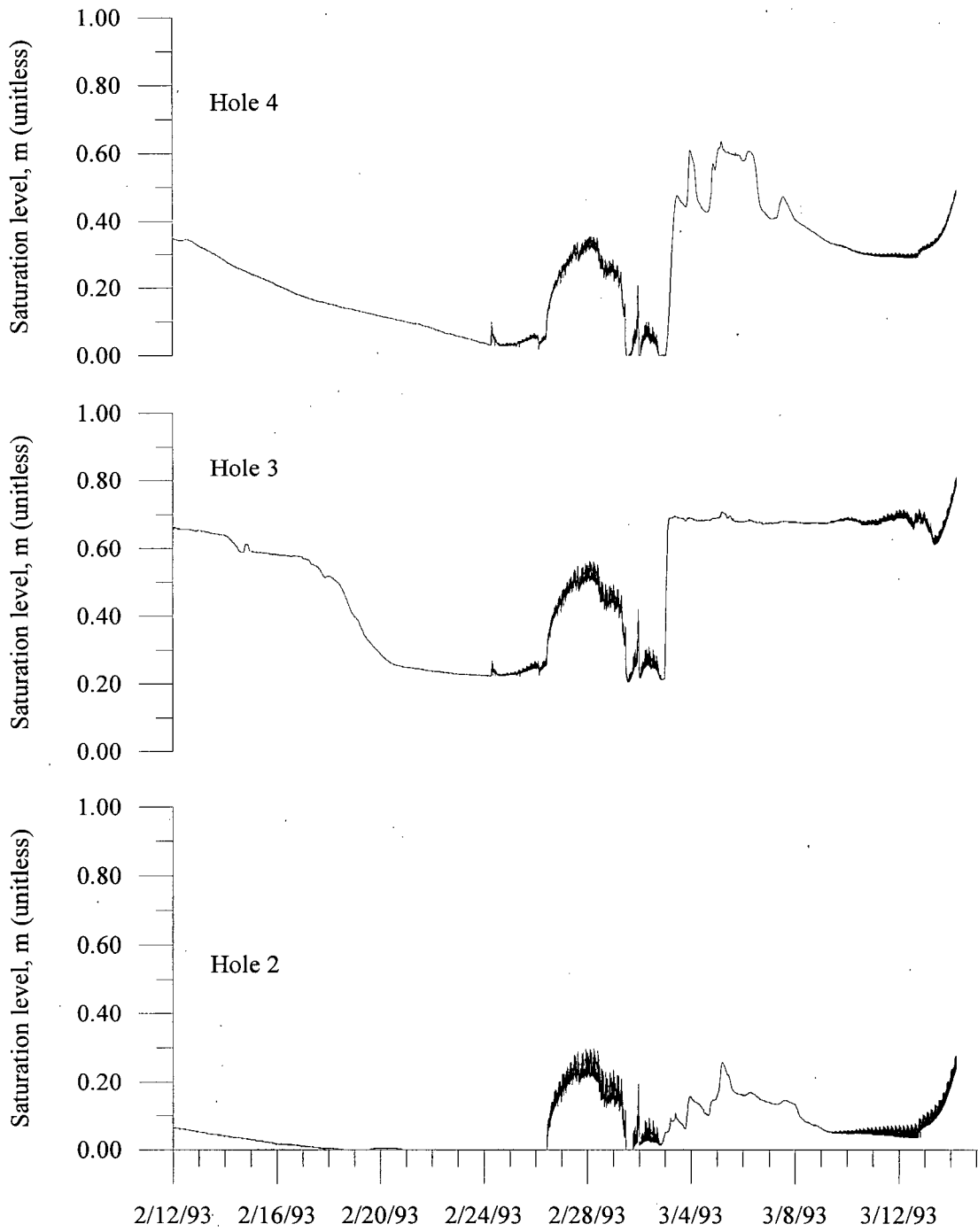
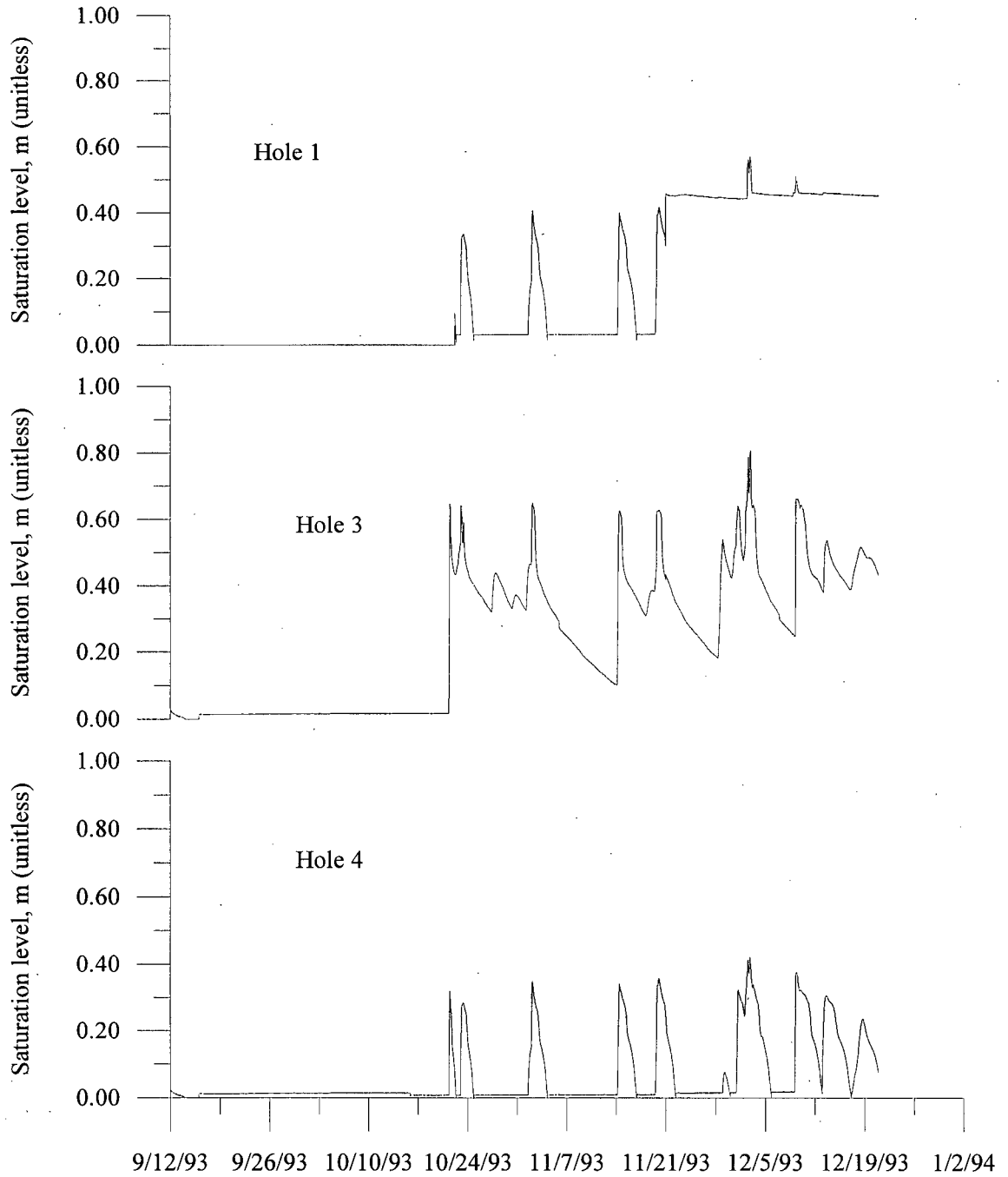


Figure 6.9b Old-growth site groundwater time series



nearly 120 mm in a 24-hour period on March 4, 1993. The high frequency oscillations visible in the saturated layer thickness in the three time series in Figure 6.9a are believed to result from fluctuations in the power supply to the pressure transducers associated with temperature fluctuations. As batteries at this site were drawn down, the power supply at lower temperatures was not sufficient to continuously power the pressure transducers.

The time series in Figure 6.9b cover the period from September 12, 1993 to December 22, 1993. The saturated layer at this site became established at this site following storm 93S22. Well 1 did not respond to this first storm and there is no explanation for this observation. The same well shows a large jump in the base level of the saturated layer around November 19, 1993 that turned out to be associated with the pressure transducer being lifted above the base of the pipe. Subsequent site inspection revealed animal disturbance to the cable of the transducer. The time series at Well 1 and Well 4 show what is believed to be the influence of macropore or void-assisted drainage. The time series at Well 3 is believed to be a mixture of macropore/void and matrix drainage with rapid drainage occurring above  $m=0.45$ . The steep recession above  $m=0.45$  at this hole represents the influence of large voids in the upper portion of the soil profile that allow for rapid drainage. Below  $m=0.45$  the drainage of the soil profile is through the soil matrix which is slower than the upper portion due to the lower porosity of the matrix portion of the soil. The maximum recorded level of the saturated layer at this site was  $m=0.8$  on December 4, 1993 which coincided with the peak flow event during that year for the Tsitika River.

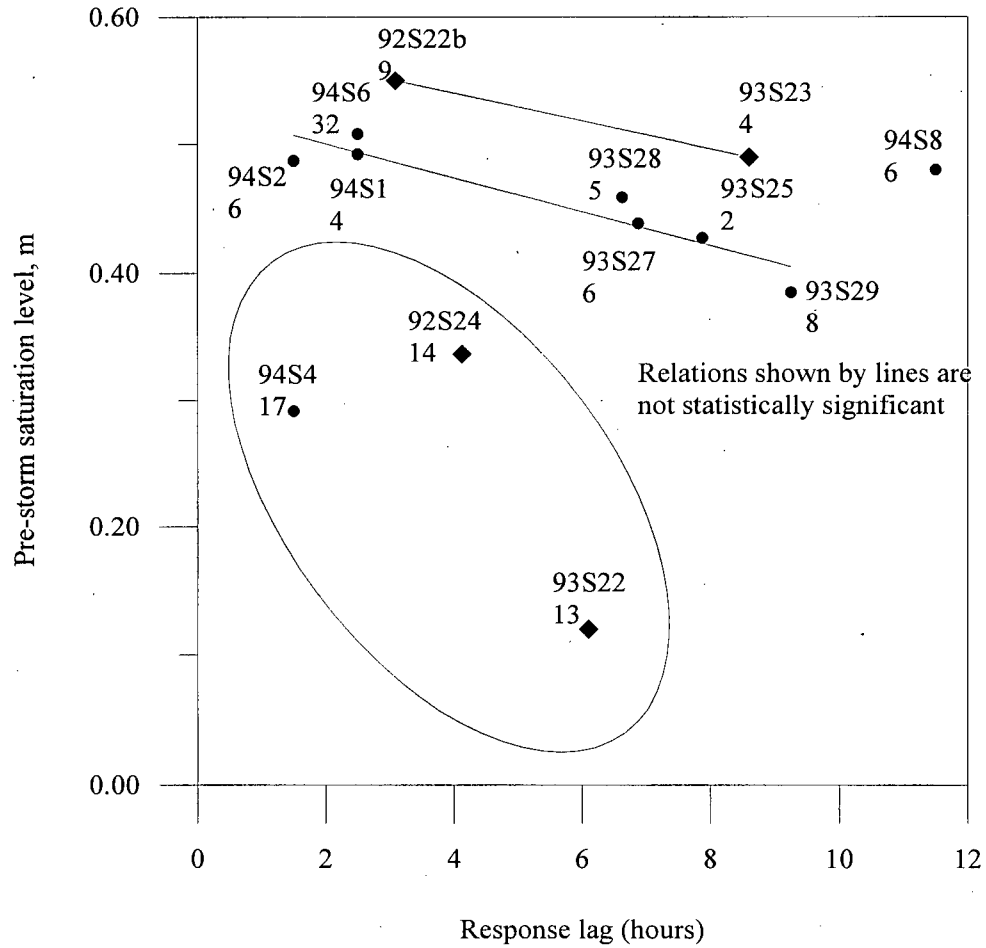
### 6.3.2 Analysis of groundwater responses

In this section results are presented by site for the following response characteristics: lag time, effective porosity, groundwater response rate, groundwater recession rate, and estimated snowmelt input. Rainfall intensities and period totals were obtained from site Russ4 which was connected to the same datalogger as the clear-cut monitoring wells.

#### 6.3.2.1 Groundwater response to storm input lag determination

Response lag represents the time between the onset of precipitation, time  $t_0$ , and the onset of groundwater rise, time  $t_1$ , (see Figure 4.1). Figure 6.10 shows the average lag time for all boreholes as a function of the pre-storm groundwater saturation level at the clear-cut monitoring site. The points in Figure 6.10 are separated into two groups for the purpose of discussion. The points for storms 93S24, 93S22, and 94S4 all had large 3-hour rainfall intensities during the early portion of the storms and exhibited short lag times for storms with a low pre-storm groundwater saturation level. During these events it is believed that macropore assisted infiltration was a factor contributing to the rapid response times for these events. The second group of points represents a cluster with pre-storm water saturation levels between 0.4 and 0.6. Examination of the points in this second group show that rain-on-snow events appear to have shorter lag times than events without a snowpack for events with similar pre-storm groundwater saturation levels most likely due to the additional water released from the snowpack. The exception to this is event 94S8 which had low intensity rainfall during the initial hours of the event. The equations for the best-fit lines plotted on Figure 6.10 for the rain-on-snow events, excluding 94S8, and the snow-free events are shown in Table 6.4. These best-fit lines are

Figure 6.10 Site averaged pre-storm saturation level versus time lag in response for the clear-cut monitoring site.



93S22	Storm ID
13	Peak 1 hour rainfall intensity (mm)
◆	Rainfall with no snowpack
●	Rain-on-snow storm

not statistically significant and represent lines fitted to show a general relation between the variables. The results of the analysis of pre-storm saturation level and response lag suggest that the presence of a snowpack reduces response lag. The relationships for both rain-on-snow and snow-free events suggest that when  $m$  is above 0.55 there is less than a two hour lag in response of the groundwater table to surface water inputs. This shows the rapid response of the groundwater table to inputs during high antecedent moisture conditions.

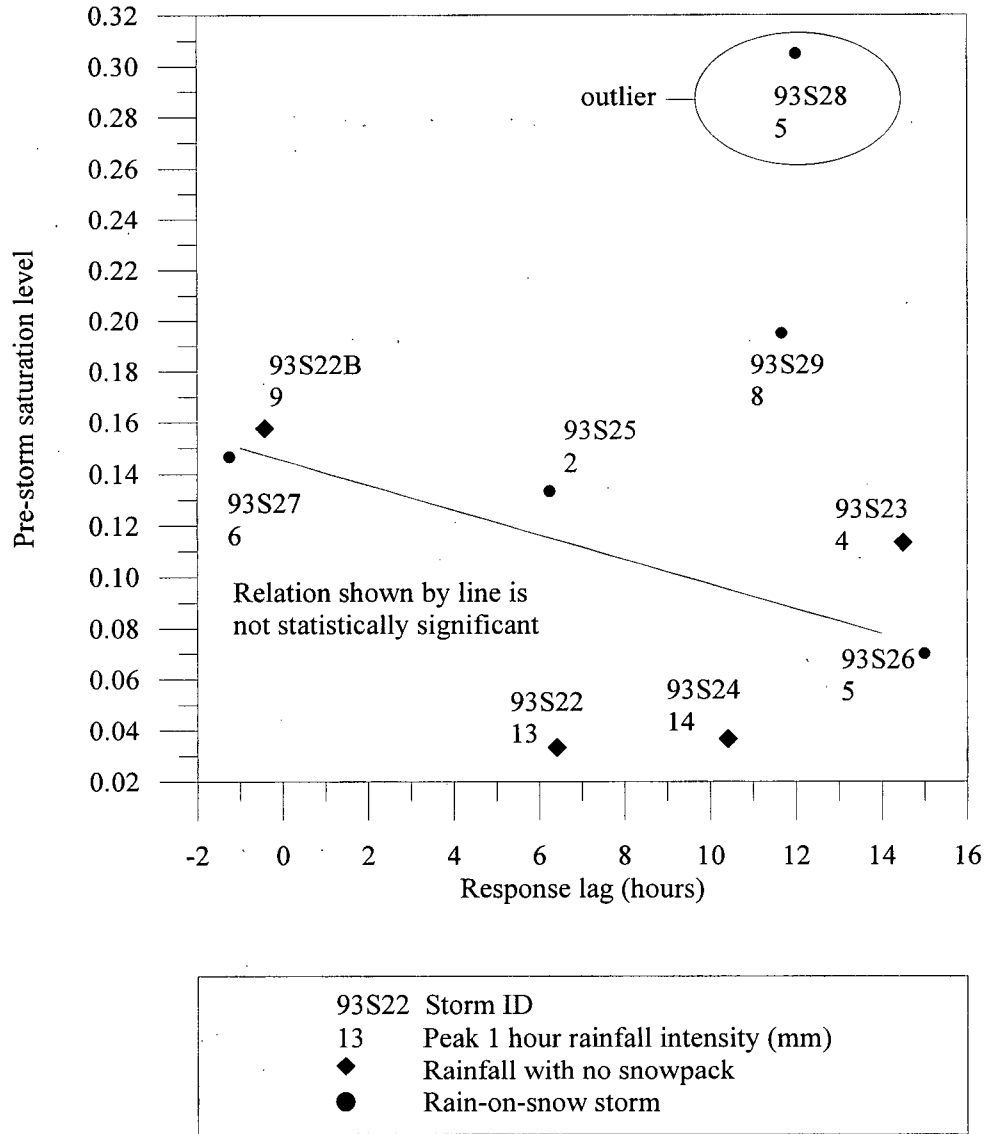
Figure 6.11 shows the lag time as a function of the pre-storm groundwater saturation level at the old-growth site. The data from this site do show a weak trend between prestorm groundwater level and response time for the rain-on-snow and snow-free events, although the trend is not distinct enough to separate the data points into distinct event types. Storm 93S28 was an outlier in that although there was a high pre-storm saturation level, the lag in response was close to 12 hours. During this storm the freezing level was observed to be close to the elevation of the old-growth site, which is believed to explain why this point did not have a quicker response time. The best-fit line for all events on Figure 6.11 is listed in Table 6.4 and it is important to note that this relationship is not statistically significant. The lack of a statistically significant relationship for the old-growth site is not surprising given the lack of on-site rainfall data.

Table 6.4 Relation of lag time and pre-storm saturation level.

Event type:	Rain-on-snow	Snow-free	All events
Clear-cut site	$\text{lag} = -76.9 m + 40.8$	$\text{lag} = -90.9 m + 52.7$	N/A
Old-growth site	N/A	N/A	$\text{lag} = -173.9 m + 25.7$

Note: equations in Table 6.4 are not statistically significant

Figure 6.11 Site averaged pre-storm saturation level versus time lag in response for the old growth monitoring site.



One observation that can be made in comparing the two groundwater monitoring sites is that pre-storm groundwater levels at the old-growth site were generally lower than those at the clear-cut site. This was believed to be a result of the differences in the soil profile and the higher elevation of the old-growth site. The colluvially derived portion of the old-growth soil profile increases the void ratio of the upper soil profile and could also provide large voids and preferential flow paths at depth, as seen in soil pit OG3. Here, flow was observed through an old rockfall layer exposed in the soil pit excavation. The elevation and location of this site was an important factor in explaining differences between the two monitoring sites. The average elevation of the old-growth site is 100 metres greater than that of the clear-cut site and it is separated from the clear-cut monitoring site hillslope by a saddle. The exact influence of the hill that shields the old-growth monitoring site is not known. During some of the mixed-temperature storm types observed over the study period snowfall would be occurring at the old-growth site while rainfall was occurring at the clear-cut site.

#### **6.3.2.2 Determination of groundwater response rate**

One of the response characteristics of interest is the sensitivity of the groundwater response rate to rainfall intensity. Studies in Japan by Okimura (1982) and in Oregon by Pierson (1980) have shown that groundwater response rate is directly related to rainfall intensity. As rainfall intensity increases, rate of rise of the groundwater table also increases. The discussion of this characteristic was restricted to the clear-cut site where there was on-site rainfall information. In the following discussion of results, the point for

storm 93S22 is not included since it was the first large storm of winter 1993-94 and the seasonal water table was not yet established.

Figure 6.12 shows 1 hour rainfall intensity versus response rate from a number of observed storms. There appears to be a weak positive relation between the two variables which is described by  $y = 14.3x + 4.6$ . This relation is not statistically significant. There did not appear to be any relation between rainfall intensity and lag in response time for the same interval. Figure 6.13 shows the relation between 3 hour rainfall intensity and maximum response rate. The 3 hour graphs show more scatter than the 1 hour data as a result of the larger range in intensities over this time interval. Figure 6.13 shows a non-significant positive relation that is described by  $y = 49.31x + 6.87$  while only a weak negative relationship was found between rainfall intensity and lag in response time.

No consistent relationship was found between the maximum groundwater response rate and lag time. What the analysis did show was a main clustering of points around  $m=0.5$  and a smaller cluster occurring around  $m=0.3$ . The main clustering at  $m=0.5$  is thought to reflect the interface between the Ah and Bm horizons.

The variation in values in the previous four graphs is likely due to averaging of the individual borehole groundwater response lag times to obtain the average site lag time for individual events. Another probable source of error in the analysis is that the peak response rates could be produced by rainfall intensities slightly below the maximum storm intensity. The initial groundwater response at both sites for most storms was very rapid showing the rapid transfer of water through the unsaturated zone. If the upper portions of the soil profile have a greater porosity than the lower horizons, then the

Figure 6.12 1 hour intensity versus maximum response rate for Russ4

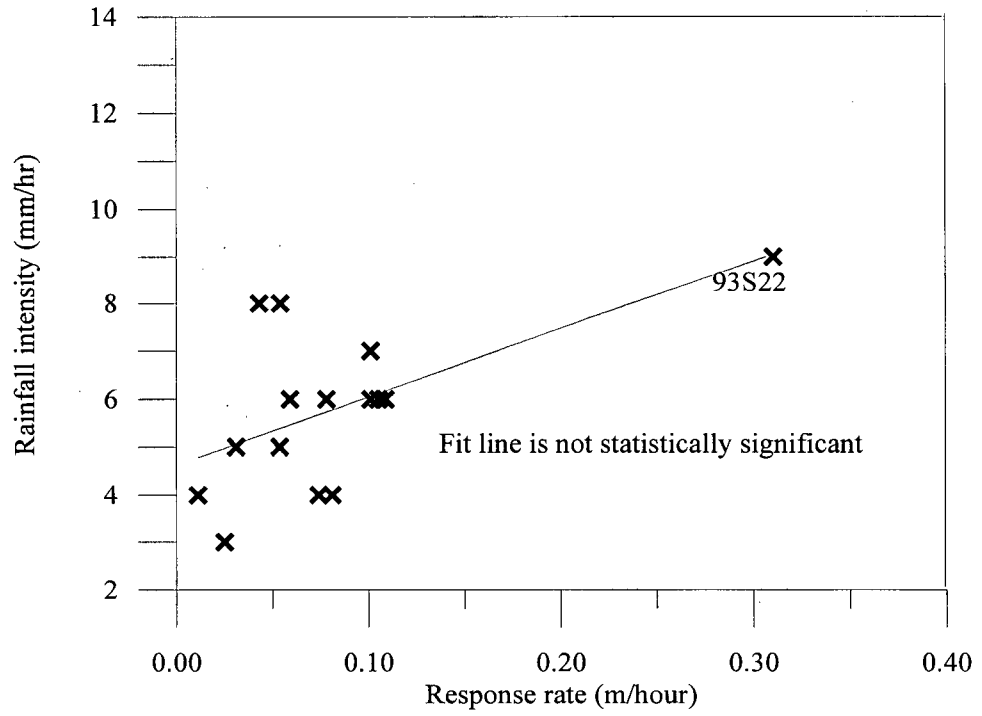
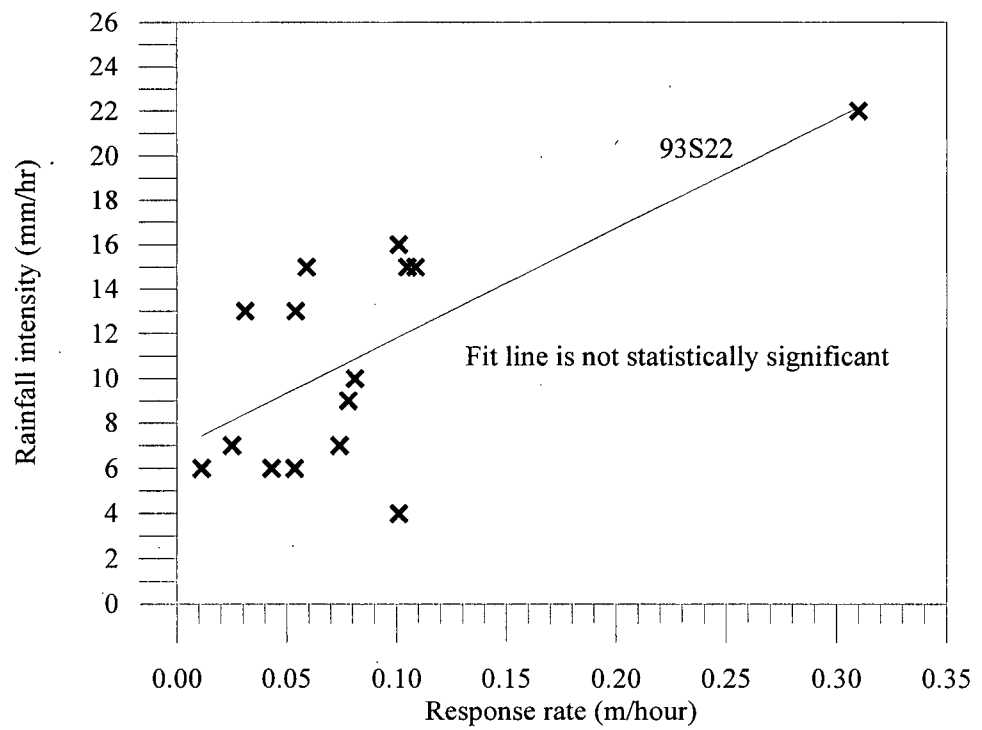


Figure 6.13 3 hour intensity versus maximum response rate for Russ4



occurrence of the maximum rainfall intensity after the groundwater table has risen to the upper portions of the soil profile would not produce a comparable groundwater response rate. In other words, the presence of a higher K layer over a lower K layer will cause attenuation of the groundwater peak.

### **6.3.2.3 Groundwater recession**

The discussion of groundwater recession and the rates described below are taken from examination of Figures 6.7a, 6.7b, 6.8a, and 6.8b. The recession rates discussed in this section refer to changes in the re-scaled hydrograph for each site, and as such have unit of  $(\text{time})^{-1}$ . As mentioned in Section 6.2, the recession rates at the groundwater monitoring sites show considerable variation between boreholes at a site. At the clear-cut monitoring site, the recession rate in the first 24 hours following a rainfall event varied from 0.06 to 0.14 per day with an average of 0.10 for holes that were matrix drained. Following this initial rapid drainage period, these holes drained at a consistent rate of between 0.01 to 0.03 per day for several days. At holes where macropores are believed to assist drainage, the recession rate in the first 24 hours following a storm averaged 0.2 with a maximum of 0.3 per day. At the old-growth monitoring site, the hole that was matrix drained had an average recession rate of 0.25 in the first 24 hours following an event. After 24 hours, this borehole drained at approximately 0.02 to 0.03 per day. The holes believed to have been macropore assisted drained rapidly at a rate of approximately 0.2 per day. The rapid drainage of all holes at the old-growth monitoring site suggests that the upper soil layer at this site is well drained by macropores or large voids. This observation concurs with the

results of visual observations from soil pits that the soil is rubbly and derived from both talus deposits and morainal deposits.

#### **6.3.2.4 Snow melt contributions to groundwater**

This section deals with the estimation of snowmelt values during the study period. The results of the estimated maximum possible 24 hour snowmelt inputs to the groundwater system are shown in Table 6.5. These values represent the maximum theoretical snowmelt from Equations 4.9 and 4.11 and as such the values would often exceed the actual snowmelt inputs at the site.

From Table 6.5 it can be seen that melt estimates made for 285 days of the study period resulted in 160 days predicting the occurrence of melt. The melt estimates listed in the table are not corrected for slope aspect and so may represent over-estimates of the actual melt that occurred on a given day. The last two columns of Table 6.5 show the number of days in a given melt class during which rainfall occurred and the average rainfall during those days. A total of 66 days with snowmelt and rainfall were predicted. These data show that rainfall did not occur on days with greater than 780 mm. of estimated melt. Rainfall occurred most frequently during days with less than 80 mm. of snowmelt and was also abundant during days with up to 160 mm. of melt. From the estimated frequencies in Table 6.5 it is assumed that maximum snowmelt inputs during storms in the Tsitika are typically in the range 200 mm to 300 mm of water.

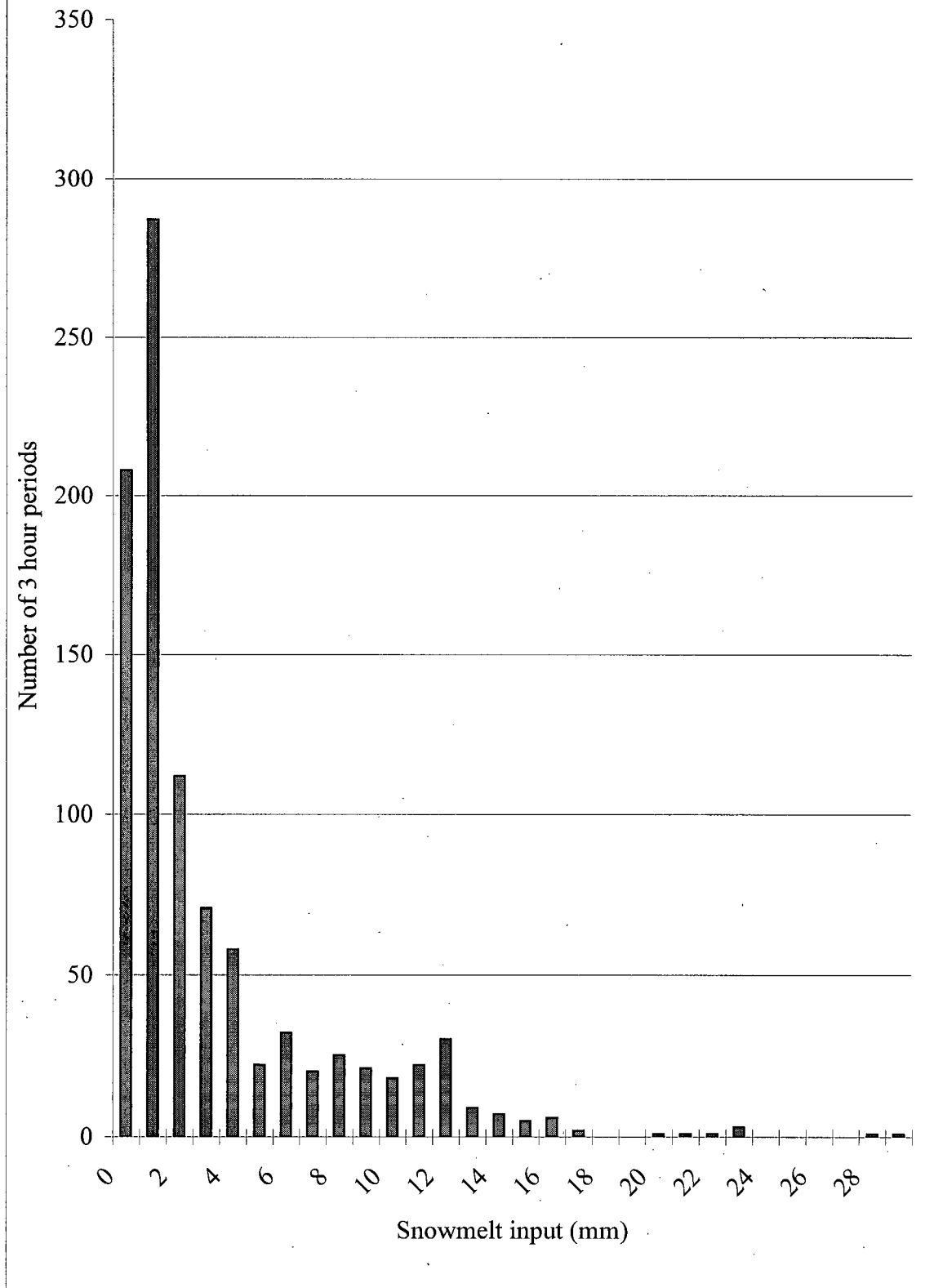
The 24 hour duration for the determination of snowmelt values in Table 6.5 is too long for modeling purposes. Estimates of the 3 hour snowmelt values during the period November 1993 to March 1994 were calculated using scaled versions of Eqn 4.9 and 4.11

Table 6.5 Estimated maximum 24 hr snowmelt frequency classes based on measured temperature and rainfall and derived from Eqn. 4.9 and 4.11.

Melt (mm)	Frequency	Cumulative %	days with rain	Average rainfall (mm)
78	64	40.00%	27	12
157	24	55.00%	14	8
235	19	66.88%	8	19
313	7	71.25%	5	11
392	6	75.00%	4	9
470	9	80.63%	3	3
549	7	85.00%	2	11
627	5	88.13%	1	1
705	5	91.25%	1	11
784	1	91.88%	1	3
862	1	92.50%	0	0
940	4	95.00%	0	0
>1000	8	100.00%	0	0

and used in the saturation model (see Figure 6.14). The histogram of melt values in Figure 6.14 shows that most frequently snowmelt input during a three hour period was less than 2 mm. The typical range of estimated values for the 3 hour snowmelt water input is 1 mm. The maximum estimated 3 hour snowmelt input was 29 mm of water equivalent. From the average rainfall it can be seen that snowmelt contributions to groundwater may be significant. In the following chapter on groundwater modeling, the storms that occurred during the modeled period are discussed as to the importance of snowmelt contributions to the groundwater table.

Figure 6.14 Histogram for theoretical 3 hour snowmelt inputs during the study period, derived from Eqn. 4.9.



## Chapter 7 Groundwater modeling

The chapter contains the results of an empirical model that was calibrated to simulate the groundwater table at the clear-cut monitoring site. The groundwater time series was simulated for rainfall events during which data were available from the clear-cut monitoring site rain gauge R4 which was connected to the same data logger as the pressure transducers. The modeling of groundwater response, as estimated by Eqn. 2.5, was done using a spreadsheet program and a 486 personal computer. The chapter is broken into two main sections that deal with the model inputs and the results of the modeling. The results of the modeling section includes discussion of the calibration of the model and the application of the model to storms during which instability is known to have occurred in the Russell Creek sub-basin.

Modeling of the groundwater time series was not done for the first large event of the storm season because of the difficulty encountered in modeling the initial development of the seasonal groundwater table. The level of the simulated saturated layer was updated using a 3 hour time interval and compared to the averaged observed saturated layer level for the same 3 hour interval. Initial modeling was conducted using a 1 hour time interval but the model was found to be too sensitive to snowmelt and rainfall inputs. The rainfall events during the modeled period are discussed in section 7.1.1 as to the importance of snowmelt input to the groundwater system.

## **7.1 Inputs to the groundwater model**

This section deals with the specific inputs used to model the response of the groundwater system. Discussion of the rainfall events that were observed to occur during the modeled period are first presented, followed by the parameterization of the model.

### **7.1.1 Rainfall events during the modeled period**

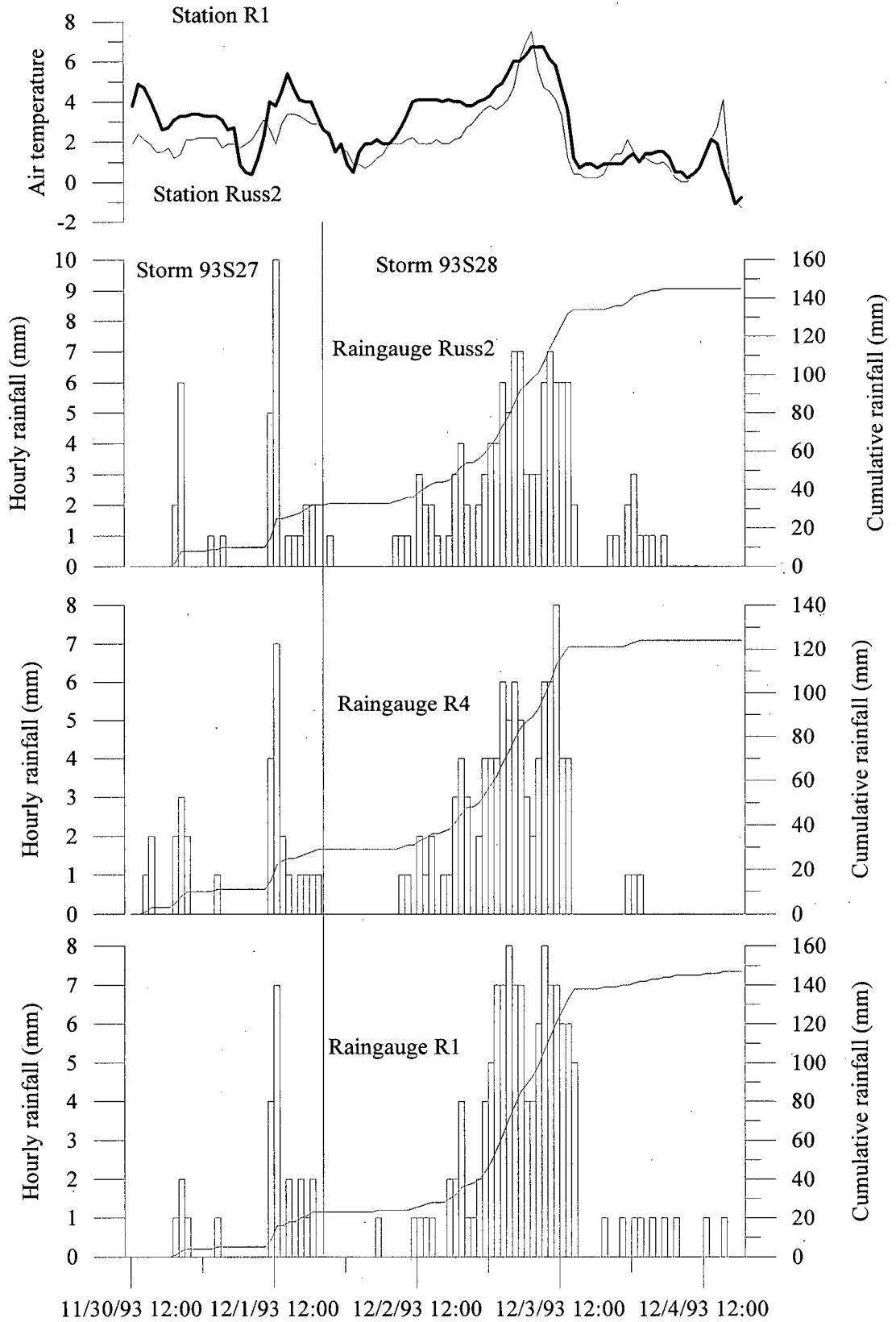
This section contains discussion of the time series for rainfall events used for the modeling. A total of nine storms, from the fifteen that occurred during the record of groundwater levels, were used for calibration of the model. The calibrated model was then run using rainfall time series from other rain gauges that were operating during the two storms (93S3 and 94S16) known to have initiated failures in Russell Creek. The discussion of individual storms in this section is limited to two large and three medium storms used for in calibration of the model.

The conditions at the monitoring sites during each event is discussed as is the probable importance of snowmelt recharge to the groundwater system. Snowpack estimates in this section were collected by Craig Nistor, U.B.C. Geography, at the lower edge of the cutblock containing the clear-cut monitoring site. Due to the sheltering effect of trees and the lower elevation of the measurement site, the snowpack estimates represent minimum depths at the monitoring site.

#### **Storm 93S28 December 2-3, 1993**

The time series for this storm is shown in Figure 7.1. Precipitation during this storm was most intense at 0100 on December 10. After approximately 0600 on that day the

Figure 7.1 Rainfall and temperature for Storm 93S28



temperature at Russ2 fluctuated around  $2^{\circ}\text{C}$  and rainfall lessened. It is possible that precipitation during the latter portions of this storm was a mixture of rain and snowfall. Snowpack depth measurements prior to this event were estimated to range from 10 cm to 40 cm at the clear-cut monitoring site. There is good agreement between the three rain gauges as to the timing of maximum rainfall intensities during this event.

#### **Storm 93S29 December 9-10, 1993**

The time series for this event is shown in Figure 7.2. Temperatures during this event at sites Russ2 and R1 were below  $2^{\circ}\text{C}$  for most of the duration of the event. At site R4 precipitation was a mixture of rain and snowfall due to the greater exposure of this site as compared to site Russ2 which is located lower in the same clear-cut as R4. Large differences are observed in the rainfall timing and totals for the three rain gauges. The lack of measured rainfall at R4 over the afternoon of December 9, coupled with the low air temperatures at Russ2, suggest that precipitation was in the form of snowfall at R4.

#### **Storm 93S24 November 14-15, 1993**

The time series for this storm are shown in Figure 7.3. Precipitation at the monitoring sites during the initial hours of this storm are believed to have been rainfall. At around 0300 on November 15, 1993 precipitation at the clear-cut monitoring site is believed to have consisted of a mixture of rain and snowfall. This is reflected by the cessation of measured rainfall at the Russ2 rain gauge with a drop in air temperature to below  $2^{\circ}\text{C}$ . A snowpack of approximately 12 cm was recorded near the elevation of the old-growth monitoring site near the time of this storm (C. Nistor, pers. comm., 1995). No

Figure 7.2 Rainfall and temperature for storm 93S29

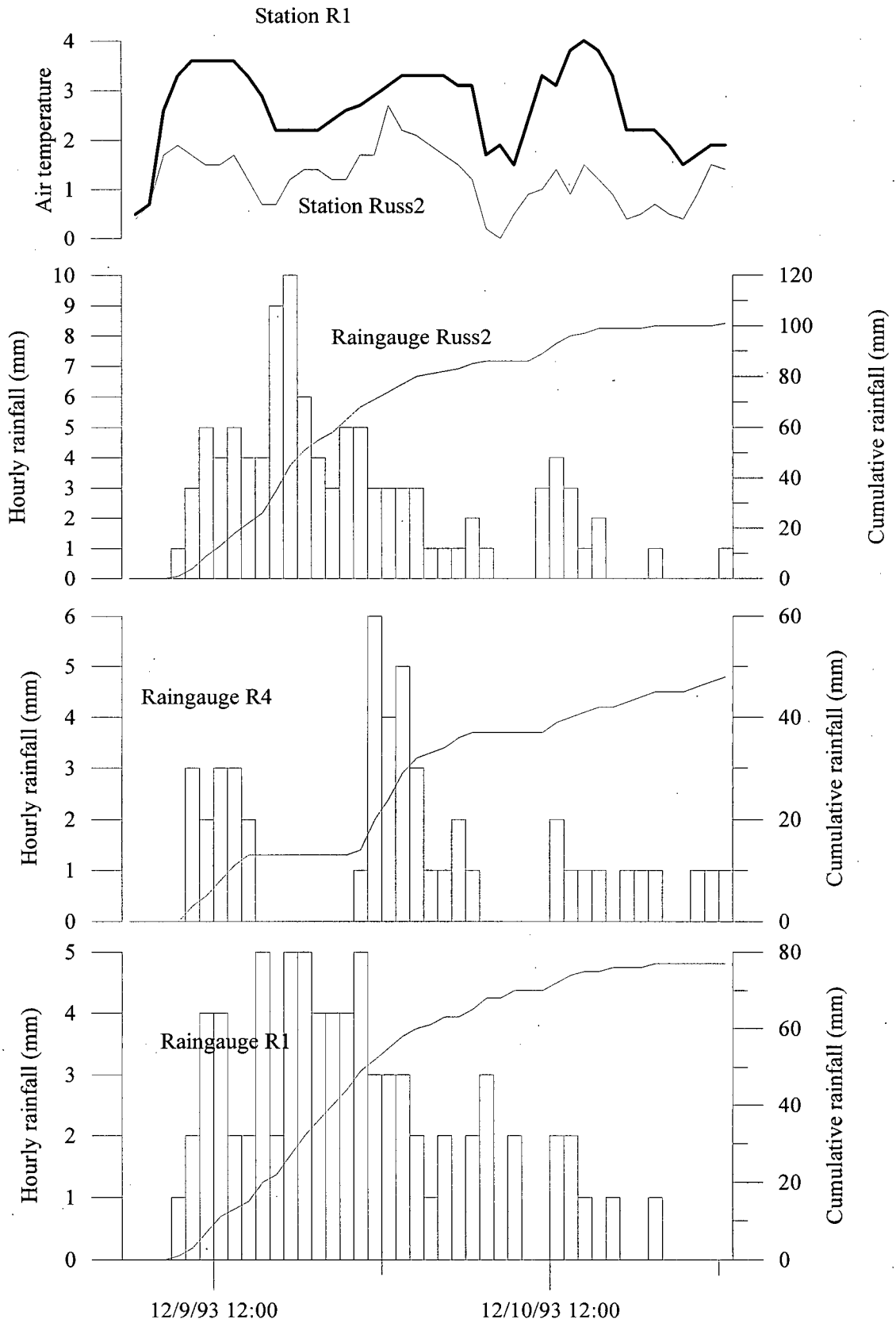
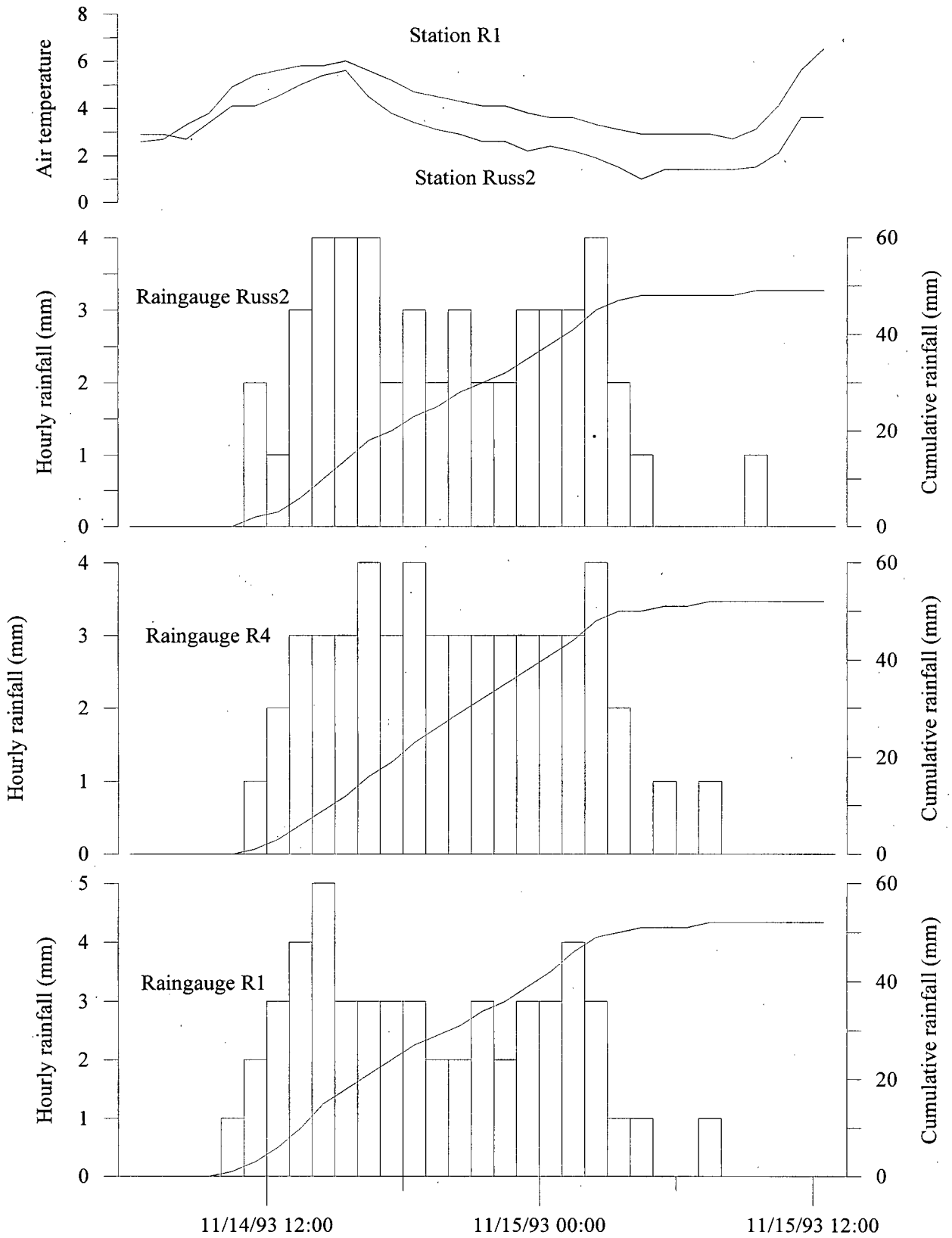


Figure 7.3 Rainfall and temperature for storm 93S24



snowpack was recorded at a site 40 m in elevation lower than the clear-cut monitoring site prior to this event. The three rain gauges show good agreement between the start of rainfall and the cumulative rainfall at each site.

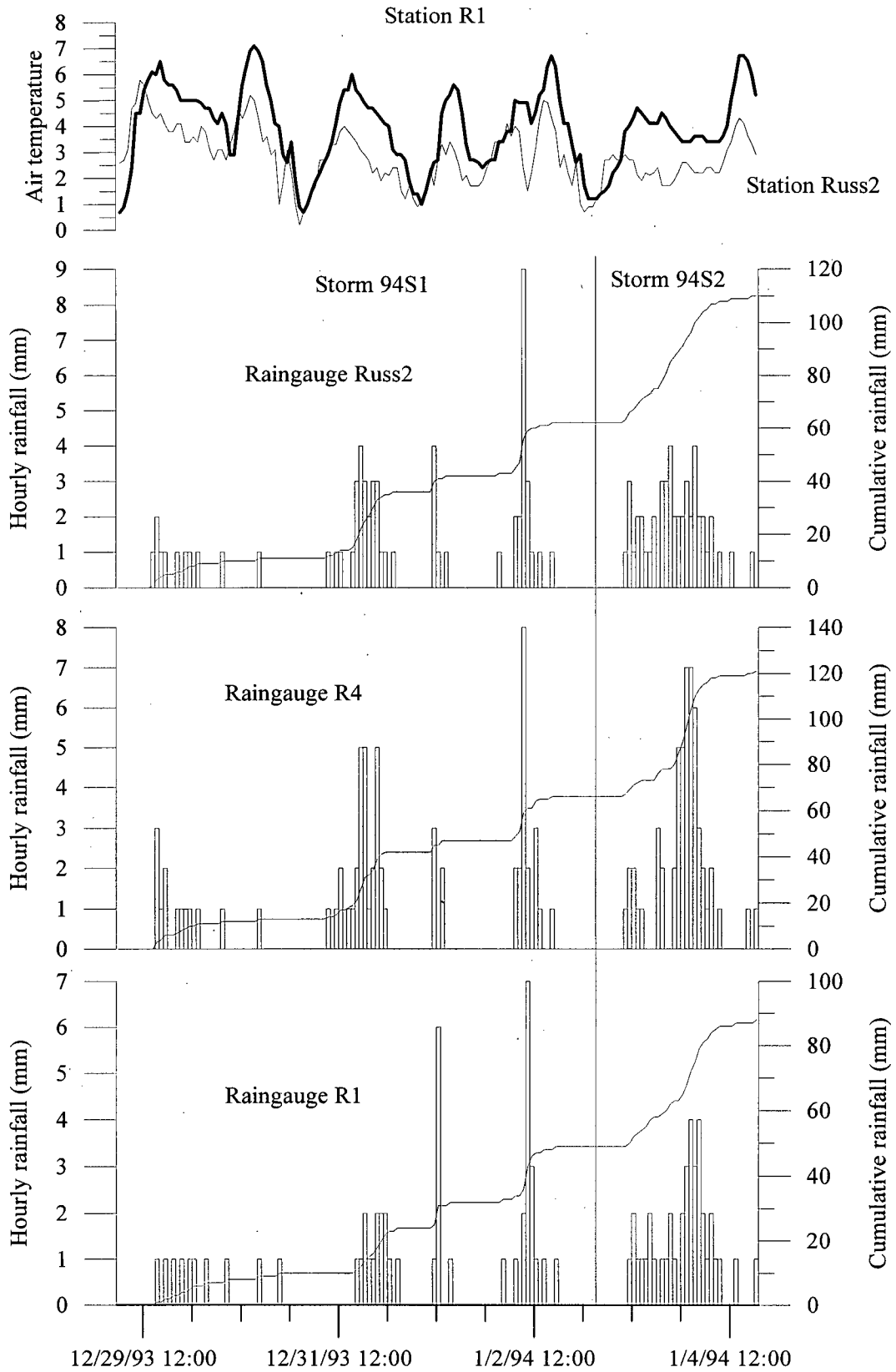
#### **Storm 94S1 December 31 to January 2, 1994**

The time series for this storm is shown in Figure 7.4 and represents the passage of multiple fronts over several days. Based on personal observations of the patterns in precipitation for the early portion of this storm it is known that precipitation on December 31 was entirely rainfall. On January 1, 1994 precipitation was a mixture of rain and snowfall. Records of discharge for a gully draining the clear-cut monitoring site showed that there were distinct peaks which correspond to the periods during which intense rainfall was recorded at site Russ2 and R4. Rain-on-snow is believed to have been an important recharge source for groundwater and streamflow during this event.

#### **Storm 94S2 January 3-4, 1994**

The time series for this event are shown in Figure 7.4 and the event was closely preceded by event 94S1. During this event it is believed that precipitation was predominantly rainfall but given the temperatures from Russ2 it is possible that at times during the event precipitation was a mixture of rain and snowfall. The streamflow records from a nearby drainage show larger flows than during the preceding event which is believed to be due to the concentration of rainfall over a shorter period of time.

Figure 7.4 Rainfall and temperature for Storm 94S1 and Storm 94S2



### **7.1.2 Snowmelt inputs to the groundwater model**

Determination of snowmelt contributions to the groundwater table was described in Section 6.3.2.4. Pre-storm snowpack thickness estimates for modeled storms were taken from field observations. To determine the amount of water in the snowpack it was necessary to assume a density for the snowpack. Initial snowpacks have a density of approximately  $100 \text{ kg/m}^3$  and as the winter progresses the snow changes form and becomes more dense with reported spring snowpack densities ranging from 300 to 500  $\text{kg/m}^3$  (Dunne and Leopold, 1978). The model determined the maximum level of melt by assuming an initial density between 0.1 and 0.5 for the pre-storm snowpack and determining the water equivalent. The individual pre-storm snowpack densities used in the modeling are contained in Section 7.2.1

### **7.1.3 Parameter determination for the groundwater model**

The lag times between the start of rainfall and the start of the groundwater response were used to determine the integration rate for rainfall inputs. The equation was determined from the relationship determined for rain-on-snow events in section 6.2.2 and the observed level of the groundwater table prior to the start of the event being modeled. The decision was made to attempt to use the rain-on-snow lag relationship as more data were available for this type of event.

Initial attempts to incorporate the lag relationship determined in section 6.2.2 were not successful as model response was well below the observed response if there was a no rain period preceding the event. The reason for this was believed to be the drainage of soil pores and the development of tension (negative pore pressures) in the unsaturated zone

during the no-rain period. For the final model it was decided to simulate the movement of water through the unsaturated zone based on the amount of incoming precipitation. The algorithm used for rainfall inputs is shown in Figure 7.5. For periods where there was greater than 24 hours without rain the incoming interval rainfall total was examined and, if the total was less than 5 mm., the water was assumed to be held in the unsaturated zone. During the next interval if the rainfall total for the two intervals was greater than 5 mm. the total rainfall from the two intervals was used to determine the increase in the groundwater table. If the rainfall total for the two intervals was less than 5 mm all rainfall input was assumed to be held in the unsaturated zone until the next interval when ,regardless of the rainfall total for the interval, all rainfall was assumed to have reached the saturated zone.

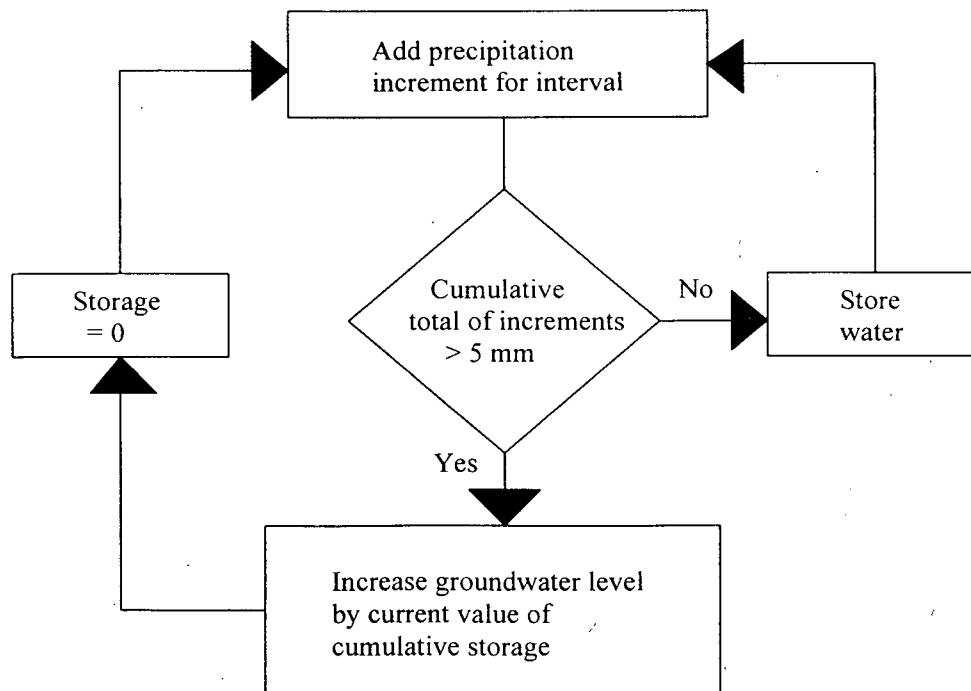


Figure 7.5 Algorithm for modeling saturation response to rainfall and snowmelt inputs

The 5 mm. rainfall threshold value is meant to reflect gravity drainage of the soil matrix during a no rainfall period. Following a no rainfall period, rainfall infiltrating into the soil would be used to satisfy any negative pore pressures within the matrix. Once any water deficits within the unsaturated matrix were satisfied additional water inputs would then be transmitted through the unsaturated zone to the saturated layer. The determination of the 5 mm. rainfall total was based on testing of the model. When a lower threshold was used then the model would yield unrealistic responses from rainfall inputs of 1 mm. to 4 mm. in consecutive intervals following a no rainfall period.

The soil profile in the model was represented as a two layered system with different porosities. This reflects the higher porosity Ah Horizon overlying the lower porosity Bm Horizon observed in soil pits. The relative thickness of the individual soil layers was based on observed information from soil pits.

Initial modeling, using a variable effective porosity,  $n_e$  value, yielded gross inaccuracies in the level of the saturated layer. In the final model a single value of effective porosity was chosen for each soil layer. For the upper soil layer a value of  $n_e = 0.50$  was chosen while a value of  $n_e = 0.12$  was chosen. The value of effective porosity used in the model represented the value of  $n_e$  at a pressure of -0.25 m of head determined from soil moisture retention tests the laboratory. The relationship determined from the gravity drainage tests was rejected as the values of  $n_e$  estimated by that test yielded extremely large fluctuations in the simulated saturated layer thickness. Given the lack of snowmelt data and the use of averaged groundwater data used in the modeling the choice of the value for  $n_e$  was not considered to be the dominant limiting factor in the model results.

Based on the observed groundwater time series at the two monitoring sites it was apparent that modeling the recession rates for the soils was not a simple matter.

Recession rates were chosen for the model based on examination of observed recessions for the averaged saturated layer time series. The recession rate chosen represents the slope of the recession curve for the averaged saturated layer. As the modeling of the groundwater was done using rescaled hydrographs, the breakpoints in the recession rates correspond to normalized saturated zone thicknesses,  $m z/z$ , and not actual saturated layer thickness. The recession rates used to simulate the decay of the groundwater table are shown in Table 7.1.

Table 7.1 Recession rates for groundwater modeling

Relative saturation level (m)	Recession rate ( $\Delta m/3$ hr.)
> 0.7	0.0530
0.65	0.0400
0.6	0.0350
0.55	0.0300
0.525	0.0250
0.5	0.0200
0.475	0.0090
0.45	0.0040
0.425	0.0015
<0.425	0.0010

When rainfall was observed the recession rate was subtracted from the increase in the saturated layer thickness to simulate continuous drainage of the soil. The use of a minimum rainfall threshold of 2 mm was arbitrarily chosen as it was found that fluctuations could develop in the simulated saturated layer thickness if 1 mm of rainfall was allowed to influence the recession rate.

## **7.2 Results of modeling of the groundwater system**

This section deals with the results of the empirical modeling of the groundwater table at the clear-cut site. The section is divided into two parts that deal with the modeling of the groundwater table over individual or closely spaced groups of events and a section that deals with the application of the model to estimate water levels during storm 93S3 and 94S16 which were known to have initiated instability in Russell Creek. For both sections the model results are presented in terms of the relative saturation level,  $m$ , of the soil profile based on the average of three groundwater wells at the site. This stratification of  $\Delta m/\Delta t$  is justified given the coarser texture of the uppermost soil layer.

### **7.2.1 Calibration of model using individual or grouped rainfall events**

This section deals with the results of the modeling of the individual, or grouped, rainfall events discussed in section 7.1.1. A summary of the snowmelt inputs and the groundwater response results for selected modeled storms is shown in Table 7.2. All modeled results in this section are based on the same 3 hour interval from site R4 discussed in the previous section. The first two storms were modeled without snowmelt inputs to the groundwater system based on field observations of the snowpack near the monitoring site.

Table 7.2 Summary of model storm characteristics for modeled storms

Storm	Estimated Snowpack Thickness (cm)	Assumed Snowpack Density (gm/cm <sup>3</sup> )	Maximum snowmelt contribution (mm)	Observed response	Estimated response
93S23	0	0	No snowpack	0.69	0.59
93S24	0	0	No snowpack	0.60	0.60
93S25	45	0.1	125	0.56	0.51
93S26	30	0.1	60	0.60	0.45
93S27	0	0	0	0.55	0.53
93S28	0	0	0	0.60	0.64
93S29	35	0.2	11	0.59	0.57

The results of groundwater modeling for storms 93S24 and 93S25 are shown in Figure 7.6. This storm sequence represents the start up of snowmelt inputs to the model. The model shows excellent response during Storm 93S24 estimating the same 0.28 change as the observed groundwater response. The model maximum relative saturation level was 0.51 compared with the observed value of 0.56. The pre-storm snowpack level is not known for storm 93S25 but it is known that constant accumulation did occur during the period between the two storms. The start up of snowmelt input to the model was assumed to be 0000 November 17.

The results of groundwater modeling for storms 93S26, 93S27, and 93S28 are shown in Figure 7.7. The model response during 93S26 was 0.45 compared to an observed response of 0.60. The underestimation of response by the model is believed to be due to the low recorded rainfall during this storm. All of the estimated pre-storm snowpack was melted during storm 93S26 and so for the other two storms in the sequence no additional snowmelt was contributed to the model. No observations from the field site are available to determine if this in fact occurred. The model response during

Figure 7.6 Groundwater modeling for storm sequence 93S24 and 93S24

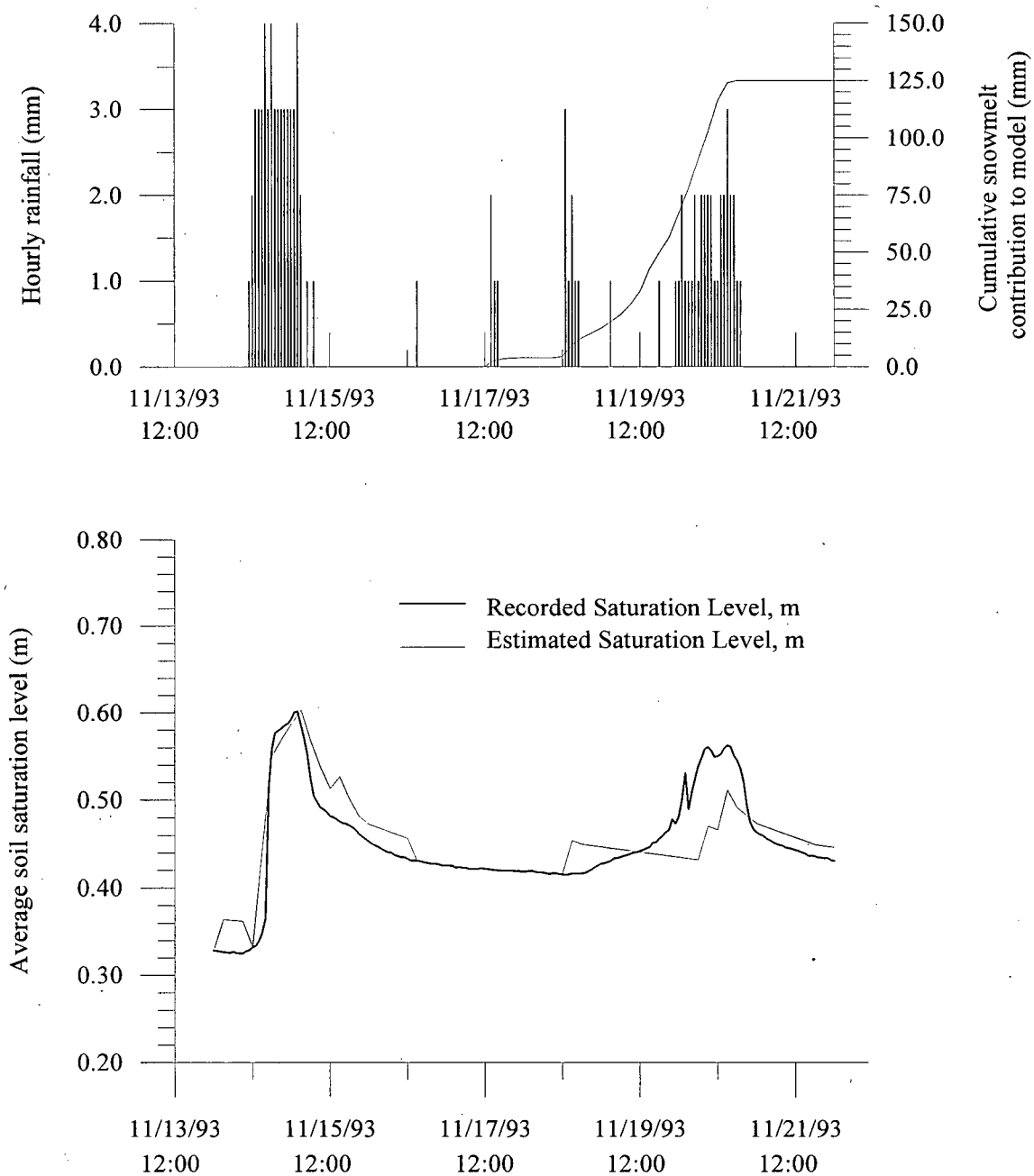
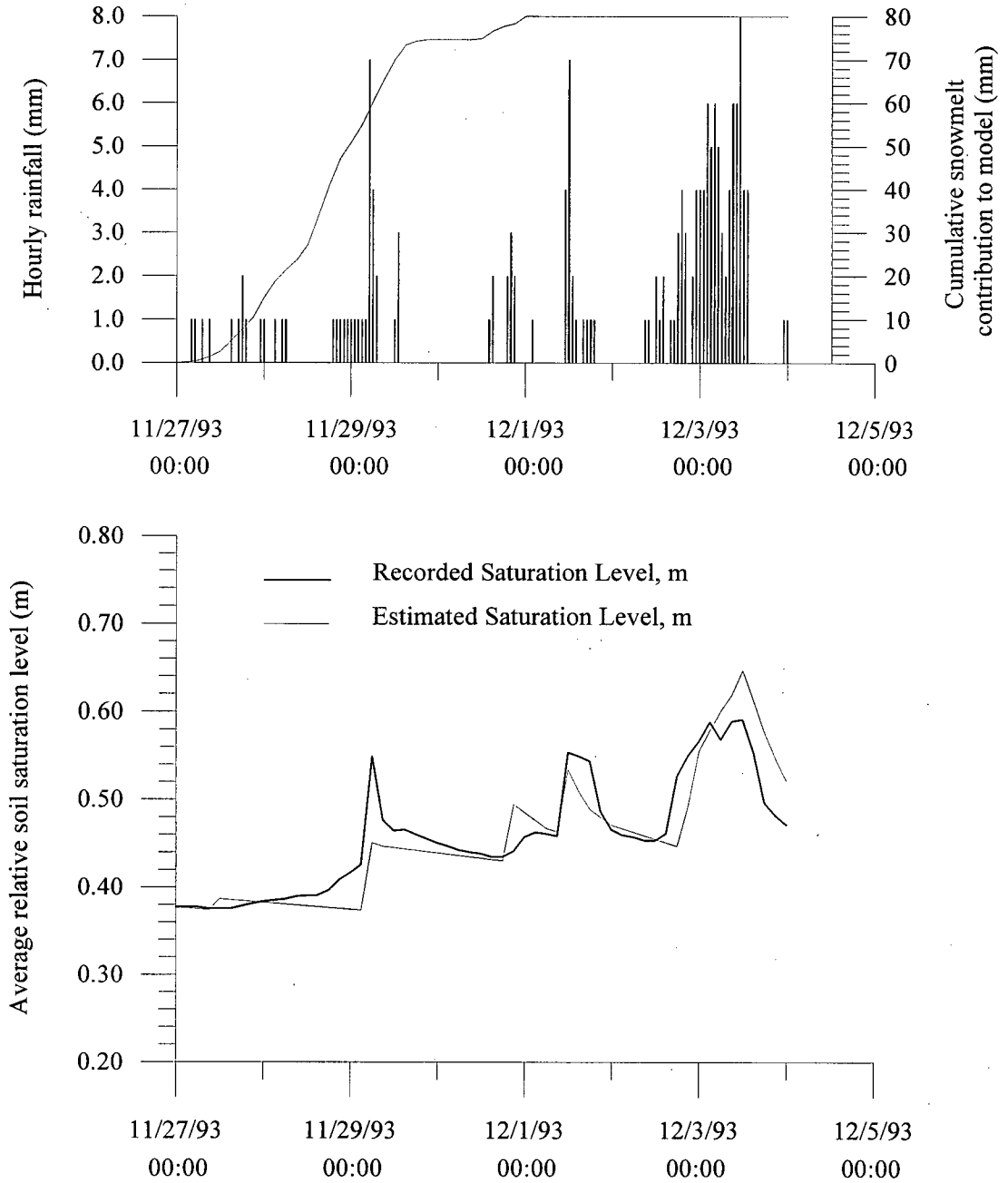


Figure 7.7 Groundwater modeling for storm sequence 93S26, 93S27, and 93S28



storm 93S27 was 0.53 compared to an observed value of 0.55. The model response during 93S28 was 0.64 compared with an observed value of 0.60. The overprediction of the response during 93S28 is believed to be due to the high total rainfall during storm 93S28.

The results of groundwater modeling for storm 93S29 are shown in Figure 7.8. The estimated maximum relative saturation level was 0.57 compared with a 0.59 observed maximum relative saturation level. The modeled response shows two sharp increases associated with the bursts of rainfall shown in Figure 7.8. The lag in the response is believed to be due to low air temperatures during this event causing plugging of the bucket of the rain gauge. Melting of the plug resulted in the rainfall burst early on December 11, 1993. A more extreme example of the freezing and melting of the tipping bucket is shown in the next storm sequence.

The results of groundwater modeling for storms 94S1 and 94S2 are shown in Figure 7.9. The observed saturation level appeared out of phase with the observed groundwater response and rainfall. This may have been the result of problems at site R4 due to freezing and melting in the aluminum funnel of the rain gauge. Field observations of tipping buckets have shown that the bucket, or funnel, may initially have a small plug of ice. Rainfall into the funnel will cause some ponding of water above the ice plug leading to the melting of the plug and a large burst of water into the tipping bucket. Examination of the temperature record for this storm show that air temperature during the period covered by the storm does fluctuate above and below  $2^{\circ}\text{C}$  which suggests that snowfall could also be responsible for blockage of the rain gauge.

Figure 7.8 Groundwater modeling for storm 93S29

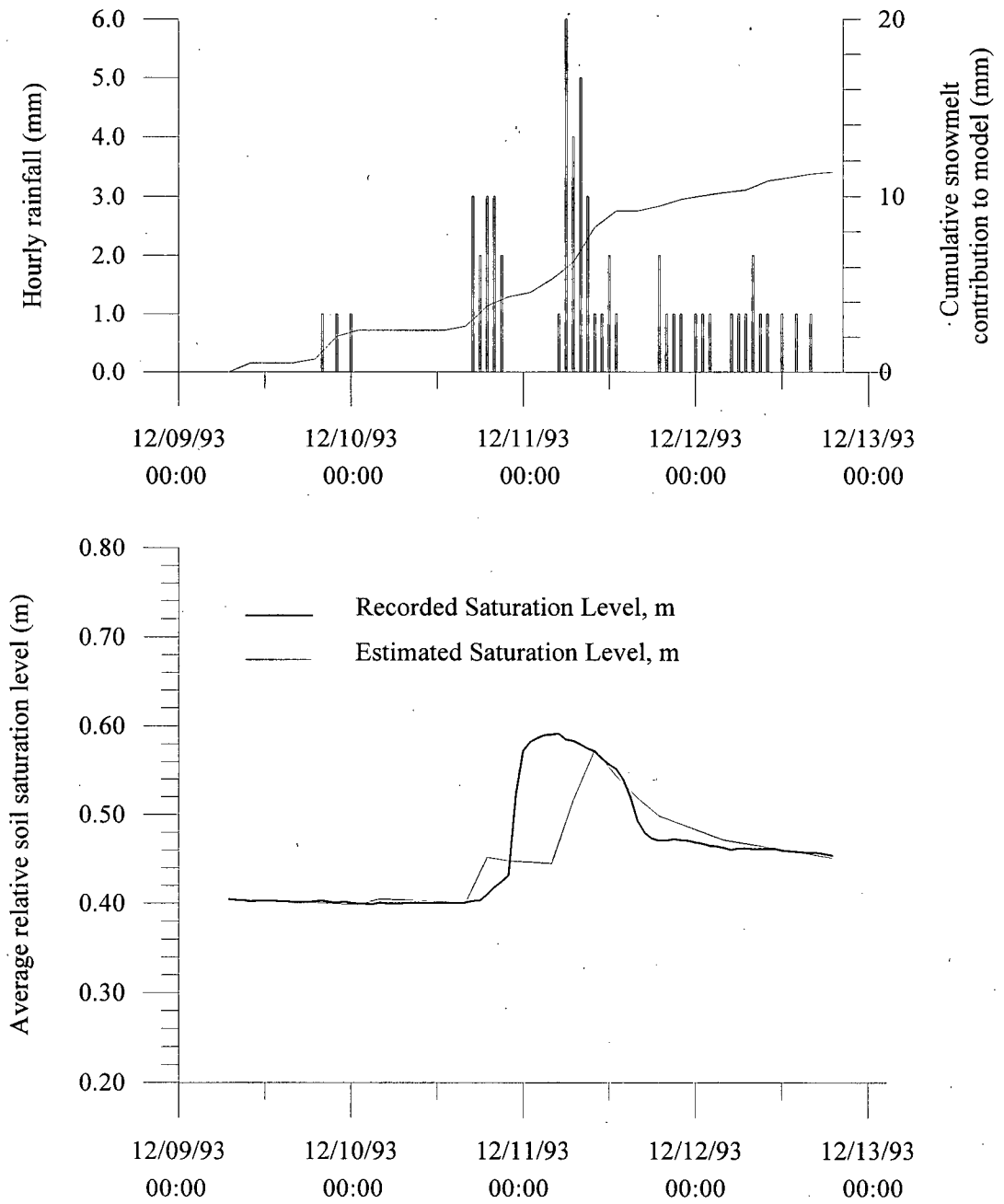
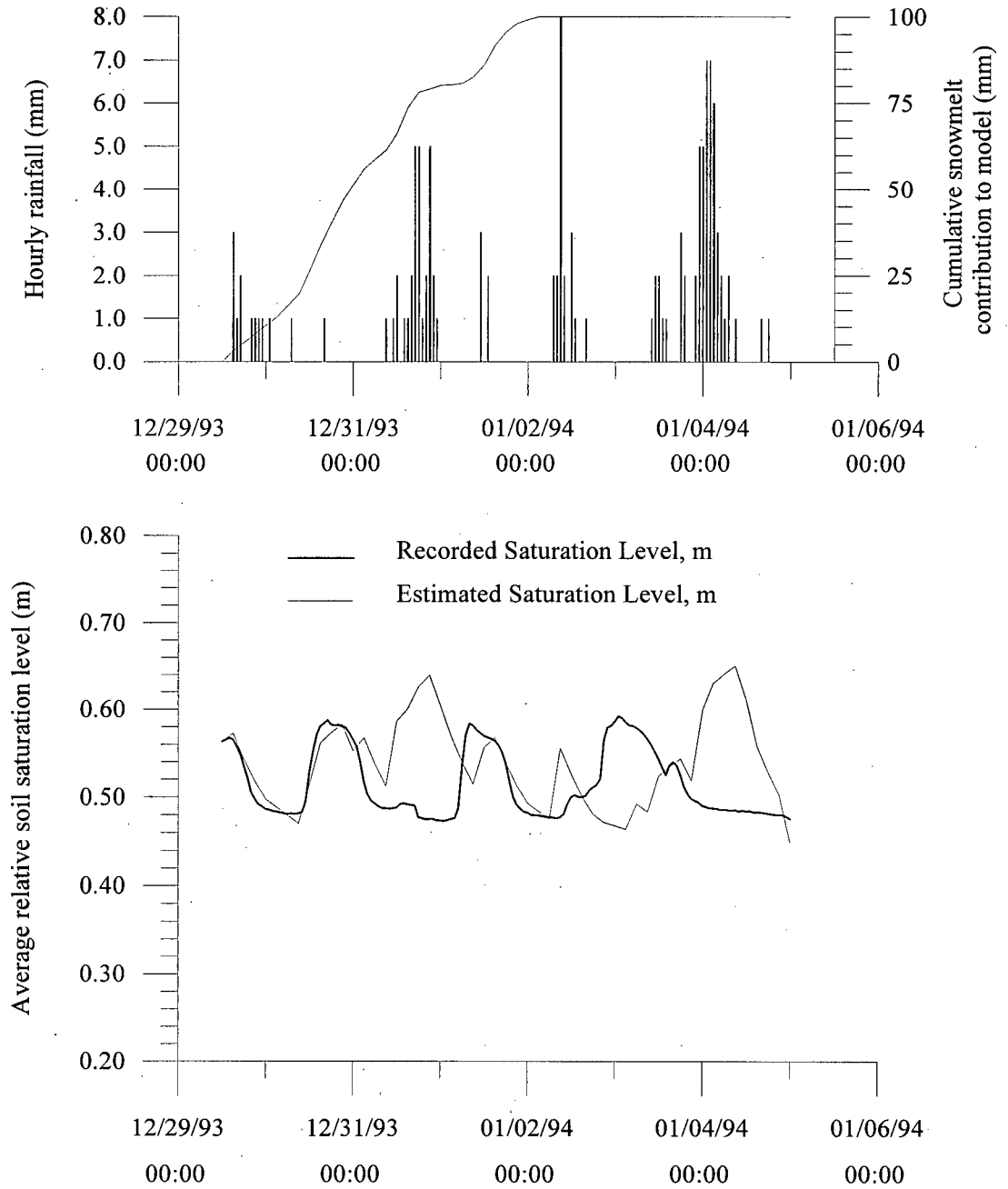


Figure 7.9 Groundwater modeling for storm sequence 94S1 and 94S2



## 7.2.2 Application of the model to storms known to have initiated instability in the Russell Creek basin

This section deals with the application of the groundwater model described above to storms 93S3 and 94S16, which are known to have initiated instability in the Russell Creek basin during the study period. No observed groundwater data were available from the two groundwater monitoring sites for either of these two storms. The application of the model to estimate maximum groundwater response levels during these two storms required the assumption of the pre-storm groundwater level. A range of pre-storm relative saturation levels between 0.4 and 0.56 were used as initial conditions for the modeling of the anticipated groundwater response.

The estimated groundwater responses for storm 93S3 are shown in Figure 7.10. The estimated maximum relative saturation levels should be considered as approximations as no snow melt information is available for this storm. It is known from field observations that there was approximately 1 metre of snow at the study area around this period but detailed pre- and post-storm snowpack depths, air temperatures and wind speed data are not available for this storm to allow for the estimation of the amount of snowmelt.

The estimated response for this storm is shown to vary with pre-storm relative soil saturation level, however there is convergence towards a similar saturation level during the middle of the storm. The maximum change in the relative saturation level ( $\Delta m$ ) was 0.18 during the latter portion of the storm. The maximum estimated saturation level was 0.67 during this event. The estimated groundwater responses for storm 94S16 are shown in Figure 7.11. It is known that approximately 30 cm of fresh snow in the area of the

Figure 7.10 Modeling of relative groundwater response for storm 93S3

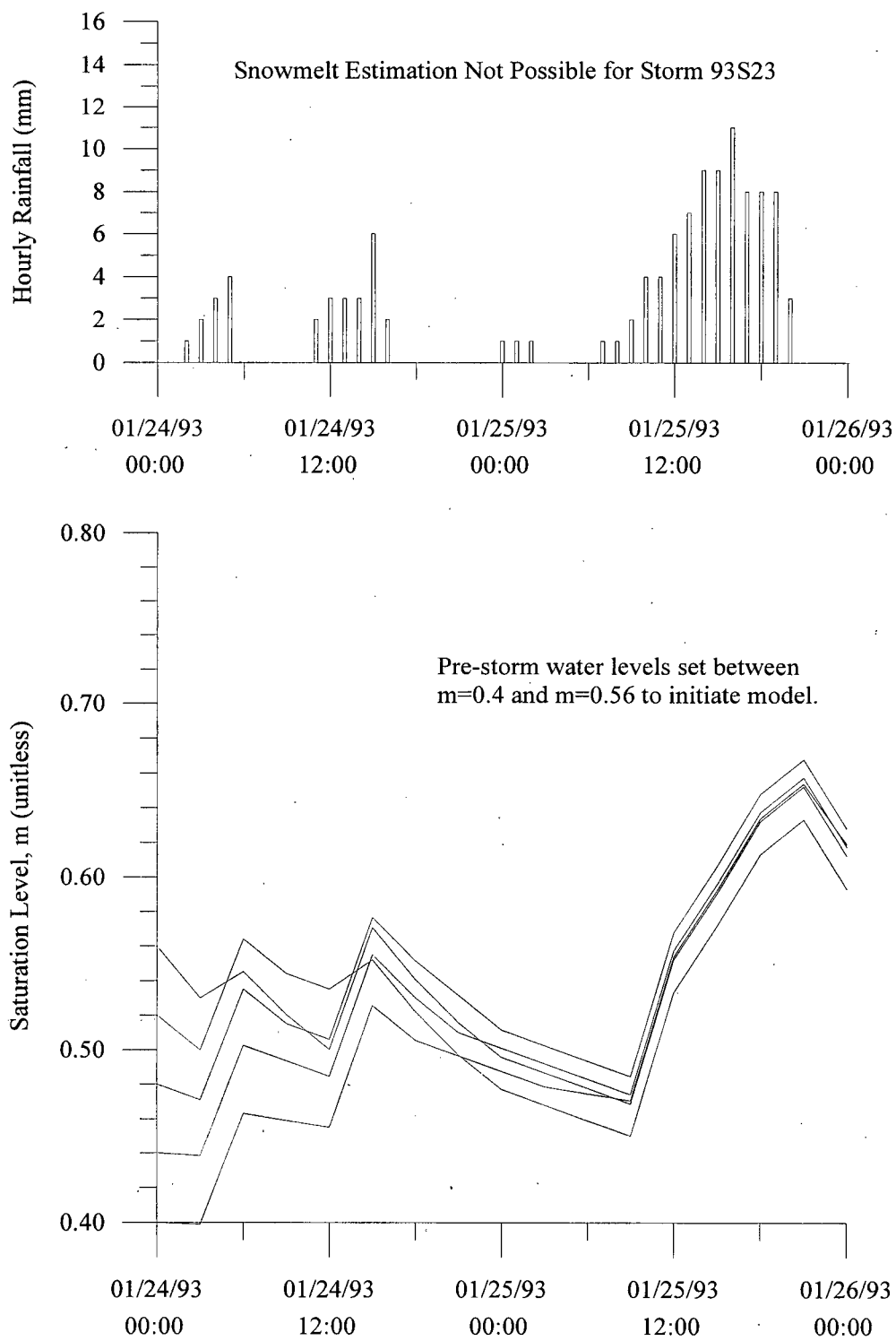
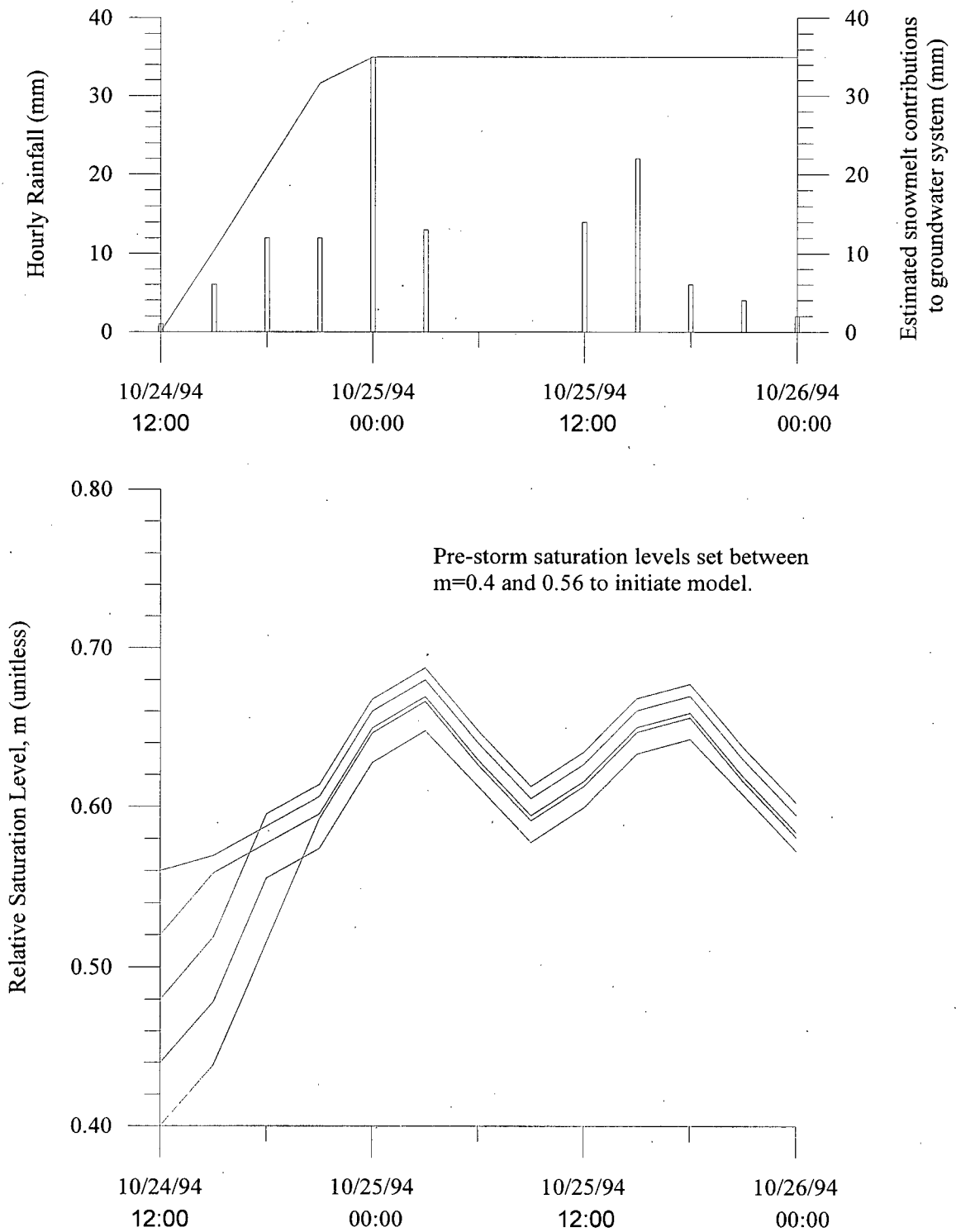


Fig 7-11 Modeling of relative saturation level response for storm 94S16



monitoring location existed prior to the storm and that all of this snow melted during the storm. Based on the assumption that the density of the fresh snow was  $0.1 \text{ gm/cm}^3$  the maximum amount of snowmelt contribution to the groundwater table was restricted to 30 mm.

The estimated response for this storm is shown in Figure 7.11 to vary with pre-storm relative soil saturation level. The maximum change in the relative saturation level ( $\Delta m$ ) was 0.38 for an initial relative saturation level of 0.40. Initial saturation levels of 0.44 and 0.48 showed similar response levels with  $\Delta m = 0.34$ .

The groundwater model can be applied to storms where no groundwater data are available, provided that data for estimates of snowmelt contributions can be determined. The model appears to give reasonable response levels based on the comparison of the two storms with the storms described in Section 7.2.1. Where snowmelt contributions cannot be estimated for an event, the groundwater response estimated by the model should be taken as representing a minimum response level.

### **7.3 Synthesis of groundwater modeling results**

The model for estimating the groundwater response during specific storms can be used to closely predict the observed maximum response during those storm events. Problems of over-prediction and under-prediction of response are believed to be due to errors in the data record for rainfall and due to the uncertainty in snowmelt estimation during these storms. The model was not able to replicate the individual trace of the observed groundwater response due to the use of a 3 hour time interval for the model.

The application of the model to storms where no groundwater record exists should be possible provided that information on pre-storm snowpack thickness, rainfall, air temperatures, and wind speed are available for the storm event. The use of multiple pre-storm relative saturation levels for these storms allows for determination of a range of predicted responses. Provided that the data input to the model is reliable the actual saturation level response should be within the range predicted by the model.

## Chapter 8 Description of failures during the study period

There were 5 failures during 3 storms in Tsitika basin during the study period. This chapter describes conditions prior to the failures as well as the locations and nature of the failed masses (Figure 8.1).

### 8.1 January 28, 1993 failure

The first storm to initiate a failure in the Russell Creek basin occurred over the period January 26 to 28th, 1993. Estimated snowpack thickness prior to the storm was 1 m. No information is available on snowpack thicknesses following the storm to allow for reasonable estimates of snow meltwater inputs. The failure occurred in an old growth drainage depression in Russell Creek sub-basin at an elevation of approximately 800 m (see Figure 8.2). Soil thicknesses are on the order of 0.4-0.9 m and the average slope in the area is  $34^{\circ}$ . The headscarp area was underlain by till and sloped steeply between  $34^{\circ}$  to  $60^{\circ}$ . The area immediately above the headscarp is another depression that may be an older headscarp (Tom Millard pers. comm.).

The failure traveled 600 metres downslope as a debris flow. In this section of the path the contact surface for the upper 150 metres was till. The lower 450 metres was scoured to intrusive bedrock in the 1-2 metre wide main channel with till visible in the path away from the channel. After 600 metres of travel, large organic debris (LOD) at the

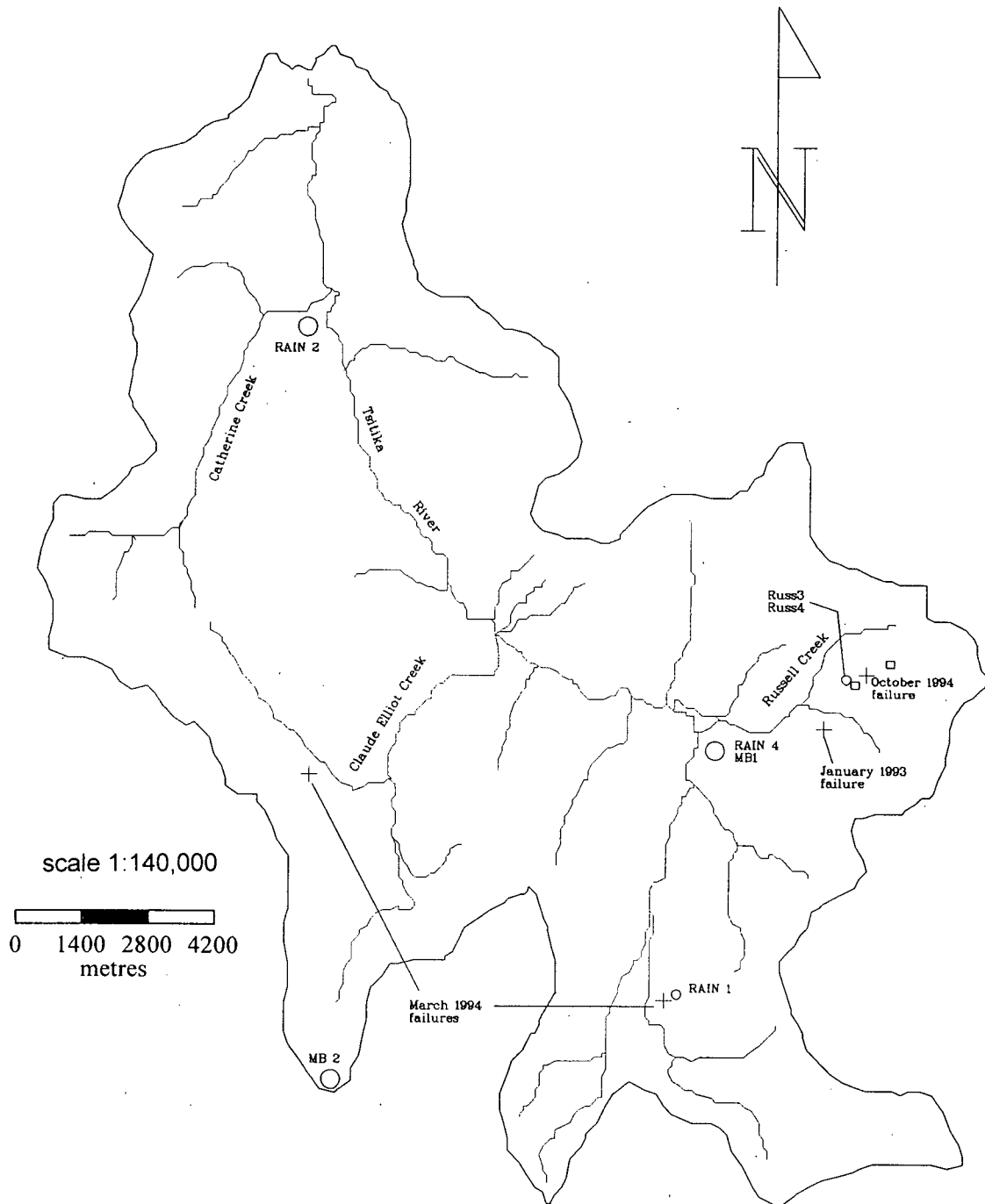


Figure 8.1 Location of failures during the study period



Figure 8.2 January 1993 failure

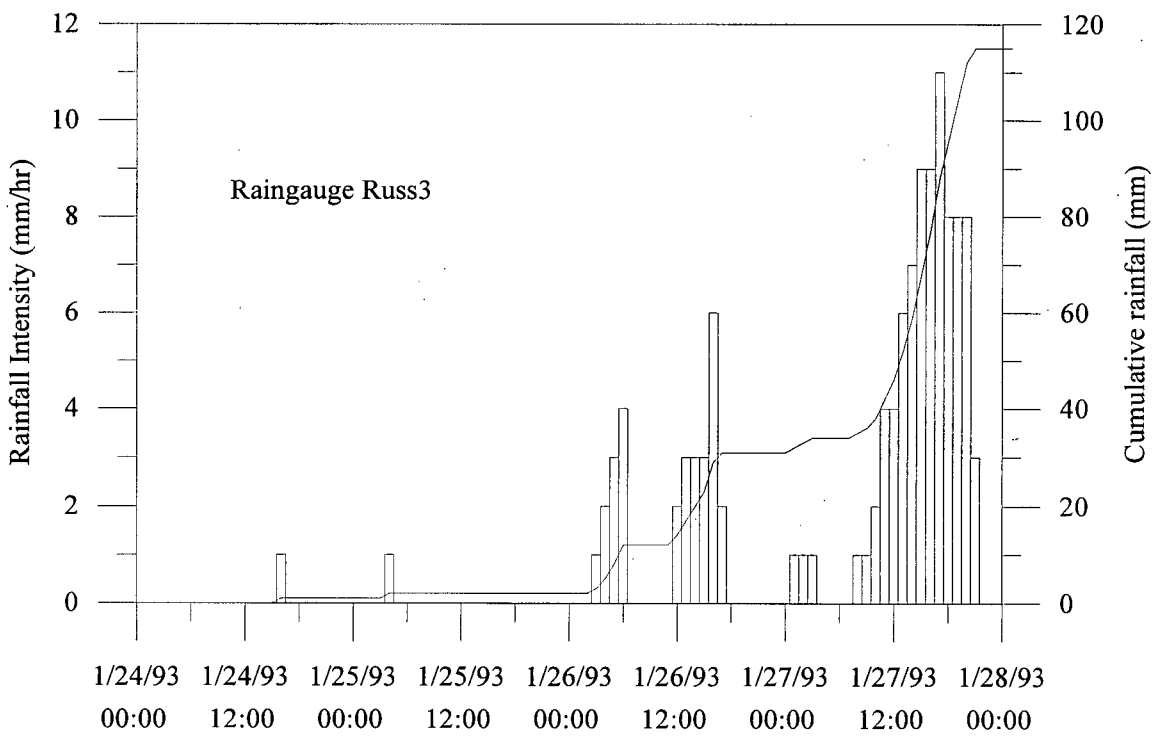
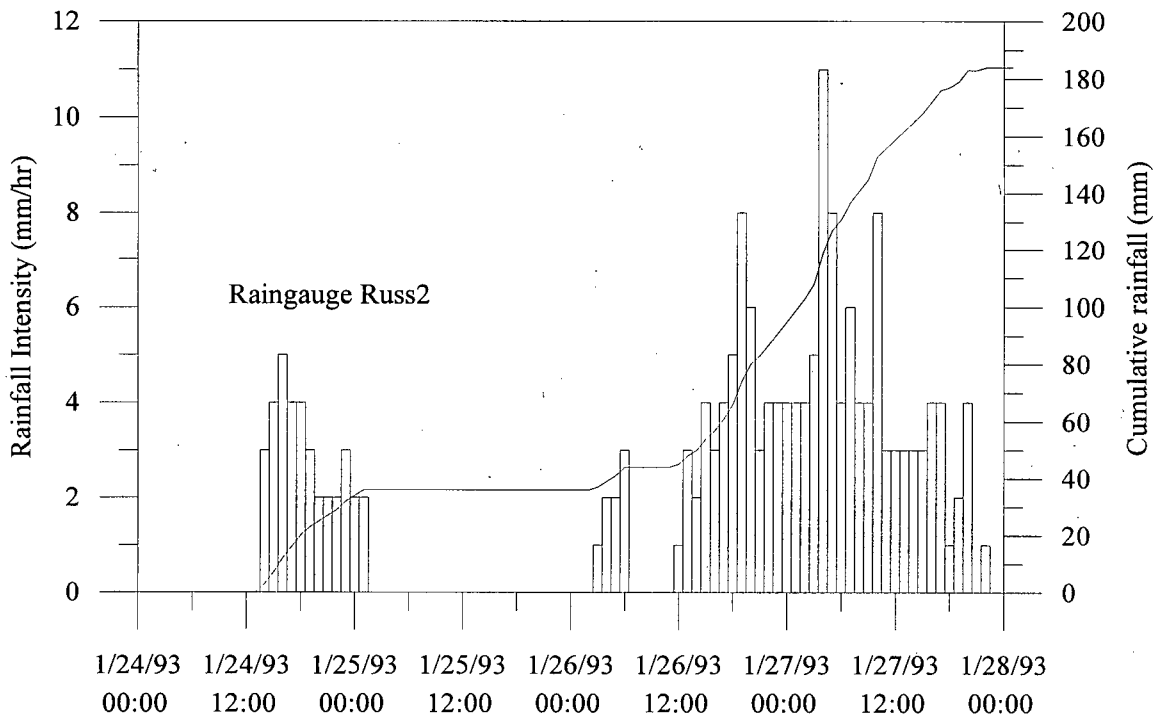
front of the torrent "bridged" against standing timber removing the LOD portion and causing some deposition of gravel and cobbles behind the logjam. Below the jam the failure continued as a flow through old growth forest to Stephanie Creek. Avulsions of the channelized flow were associated with breaks of slope on the hillslope. Material deposited during these minor avulsions consisted of sands and gravels. Of note is that there was minimal disturbance to the channel as a result of the passage of the flow. The flow entered Stephanie Creek in a bedrock canyon.

Time series for the Russell Creek rain gauges operating during Storm 93S3 are shown in Figure 8.3. Only rainfall data are available for these sites as temperature probes had not yet been installed at the rain gauge sites. No other local sources of temperature data were found for this period. Over the period shown in Figure 8.3 the observed differences in the time series for the two rain gauges is believed to be the result of temperature differences at these sites. The total rainfall for rain gauges Russ 2 and Russ3 was 184 mm and 115 mm respectively. The most intense rainfall observed at Russ2 occurred at 4:00 A.M. on January 26th while station Russ3 recorded its peak rainfall at 5:00 P.M. on the 26th. Based on the peak 24-hour interval intensities for this storm, the event had a return period of between 2 to 5 years.

## **8.2 February 28-March 1, 1994 failures**

The 94S7 storm was a mixed, moderate event that occurred at approximately the same time as the maximum snowpack depth of approximately 1 m. The storm triggered

Figure 8.3 Rainfall time series for Storm 93S3



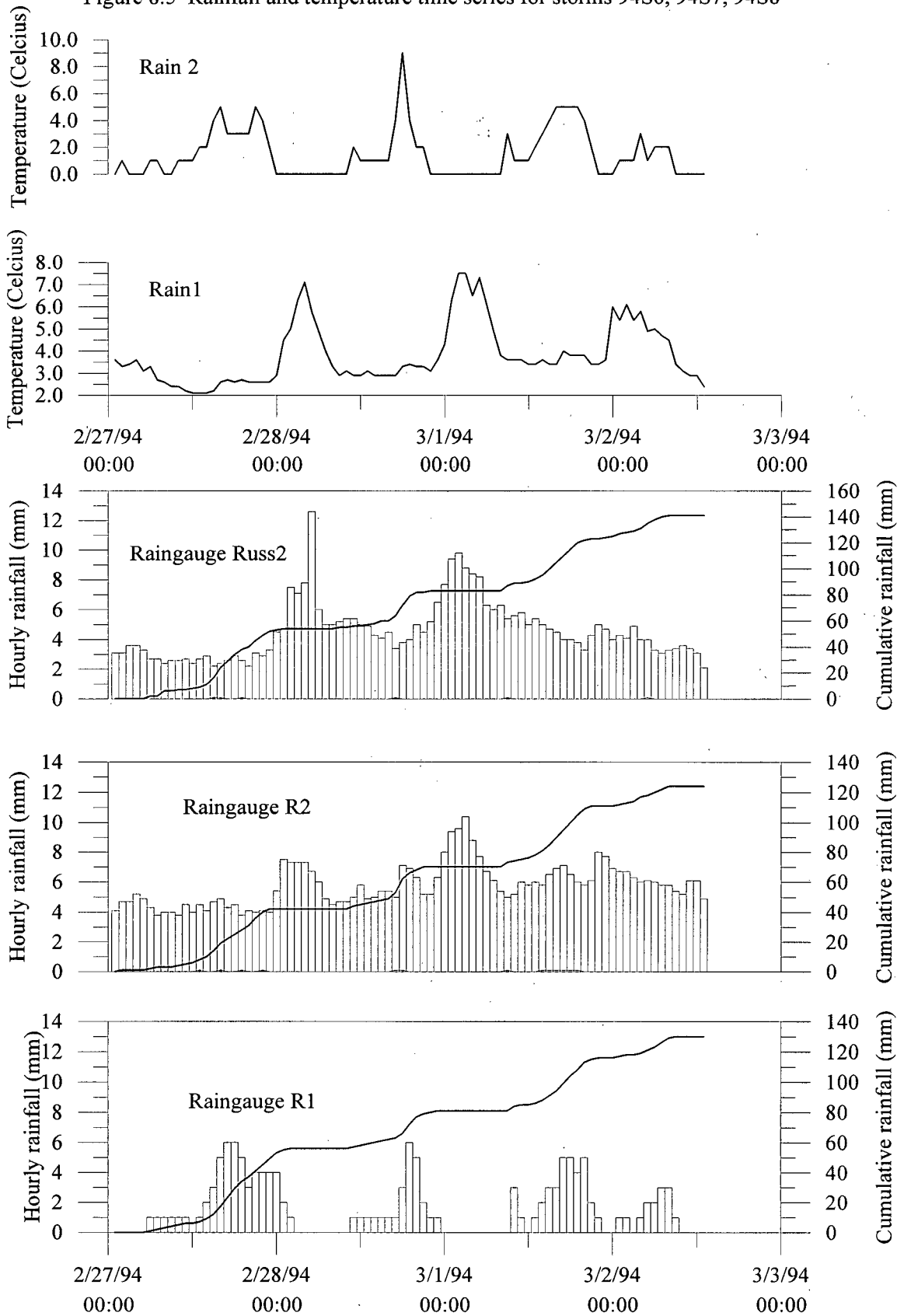
two failures in the upper reaches of the main Tsitika basin and one failure in the Claude Elliot sub-basin (see Figure 8.1). Rain-on-snow meltwater production is believed to have been a major factor in the initiation of failures during this storm. Of the three failures, only one failure was of the open-slope type (see Figure 8.4). The two other failures were logging road related (blocked culvert, side-cast failure). The failures are believed to have occurred on March 1st based upon Canfor and MacMillan Bleodel landslide event reports. No suspended sediment information on the mainstem channels are available to aid in determining a more precise timing of the occurrences.

The available time series for rainfall and temperature from 94S6, 94S7, and 94S8 are shown in Figure 8.5. The Ministry of Forests rain gauge located closest to the site of these failures was not operating properly during this storm period and so no rainfall records are available from that station. Storm 94S6 had 1 and 3 hour rainfall totals of 6 and 17 mm, respectively, at site R1 near the mouth of Russell Creek while site R2 near the confluence of Catherine Creek and the Tsitika River had 1 and 3 hour intensities of 5 and 12 mm respectively. The most intense rainfall recorded during this storm was at site Russ2, which had 1 and 3 hour intensities of 8 and 18 mm respectively. In the period between 94S6 and 94S7 was a warming trend that would have increased snowmelt. Storm 94S7 was of short duration with peak 1 hour and 3 hour intensities of 8 and 17 mm at site Russ2. The 1 and 3 hour rainfall intensities at sites R1 and R2 during 94S7 were 6 mm/14 mm and 8 mm/14 mm. The 24-hour rainfall intensities for this series of storms fall below the estimated 2 year return period.



Figure 8.4 March 1994 open slope failure

Figure 8.5 Rainfall and temperature time series for storms 94S6, 94S7, 94S8



### 8.3 October 25, 1994 failure

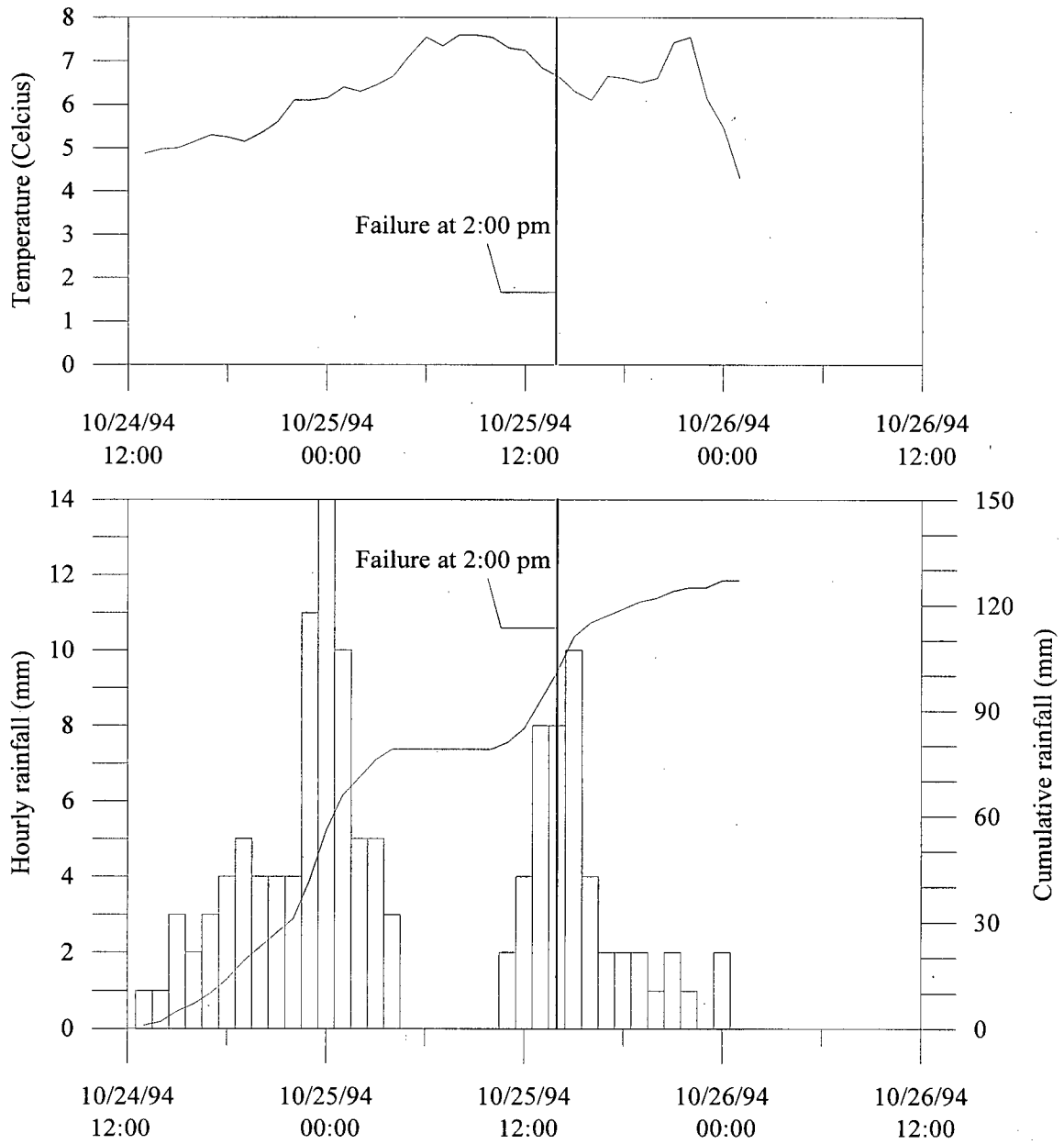
The failure occurred around 1400h on October 25th in the Russell Creek sub-basin (see Figure 8.1). The timing of this event is based on cessation of flow and turbidity data at a monitoring site maintained by Craig Nistor of the Department of Geography, U.B.C. and by observations of a logging truck driver who reported the event to MacMillan Bleodel operations staff. The headscarp of the failure was located in a depression draining to a deeply incised gully on the study slope (see Figure 8.6). The hillslope was logged in 1987 and the 8 years since logging would have reduced the hillslope to a condition of minimum root cohesion following logging. Soil thicknesses near the headscarp ranged from 70-100 cm. Till underlies the initiation zone of the failure and dips steeply at up to 60°. The failed mass travelled approximately 70 metres to the main gully, then towards Russell Creek. Large organic debris at the snout of the failed mass was deposited at points where the stream channel changed direction as well as at the edge of the clear-cut near the valley flat.

The closest rain gauge is approximately 300m from the initiation zone. At the start of the storm there were approximately 30 cm. of snow on the ground which is assumed to have melted during the storm. The snowmelt contribution to groundwater was probably at least 30 mm. Figure 8.7 shows hourly and cumulative precipitation and temperature from the two closest rain gauges Russ3 and Russ4. Rainfall occurred in two pulses of 79 and 48 mm, respectively. The failure occurred during the second pulse when the peak intensity of 13 mm/hr at 10:00 decreased the factor of safety below 1.0. The 24-hour



Figure 8.6 October 1994 failure path  
slide path is ~ 10 m wide  
the lower road visible in the picture is ~ 200 m from the headscarp

Figure 8.7 Rainfall and temperature data for storm 94S16



storm intensity has a return period of less than 2 years. Only the 6 hour rainfall intensity had a return period of between 2 to 5 years; all other intensities (1 hour, 12 hour) had return periods of less than 2 years. The lag between the maximum intensity and the subsequent burial of scientific equipment by the released sediment located 500 m downstream of the failure is four hours. This lag is in approximate agreement with the findings of Okimura (1982), discussed in Chapter 2. Groundwater wells at the site were not in operation at the time of failure to give information on water levels for the storm.

## Chapter 9 Discussion

This chapter contains the linkages between rainfall events, groundwater responses, and landsliding. The discussion is broken into three sections, each dealing with one of the above systems as well as the results of the groundwater modeling. The implications of the analyzed field data for the development of a warning system for high risk areas during high potential failure periods are also presented.

### 9.1 Rainfall events

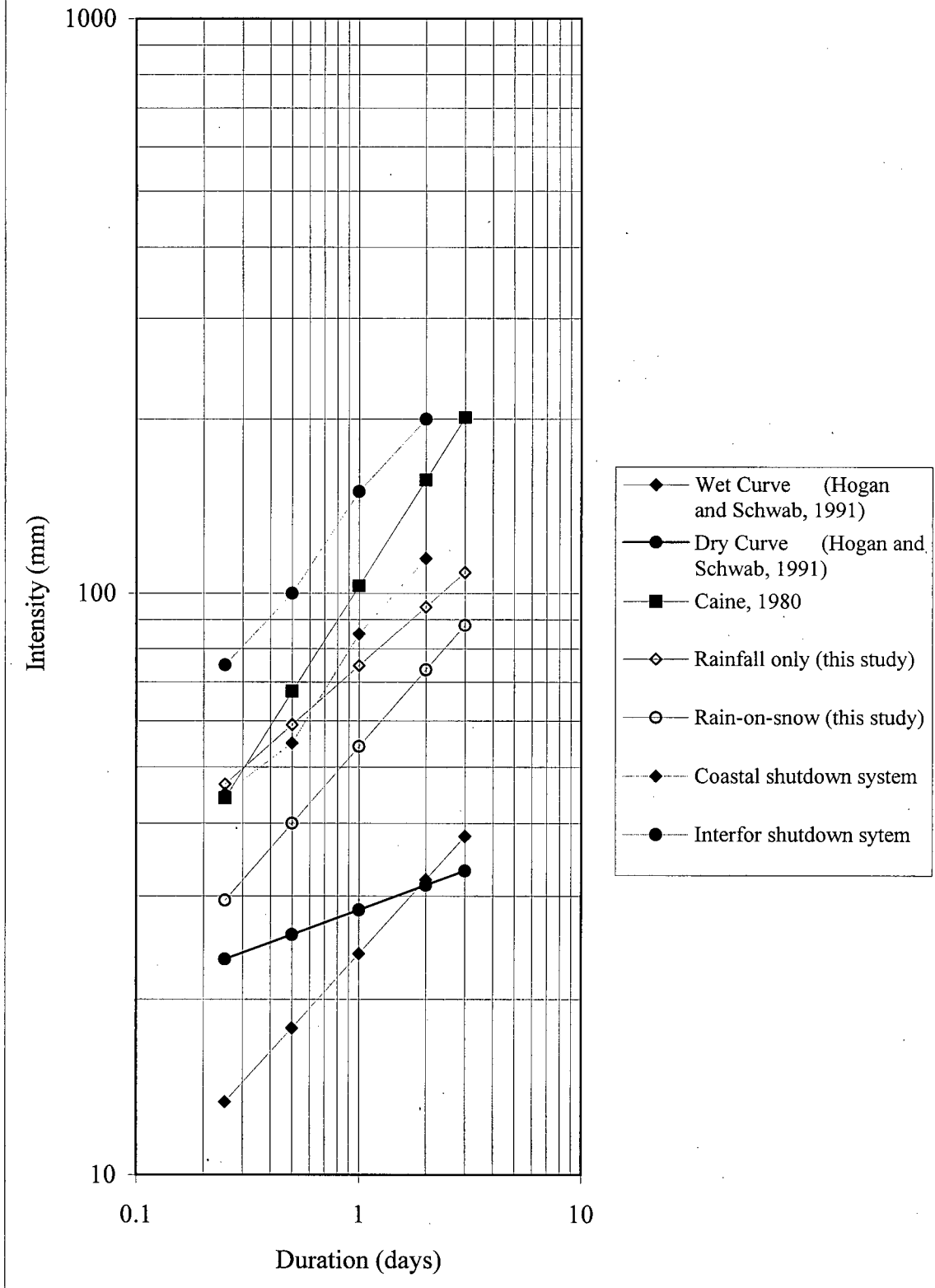
The consistent response of the observed rain gauges during medium and large events in Figure 5.1 suggest that the events influencing Tsitika basin have a much larger spatial scale than that of the watershed. This underlines the dominance of synoptic-scale disturbances in this region. However, periods of intense rainfall did not occur simultaneously at all rain gauges, which supports the notion that intense precipitation tends to occur as cells embedded within a storm (Houze, 1981). As there is good agreement between rain gauges for the timing of rainfall, it may be possible to reliably monitor watersheds on the scale of the Tsitika ( $500 \text{ km}^2$ ) with fewer rain gauges than currently being used, provided that they are located to record rainfalls representative of potentially unstable areas

Most observed rainfall events occurred from September to March. In this period, 40 medium and large events occurred with 14 depositing more than 60 mm of rainfall in 24 hours. Of the 40 events, 32 were classed as rain-on-snow events, which emphasizes the importance of snowmelt during rainfall events.

Rainfall intensities of different duration were examined for the representativeness of storm size and for their use in the determination of rainfall thresholds for slope instability. Peak rainfall intensity was found to be positively related to total storm precipitation (Caine 1980), especially storms with 24 hour intensities less than 80 mm. Storms with more than 80 mm rainfall in 24 hours did not show as strong a positive relationship between maximum intensity and total precipitation.

Intensity-duration relationships for landsliding were determined from data collected during the study and data from other published studies in the Pacific Northwest. The duration-intensity threshold for slope instability in the Pacific Northwest based on an analysis of regionally documented instability events was  $I = 25.4D^{0.34}$  for high intensity rainfall storms without significant snowmelt input, and  $I = 13.4D^{0.44}$  for storms with significant snowmelt input (Figure 9.1). Both of these limits represent lower thresholds than those identified by Caine (1980). The limits from Hogan and Schwab (1991) are both below the three previously mentioned thresholds. The other two thresholds shown on Figure 9.1 are taken from two operational safety shutdown systems currently active on Vancouver Island. These systems, and their relations to other instability thresholds, are described in Section 9.2. The rain-on-snow limit determined in this study is from events during which excess water from snowmelt is believed to have been responsible for lowering the factor of safety of a hillside hollow to unity. While intensity-duration relationships are useful, more information is needed to determine local thresholds and to determine thresholds for storms with significant snowmelt input; indeed, Church and Miles (1987) observed that a simple rainfall threshold was unworkable in southwestern

Figure 9.1 Intensity-duration envelope curves applicable to the Pacific Northwest



British Columbia because of snowmelt contributions, and this study further supports that assertion.

## 9.2 Groundwater relations

The closely timed response of the clear-cut site groundwater peak events to peak rainfall intensities shows the direct linkage of rainfall or rain-on-snow inputs and groundwater rise. The peak rate of groundwater rise during a storm is primarily a result of rainfall intensity. From the observed groundwater time series in Chapter 7 it is possible to separate storms with snowmelt recharge from those with minimal snowmelt recharge. Examples of snowmelt storms are 93S25 and 93S28, (Figure 7.6 and Figure 7.7) in which the clear-cut site showed large groundwater rises during moderate rainfall intensities. Storms with minimal snowmelt recharge are 93S27 and 93S30. Storm 93S27 (Figure 7.7) involved a three hour rainfall intensity of 11 mm and low air temperatures at the monitoring site imply that there was little snowmelt.

Groundwater rise at the old-growth site was loosely connected to the measured rainfall data from the clear-cut site. The observed differences in groundwater response at the old growth site is a result of at least two factors. The first is that precipitation was not available at this site to allow lag determination. Secondly, the site may experience somewhat different weather patterns from the clear-cut site due to differences in topography and elevation. Some storms at the old growth site may be influenced by convergence of weather systems from Tlatlos Creek basin, a sub-basin of the Eve basin (Figure 3.2) and systems travelling up the main Tsitika basin. Topographically forced convergence is believed to result in increased precipitation. This is a somewhat tenuous

hypothesis but, field experience of local weather patterns during the study period suggested that some convergence of storm systems between the two basins occurs.

Recession rates observed at the groundwater monitoring sites showed variation between boreholes. The observed variations reflect the influence of macropores or a higher porosity layer on soil drainage in the upper soil profile. Examination of soil pits at the two monitoring sites showed that the upper Ah Horizon was less dense than the mineral soil layer below and would have a higher porosity. This would produce a lesser rate of rise of saturation level than in the underlying mineral soil.

The average level of the contact between the two soil layers was  $m=0.53$  and  $m=0.61$  for the clear-cut and old growth monitoring sites respectively. From the saturation responses in Chapter 7 at the clear-cut site, saturation level consistently peaked between  $m=0.48$  and  $m=0.69$  which suggests that the upper Ah Horizon had only a thin ( $m \approx 0.04$  to  $0.16$ ) saturated thickness during storms with intense rainfall and/or high snowmelt inputs. The mineral soil layer at this site was completely saturated during most of the storms examined in Chapter 7.

### **9.3 Groundwater modeling at the clear-cut site**

Using the model I was able to closely estimate the observed change in relative saturation level for a number of storms and in some cases the agreement between observed and modeled responses was excellent. Cases in which the model failed to closely estimate the observed response were associated with the rainfall record problems due to snowfall or a frozen rain gauge funnel. Where a frozen funnel exists at the start of a storm, the ice plug may be melted by the release of latent heat from ponded water and

rising air temperatures. Ice plugs typically occur during mixed rain and snow events where the air temperature is below  $2^{\circ}\text{C}$ . Melting of the plug results in the release of the ponded water into the tipping bucket and can be detected on the rain gauge time series as a large pulse of rainfall. An example of this is shown in Figure 7.9 where the rainfall time series lags the observed response time series for the period December 30, 1993 to January 3, 1994.

Rainfall data from more storms should be used to further calibration of the model for the Russell Creek basin. The inclusion of on-site information on snowmelt contributions to groundwater during storm events is required to allow for proper calibration of the model. In the absence of this information, U.S. Army Corps. of Engineers snowmelt formulas allow a reasonable estimation of snowmelt contributions.

#### **9.4 Relations to landsliding**

Detailed discussion of the three storms that initiated instability during the study period was given in Chapter 8. Storms 93S3 and 94S16 were two of the three largest storms recorded during the study period and both initiated channelized debris flows in the Russell Creek basin. Storm 94S7 initiated three failures in the Tsitika basin but was only a medium-sized rainfall event. Examination of these storms shows the importance of antecedent moisture conditions and snowmelt. As instability can be associated with medium rainfall events more attention must be given to fluctuations in temperature prior to events as this can give some warning as to the potential importance of snowmelt.

Return periods for 1, 6, 12, and 24 hour rainfalls for the three storms are listed in Table 9.1. It can be seen that storm 94S7 was an average annual rainstorm with all

durations having a return period of one year or less. Storm 94S16 had similar return periods for 1 and 12 hour durations while the six hour duration during this storm had a return period of only 3.8 years. The return period for the 24 hour duration of Storm 94S16 was 11.8 years. Storm 93S3 had a 1 hour duration return period of 1.4 years, which is not significant. The 24 hour duration return period of 25 years for Storm 93S3 was the highest recorded during the study period. The data in Table 9.1 should not be taken as showing the importance of forest cover in slope stability due to the limited sample size of storms known to have initiated failures and the methods for inventorying landslides during the study period. A more systematic inventory of landslides from individual storms needs to be done to examine the differences in slope instability thresholds for forested versus cleared areas in a watershed.

Table 9.1 Return period of 1, 6, 12, and 24 hour rainfall intensities for storms with failures

Storm ID	Return period (years)			
	1 hour	6 hour	12 hour	24 hour
93S3	1.4	7.1	5.6	25
94S7	1.0	1.0	1.0	< 1
94S16	2.8	3.8	2.9	11.8

Two of the three natural failures that occurred over the course of the study had failure planes dipping greater than  $35^\circ$ . The dip of the failure plane was greater than the slope angle in the area around the headscarp. All three slope failures occurred in hollows where convergence of groundwater flow occurs. Generally, it appears that response during intense recharge events quickly raises the saturation level in hollows and can lead to instability. Recognition of potentially unstable sites based on slope angle and surface expression should be possible in the Tsitika basin. Hollows situated on slopes steeper

than 30° are potential failure sites, especially if there is evidence of instability in other hollows in the vicinity. Hollows on steep terrain may undergo a similar cycle of instability and recharge to that identified for gullies by Oden (1994) but over a greater time scale.

### 9.5 Implications for a warning system to shutdown logging operations during periods of potential slope instability

The intent of a warning or shutdown system would not be to predict the exact initiation site of a landslide, but to provide warnings of potential landsliding when conditions are favourable in a general area. The system would be specifically aimed at avoiding high risk areas, such as terrain in stability classes IV and V terrain and gully systems that show signs of past instability.

#### 9.5.1 Interfor Shutdown System

The Interfor shutdown system was developed in 1991 as a result of a worker fatality in the Brooks Bay area on Vancouver Island and is currently used by all Interfor operations. The system identifies rainfall limits above which all operations must cease, and is based on the two year return period rainfall totals (Table 9.2)

Table 9.2 Rainfall limits for the Interfor Shutdown System

Time period	Rainfall (mm)
12 hours	75
24 hours	100
48 hours	150
72 hours	200
Operations can resume when the 24 hour rainfall falls below 50 mm	

### 9.5.2 Wet and Dry Coastal Shutdown Systems

The coastal shutdown systems were developed in early 1994 to stimulate discussion at a Federal Research Development Agency sponsored seminar (Chatterton pers. comm.). The system was designed for Vancouver Island and the Lower Mainland and is currently being considered for use in the Prince Rupert Forest Region. The system uses a water balance approach to determine the stability of a hillslope. The system developed by Chatterton is broken into the Wet and Dry regions for Vancouver Island and the Lower Mainland of British Columbia, a division based on Coligado (1982). The Wet Region consists of the western coastline and the northern tip of Vancouver Island. The Dry Region consists of the east flank of Vancouver Island.

The rainfall limits proposed by Chatterton for the Wet and Dry Coasts are shown in Table 8.3. The governing equation of the water balance approach is:

$$Wb_i = (P_i - RR) + (P_{i-1} - RR) \quad (\text{Eqn. 8.1})$$

where:

$WB_i$  is the water balance of the soil for time period  $i$  ( $i = 12, 24, 48$  hours)

$P_i$  is the precipitation input from rainfall and snowmelt over time period  $i$

$RR$  is the regional recession, or recovery rate of the soil.

The water balance thresholds for instability of the Wet Coast were obtained from Chatwin et al. (1995) and were found to be comparable with the 2-year extreme rainfall event determined by Coligado (1982) and the thresholds used by the Interfor. For the Dry Coast area, thresholds were determined using the 2-year extreme precipitations for various durations.

The recession rates used in the coastal shutdown system represent the rate at which water drains from the soil. The values for the regional recovery rates shown in Table 8.3 were determined by Chatterton from the slope of the instability threshold curve in Chatwin et al. (1995), and therefore do not represent a newly derived physical or empirical measure of the actual rate at which water drains from the soil. The inclusion of snowmelt input to the water balance is considered to be an improvement over the Interfor system since snowmelt during rain-on-snow events can be a significant initiation factor for slope stability problems.

Table 9.3 Shutdown Criteria for The Wet and Dry Coast Systems  
(from Chatterton, 1995)

Time period	Wet Coastal Limits	Dry Coast Limits
12 hours	75 mm	40 mm
24 hours	100 mm	55 mm
48 hours	150 mm	85 mm
72 hours	200 mm	115 mm
Recovery rate	50 mm/24 hours	30 mm/24 hours

### 9.5.3 Relation of current shutdown thresholds to regional intensity-duration instability thresholds

This section compares how the two operational thresholds described above compare to the regional intensity-duration instability envelope curves in Figure 9.1. The Interfor system has a higher threshold than any of the instability curves. This is not too surprising as the thresholds apply to the west side of Vancouver Island. The Dry Coastal shutdown system thresholds are comparable to the rainfall-only limit determined in this study. At 6

hour and 12 hour durations, the Dry Coastal shutdown thresholds are below the instability envelope, but the shutdown threshold is above the instability envelope for 1-day and 2-day durations.

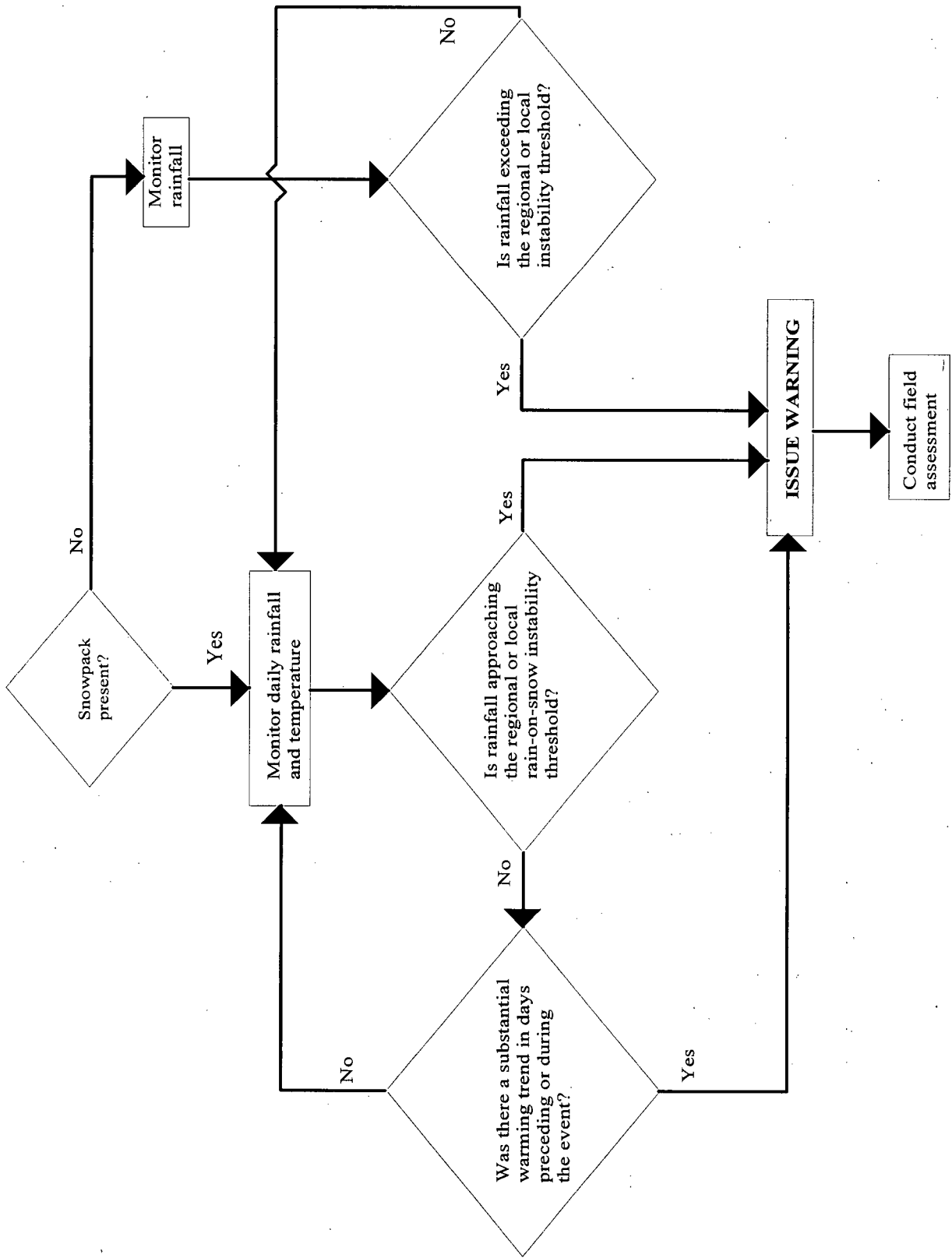
#### 9.5.4 Design of a warning system for operational shutdown

The results of rainfall and landsliding analysis and the rainfall intensity envelope show that it may be possible to develop a rational warning system based on hydrological analysis. Reliable real-time data from sites near to potentially unstable terrain would be required as input. Significant changes in hillslope stability conditions can occur on an hourly time scale, but it is not essential to monitor conditions at this interval. A minimum sampling interval of 6 to 12 hours would probably suffice as input to a warning system. A simplified schematic diagram for a warning system is shown in Figure 9.2.

The shutdown level should be determined by applying a safety factor to the known threshold level for landsliding in an area. However, information on the rainfall-landslide threshold is not available for most areas of the Pacific Northwest and would be laborious to obtain. The system could be based on regional thresholds like those in Figure 5.3, but should incorporate local adjustments where this information is available.

A limitation to warning systems involves the issuing of false alarms. If incorrect alerts occur frequently the financial costs can become considerable. Two steps are suggested to reduce false alarms. The first is to have the sampling input interval,  $i$ , shorter than the interval,  $j$ , used to decide if an alert should be issued. If decisions to issue an alert are based on 12 hour rainfall and temperature data, they should be updated at 6 hour intervals. The 12 hour value of  $T_i$  is updated at interval,  $i$  and represents the sum of  $S_j$

Figure 9.2 Schematic for an early warning system



and  $S_{j-1}$ , where,  $S_j$  represents the 6 hour data values from the remote site. When the 12-hour values indicate a high potential for instability, data from the remote site are monitored for an additional 6 hours. If at this point the data from the remote site still indicate high risk, an alert should be issued calling for operations to cease in high risk areas, or warning of potentially unsafe conditions. To be most cost effective, the issuance of a warning or caution should be issued in the morning prior to the deployment of workers.

A second step to reduce incorrect alerts is assessment of conditions near the remote area to determine if the data from the remote site are reliable. Where remote sites are accessible it would be possible for an observer to make field visits to the remote site, or a series of fixed observation control points, as a check of conditions near potentially unstable terrain. An example of an observation control point is visual assessment of streamflow and turbidity at a large culvert or bridge site. The observer should be familiar with the area near the remote site and should have an understanding of unstable conditions on steep slopes.

During storms where high risk sites may be unsafe (i.e. storms above the threshold for instability), shutdown should be implemented on operations in those areas. Terrain with hollows and gullies and steep slope areas are terrain types that represent high risk areas. Also included should be areas that show evidence of recent slope instability. Total shutdown of operations is unnecessary on low risk ground. During threshold storms, alerts can be given to personnel using road networks that cross high risk areas to watch for signs of slope instability. The probability of encountering a debris flow is lower for

workers in moving vehicles than for those on hillslopes, but those in moving vehicles represent sources of information on local conditions and event occurrence.

## **Chapter 10 Conclusions and Recommendations**

### **10.1 Rainfall and landsliding conclusions**

During the study period there was good agreement between rainfall duration and intensity and landsliding. Failures during storms 93S3 and 94S13 were a result of intense rainfall in the study basin and these two storms ranked as two of the most intense of the study period. Storm 94S7 was a medium-sized storm that coincided with warm air temperatures and gusty winds and occurred near the time of maximum snowpack thickness in that winter.

The occurrence of failures in October, January and March show that it is necessary to monitor rainfall for at least six months. Most of the precipitation monitoring sites maintained by licensees on Vancouver Island are used for monitoring fire conditions and thus are maintained only from mid-May to mid-October.

Regular inventories of landslides are needed to note occurrences that may not be visible to personnel operating in an area. The inventory should ideally be updated following every major storm but this may prove to be uneconomic. Realistically, landslide inventories could be conducted several times during the storm season to determine which storms most likely triggered given events.

### **10.2 Groundwater conclusions**

The observed rainfall and groundwater time series for Russell Creek showed that there was a consistent response to rainfall and snowmelt inputs. Peaks in the groundwater time series usually occurred close to the peak of rainfall intensity. Peak relative saturation

levels at both the old-growth and clear-cut sites were consistently around  $m=0.60$ . However, the time series at both sites show considerable variation between boreholes as well as between-site variation. The maximum rate of groundwater rise was related to peak rainfall intensities during all observed events. Rainfall intensities around 10 mm/hr were sufficient to initiate rapid rise of the saturation level. In-depth examination of the data may determine if this a reliable threshold rainfall intensity associated with maximum response rate. Data from several more years of storm events should be collected to allow for a more comprehensive examination of response rates.

Information on snowpack dynamics should be used in conjunction with rainfall and temperature data when monitoring hillslope conditions for periods with a high probability of failure. As groundwater time series are not readily available for much of the Pacific Northwest, and given the large variation in groundwater responses over small distances, real-time rainfall intensity values in conjunction with a knowledge of local antecedent conditions should be used as a surrogate for indicating peaks in the groundwater table. Lag times in groundwater response are between one to five hours during large storms, depending on initial water table positions at the start of the storm.

Due to equipment problems encountered during the study the groundwater levels were recorded during only one storm causing failures. A lack of groundwater data for the other two storms causing failures limits the conclusions that can be drawn concerning groundwater levels. The studies discussed in Chapter 2 have also shown that there is a relationship between the peak groundwater level and the incidence of landsliding.

### **10.3 Groundwater modeling conclusions**

The groundwater model used in this thesis can be used to estimate the magnitude of groundwater rise at the clear-cut site. Through use of the model it was possible to estimate the timing of the individual groundwater peaks during some heavy rainfall periods. Use of a three-hour time interval in the model is justified based on the model results.

The use of a tipping bucket rain gauge to collect data for input to the groundwater model limited the period over which data could reliably be collected. Sites used for collecting model input data should make use of a total precipitation gauge and possibly snowmelt lysimeters to better modeling of rain-on-snow events. More detailed information on snowpack thickness and density is also required to allow for determination of snowmelt contributions. A snow pillow would have been a valuable addition in this study.

### **10.4 Comparison of study findings to the study hypothesis**

The first objective was to show that variations in precipitation were positively correlated with fluctuations in the groundwater table on steep slopes. Based on observed groundwater response to rainfall, this objective can be accomplished based on examination of the time series for the two variables. The second objective was to document the incidence of slope failures occurring during major rainstorms and periods of groundwater rise in Russell Creek and in Tsitika basin. Documentation of five recorded slope failures was achieved through the collection of landslide event reports from MacMillan Bleodel and Canadian Forest Products operations staff. It is likely that

these events were not the only instability events in Tsitika basin during the study period. The third objective was to assess the critical sequence of events required to destabilize steep slopes typical of forested terrain in coastal British Columbia. Rainfall intensity-duration relationships for the three storms known to have initiated instability were compiled along with similar information obtained from other studies in the Pacific Northwest. From the gathered dataset, threshold levels for slope instability associated with rainfall and rain-on-snow events were developed for the Pacific Northwest. The determined relationships represent regional thresholds and could be subjected to local calibration under operational conditions.

Saturation levels during storms initiating landslides were not higher than the level during storms in which instability was not observed. Saturation levels at the site were consistent in response levels for large storms and for storms with high snowmelt. As the observed instability in the Tsitika basin occurred in hollows on steep hillslopes, the saturation level at the failure initiation sites was believed to be greater than that at the monitoring sites.

There appear to be two possible sequence of events required to destabilize steep hillslopes in Tsitika basin based on a few data points. The first is high intensity rainfall greater than 12 mm/hr and 24-hour totals above 100 mm. During a storm typical season these events may occur once or twice. The second sequence of events to destabilize hillslopes is high antecedent rainfall and warm air temperatures coincident with a melting snowpack. Storms of this variety have antecedent rainfall exceeding 50 mm and peak rainfall intensities around 10 mm/hr. Snowmelt during these events is an important contributor to groundwater recharge.

The fourth objective was to develop a numerical groundwater model to predict periods of probable slope instability. The model developed closely predicted the timing and level of groundwater rise for some of the storms. The transferability of the model from one location to another without further calibration is questionable. The main use of a groundwater model in the study area appears to be to predict periods when there is potential for instability to occur. The modeling approach appears to operate better than a rainfall alone approach due to the inclusion of snowmelt inputs.

The study hypothesis stated in Chapter 1 was that antecedent conditions and rainfall, through groundwater peak events, are linked to the incidence of slope instability. It was shown through the analysis of rainfall that the incidence of landsliding was linked to rainfall and antecedent conditions. It was also shown that groundwater peak events were related to rainfall and antecedent conditions. The model used to estimate saturation level response was based on measurements from groundwater wells on a typical steep, middle slope segment and does not estimate flow convergence. Given that linkages between rainfall and groundwater and rainfall and landsliding were clearly identified, the study hypothesis is accepted.

## **10.5 Recommendations**

This section deals with recommendations based on the findings and discussions earlier in this thesis. The goal of this section is to put forward recommendations to reduce risk for workers operating on or near potentially unstable terrain.

**Recommendation 1**

The current collection of hydrometeorological data by licensees is based on 24 hour summations, often collected manually. While this may be sufficient for forecasting fire weather, it is not sufficient for slope stability evaluations. Monitoring stations should be automated to permit telemetric access and should use a sampling interval of six hours since stability conditions can change rapidly.

**Recommendation 2**

While it is true that high intensity rainstorms can cause instability, it has also been shown that instability can occur during moderate intensity rain storms with certain antecedent or modifying conditions. Modifying conditions include wind throw and snowmelt. To allow for a comprehensive system, total precipitation and rainfall index sites should be chosen from all available stations. An index site is a site whose precipitation totals can be shown to be representative of nearby, potentially unstable slope segments. Examination of landslide event reports and precipitation totals for existing sites is a means of determining index sites.

**Recommendation 3**

Ideally, remotely sensed data from rain gauges should be examined on a regular basis to review the status of working conditions prior to crew deployment. Rainfall data from stations should be used with effective shutdown guidelines to determine shutdown of operations. Shutdowns could vary in magnitude from a total work stoppage to more localized shutdowns. For example, open-slope logging on well drained sites could be permitted whereas logging in terrain with hollows or near gullies would be closed. It is

recommended that analysis be conducted on the Interfor and Water Balance shutdown systems to determine their range of applicability on northern Vancouver Island.

#### **Recommendation 4**

To better understand the relation between rainfall and landsliding in mountainous terrain it is necessary to ensure that the incidence of landsliding is adequately recorded. It is recommended that all landslide event reports from licensees and other agencies should be compiled at the regional level. Analysis of event reports with respect to precipitation levels and antecedent conditions should be conducted and the results used to refine local shutdown limits.

#### **Recommendation 5**

The measurement of groundwater response during this study yielded interesting insight into storm responses. However, the lack of physical data on snowmelt rates is a drawback. It is recommended that groundwater monitoring to storm response be continued with the addition of pressure pillows or lysimeters to determine the relative contribution of snowmelt during rain-on-snow storms.

## References

- Beven, K. 1981. Kinematic subsurface stormflow. *Water Resources Research*, vol 17, no 5, pp 1419-1424.
- Beven, K. 1982. On subsurface stormflow: prediction with simple kinematic theory for saturated and unsaturated flows. *Water Resources Research*, vol 18, no 6, pp 1627-1633.
- Beven, K. and Germann, P. 1982. Macropores and water flow in soils. *Water Resources Research*, vol 18, no 5, pp 1311-1325.
- Brand, E.W., Dale, M.J., and Nash, J.M. 1986. Soil pipes and stability in Hong Kong. *Quarterly Journal of Engineering Geology*, London, vol. 19, pp 301-303.
- Buchanan, p. 1990. Debris avalanches and debris torrent initiation, Whatcom County, Washington, U.S.A. Master's thesis, University of British Columbia, Department of Geological Sciences, Vancouver. 237 pp.
- Buchanan, P. and Savigny, K.W. 1990. Factors controlling debris avalanche initiation. *Canadian Geotechnical Journal*, vol 27, pp 659-675.
- Caine, N. 1980. The rainfall intensity-duration control of shallow landslides and debris flows. *Geografiska Annaler*, vol 62A, pp 23-27.
- Chamberlin, T.W. 1972. Interflow in a mountainous forest site in coastal British Columbia. *In Mountain Geomorphology*. O.H. Slaymaker and H.J. McPherson (Eds.). Tantalus Research. Vancouver, B.C. pp. 121-126.
- Cannon, S.H. and Ellen, S. 1985. Rainfall conditions for abundant debris avalanches, San Francisco Bay Region. *California Geology*, pp 267-272.

- Chatterton, A.N., Muholland, M.J., and Willington, R.P. 1985. ROCMOD2: A computer model to simulate the effects of forest harvesting on rain-on-snow peak flows. Unpublished report by British Columbia Forest Products Ltd. Resource Planning Group. 85p.
- Chatterton, A.N. and Willington, R.P. 1987. ROCMOD3: An improved and re-calibrated version of ROCMOD2. Unpublished first draft report by British Columbia Forest Products Ltd. Resource Planning Group.. 30p.
- Chatwin, S.C., Howes, D.E., Schwab, J.W. and Swanston, D.N. 1994. A guide for management of landslide-prone terrain in the Pacific Northwest (2nd. edition). British Columbia Ministry of Forests Land Management Handbook no. 18. 212p.
- Church, M.C. 1988. Floods in cold climates. *In Flood Geomorphology*. V.R. Baker, R.C. Kochel, and P.C. Patton (Eds.). John Wiley & Sons, Inc. New York, N.Y. pp 205-229.
- Church, M.C. and Miles, M.J. 1987. Meteorological antecedents to debris flow in southwestern British Columbia; some case studies. *Reviews in Engineering Geology*, vol. VII. pp 63-79.
- De Vries, J. and Chow, T.L. 1978. Hydrologic behavior of a forested mountain soil in coastal British Columbia. *Water Resources Research*, vol 14, no 5, pp 935-942.
- Dunne, T. and Black, R.D. 1970. An experimental investigation of runoff production in permeable soils. *Water Resources Research*, vol. 6 no. 2. pp. 478-490.
- Eisbacher, G.H. and Clague, J.J. 1981. Urban landslides in the vicinity of Vancouver, British Columbia, with special reference to the December 1979 rainstorm. *Canadian Geotechnical Journal*, vol. 18. pp. 205-216.
- Givone, C. and Meignien, X. 1990. Influence of topography on spatial distribution of rain. *Hydrology of Mountainous Areas, Proceedings of the Strbske Pleso Workshop, Czechoslovakia, June 1988*. IAHS Publication no. 190. pp. 57-65.

- Harp, E.E., Wells II, W.G. and Sarmiento, J.G. 1990. Pore pressure response during failure in soils. *Geological Society of America Bulletin*, vol 102, pp 428-438.
- Haneberg, W.C. 1991. Pore pressure diffusion and the hydrologic response of nearly saturated, thin landslide deposits to rainfall. *Journal of Geology*, vol 39, pp 886-892.
- Hogan, D.L. and Schwab, J.W. 1991. Meteorological conditions associated with hillslope failures on the Queen Charlotte Islands. B.C. Ministry of Forests, Land Management Report No. 73, 36 p.
- Hogg, W.D. and Carr, D.A. 1985. Rainfall Frequency Atlas for Canada. Canadian Climate Program publication En56-67/1985, 90 p.
- Houze, R.A. 1981. Structures of atmospheric precipitation systems; a global survey. *Radio Science*, vol. 16. pp. 671-689.
- Innes, J.L. 1983. Debris flows. *Progress in Physical Geography*, no. 7. pp. 469-501.
- Jackson C.R. and Cundy T.W. 1992. A model of topographically driven, saturated subsurface flow. *Water Resources Research*, vol 28, no 5, pp 1417-1427.
- Keefer, K.K., Wilson, R.K.M., Mark, R.E., Brabb, E.E., Brown, W.M., Ellen, S.D., Harp, E.L., Wiczorek, G.F., Alger, C.S. and Zatzkin, R.S. 1987. Real-time landslide warning during heavy rainfall. *Science*, vol 238, pp 921-925.
- Kimmins, J.P. 1987. Forest Ecology. Macmillan Publishing Company. New York, N.Y. 531 p.
- Loukas, A. 1991. Analysis of the response and the rainfall distribution in a mountainous watershed. Unpublished M.A.Sc. thesis. University of British Columbia.
- McDonnell, J.J. 1990a. The influence of macropores on debris flow initiation. *Quarterly Journal of Engineering Geology*, London, vol 23, pp 325-331.

- McDonnell, J.J. 1990b. A rationale for old water discharge through macropores in a steep, humid catchment. *Water Resources Research*, vol. 26, no. 11, pp 2821-2832.
- Maynard, D. 1991. Tsitika river watershed sediment source inventory. Unpublished report prepared for the Research Branch, B.C. Ministry of Forests. 49 p.
- Megahan, W.F. and Clayton, J.L. 1983. Tracing subsurface flow on roadcuts on steep, forested slopes. *Soil Science of America Journal*, vol. 47, no. 6. pp. 1063-1067.
- Meidinger, D. and Pojar, J. (Eds.). 1991. *Ecosystems of British Columbia*. British Columbia Ministry of Forests. Special Report Series no. 6. 330 p.
- Mosley, M.P. 1979. Streamflow generation in a forested watershed, New Zealand. *Water Resources Research*, vol. 15. pp. 795-805.
- Okimura, T. 1983. Rapid mass movement and groundwater level movement. *Zeitschrift für Geomorphologie, Supplement* 46. pp. 35-54.
- O'Loughlin, C.L. 1972. An investigation of the stability of the steepland forest soils in the coast mountains, southwest British Columbia. Unpublished Ph.D. thesis. University of British Columbia.
- Pierson, T.C. 1983. Soil pipes and slope stability. *Quarterly Journal of Engineering Geology, London*, vol. 16, pp 1-11.
- Rollerson, T.P. 1992. Relationships between landslide attributes and landslide frequencies after logging: Skidegate Plateau, Queen Charlotte Islands. B.C. Ministry of Forests Land Management Report number 76. 13 p.
- Sidle, R.C. 1992. A theoretical model of the effects of timber harvesting on slope stability. *Water Resources Research*, vol 28, no 7, pp 1897-1910.
- Sidle, R.C. and Swanston, D.N. 1981. Analysis of a small debris slide in coastal Alaska. *Canadian Geotechnical Journal*, vol 19, pp 167-174.

- Side, R.C., Pearce, A.J., O'Loughlin, C.L. 1985. Hillslope Stability and Land Use. Water Resources Monograph Series Number 11. American Geophysical Union. 140pp.
- Sterling, S.M. 1997. The influence of bedrock type on the magnitude, frequency and spatial distribution of debris torrents on northern Vancouver Island. Unpublished M.Sc. thesis. University of British Columbia. 117pp.
- Tischer, E. 1986. Hydrologic behaviour of a forested mountain slope in coastal British Columbia. Unpublished M.Sc. thesis. University of British Columbia. 164pp.
- University of British Columbia Mountain Hydrology Group. 1994. U.B.C. Watershed Model Manual Version 3. Unpublished reference manual. 75p.
- VanDine, D.F. 1985. Debris flows and debris torrents in the southern Canadian Cordillera. *Canadian Geotechnical Journal*, vol 22. p. 44-68.
- Wieczorek, G.F. 1983. Effect of rainfall intensity and duration on debris flows in central Santa Cruz Mountains, California. *Reviews in Engineering Geology*, vol 7. p. 93-104.
- Wu, T.H., McKinnell III, W.P., Swanston, D.N. 1979. Strength of tree roots and landslides on Prince of Wales Islands, Alaska. *Canadian Geotechnical Journal*, vol 16. p 19-33.

## Appendix A Results of Soil Sample Sieve Analysis

Table A.1. Size distributions of sediment samples

Sample Id.	%gravel and pebbles	%sand	%fines
CC1	26.61	68.72	4.13
CC2	25.67	69.55	3.37
CC3	37.61	54.71	6.69
CC4	26.61	68.72	4.13
CC5	25.67	69.55	3.37
CC6	38.08	54.71	6.69
CC7	8.07	83.37	8.56
CC8	21.88	73.38	4.74
CC9	5.72	85.30	8.98
CC10	30.03	59.65	10.32
CC11	39.02	54.51	6.47
<b>Average</b>	<b>25.91</b>	<b>67.47</b>	<b>6.13</b>
OG1	54.39	49.30	4.78
OG2	88.03	10.93	1.01
OG3	60.65	30.09	3.53
OG4	77.89	19.81	2.30
OG5	15.58	78.88	5.53
OG6	5.53	89.47	5.01
OG7	15.63	76.85	7.52
OG8	16.20	74.91	8.89
OG9	36.22	55.76	8.02
OG10	53.13	41.20	5.67
OG11	39.21	53.70	7.09
OG12	37.74	58.13	4.14
OG13	42.68	53.07	4.25
OG14	13.79	77.81	8.40
OG15	51.37	45.77	2.86
<b>Average</b>	<b>40.53</b>	<b>54.38</b>	<b>5.27</b>
R1	12.45	81.79	5.77
R2	16.11	78.48	5.41
R3	51.76	45.23	3.01
<b>Average</b>	<b>26.77</b>	<b>68.50</b>	<b>4.73</b>

CC clear-cut monitoring site  
OG old growth monitoring site  
R January 1993 failure site